ABSTRACT

COMPUTER SIMULATION OF AUTOMOTIVE DISC BRAKE NOISE

by

Vadims Milovs

Disc brake noise continues to be a major concern throughout the automotive industry despite efforts to reduce its occurrence. Many articles are written on this subject, but there still is no agreement on what exactly causes disc brake noise and what part of the braking system is responsible for it

The goal of current research was to build a simplified but inclusive mathematical model of a disc brake system and investigate it using Matlab software. The two-dimensional model including damping, Stribeck effect and stick-slip friction was built.

The model is unique in a way that all the similar models have been built using complicated FEM software. It is also unique because it considers the stick-slip phenomenon that has not been considered as a potential source of noise in most models.

The simulation was run in Simulink and gave some valuable insights into the brake noise problem. During this investigation, by changing systems parameters, such as damping coefficients, wheel rotation velocity and pad pressure, the stable and the unstable regions of the system were found.

Probably the main conclusion made from the simulations is that the unstable tangential oscillations can develop in the brake system due to the Stribeck effect (velocity-dependant friction coefficient). Another remarkable conclusion based on the simulation results is that the pad while experiencing stick-slip transitions suppresses the unstable disk oscillations. This seems to be an unobvious effect related to non-linear stick-slip oscillations of the pad, which deserves an additional study.

COMPUTER SIMULATION OF AUTOMOTIVE DISC BRAKE NOISE

by
Vadims Milovs

A Thesis
Submitted to the Faculty of
New Jersey Institute of Technology
In Partial Fulfillment of the Requirements for the Degree of
Master of Science in Mechanical Engineering

Department of Mechanical Engineering

January 2003

APPROVAL PAGE

COMPUTER SIMULATION OF AUTOMOTIVE DISC BRAKE NOISE

Vadims Milovs

Dr. Avraham Harnoy, Thesis Advisor — Date
Professor of Mechanical Engineering, NJIT

Dr. Zhiming Ji, Committee Member — Date
Associate Professor of Mechanical Engineering, NJIT

Dr. Boris Khusid, Committee Member — Date
Associate Professor of Mechanical Engineering, NJIT

BIOGRAPHICAL SKETCH

Author: Vadims Milovs

Degree: Master of Science

Date: January, 2003

Undergraduate and Graduate Education:

- Master of Science in Mechanical Engineering
  New Jersey Institute of Technology
  Newark, New Jersey, 2003

- Batchelor of Science in Mechanical Engineering
  Ben Gurion University of the Negev
  Beer Sheva, Israel, 1996

Major: Mechanical Engineering

To my beloved parents, my brother Tom, his wife Julia and their son Daniel Aaron.

ACKNOWLEDGEMENT

I express my appreciation to Dr. Avraham Harnoy, Professor in the Department of Mechanical Engineering, New Jersey Institute of Technology for his guidance and suggestion in preparation of this thesis.

Particular acknowledgement to Dr. Bernard Friedland, Professor in the Department of Electrical Engineering, New Jersey Institute of Technology for the knowledge of Matlab, Simulink and modern control systems I acquired from his course.

I wish to thank my family and my friends: Andrey Titov, Larry Murray, Frank Maddin, Deirdre Coffey, Jose Mario, Hakan Altan, Ilja Nabutovsky, Alex Isakbaev, Misha Hahalev, Vadik Stupin, Mark Mirochnik, Boris Greenberg, Dima Lukatsky, Jaroslav Tenzer, Kirill Gitman, Sasha Slivkin, Jura Bazilev and many others, who encouraged me in my graduate studies and gave me a lot of help and support.

I would like to express gratitude to my friends in Brooklyn, the Fraiman family, Alik, Valentina, Boris and Michael, for being my second family in USA.

Special acknowledgement to Mr. Janis Priede, my Latvian friend, whose valuable advice helped me through this work.

TABLE OF CONTENTS

TABLE OF CONTENTS
(Continued)

LIST OF TABLES

LIST OF FIGURES

CHAPTER 1

INTRODUCTION

Disc brake noise continues to be a major concern throughout the automotive industry despite efforts to reduce its occurrence. Over the years, disc brake noise has been given various names that provide some definitions of the emitted sound such as grind, grunt, moan, groan, squeak and squeal. In order to simplify and categorize all this cases, it is convenient to divide brake noise into three larger categories: low frequency noise, low frequency squeal and high frequency squeal [4]. High frequency squeal is the most problematic of all.

Many articles are written on this subject, but there still is no agreement on what exactly causes disc brake high frequency squeal and what part of the braking system is responsible for it. One thing known for sure is that disc brake noise is caused by frictional instabilities that cause sound-emitting oscillations. All friction-excited oscillations have one common feature – the source of oscillation is an energy-dissipating frictional event. There is only one way to end friction-excited oscillations and that is to stabilize the system. This can be done by reducing the frictional excitation and/or by changing the friction material. It can also be accomplished by providing damping at the excitation site.

The goal of current research is to build a simplified but comprehensive mathematical model of a disc brake system and investigate it using Matlab software. During this investigation, by changing systems parameters, such as elasticity and damping coefficients, the stable and the unstable regions of the system have to be found. The knowledge of these stability regions can help in making the conclusions about

certain parameter's influence on system's stability and ultimately in understanding of how to avoid the brake squeal.

Experimental observations previously made by researchers indicate that high frequency squeal is related to circumferential (in-plane) disc oscillations. On the other hand, both experiment and theory suggest that the audible noise is usually emitted by flexural (out-of-plane) oscillations.

Thus, two basic questions arise:

- What is the physical mechanism responsible for the onset of the circumferential oscillations?
- How do the circumferential oscillations cause the flexural ones?

As to the origin of circumferential vibrations, the potential physical mechanism responsible for this instability is the Stribeck effect (decrease of the friction coefficient with velocity). This effect could, in principle, give rise to self-sustained circumferential oscillations. Note that the energy of oscillations is obviously coming from the rotation of the disc related with the circumferential DOF.

The major problem is the physical coupling between circumferential and flexural modes that oscillate in mutually perpendicular directions. To obtain self-sustained oscillations, a two-directional coupling between the involved DOFs is necessary. For this reason, an additional feedback mechanism is needed to account for excitation of the flexural vibrations from the circumferential ones. It seems that the best candidate for such a feedback mechanism is the so-called follower force. The follower force hypothesis was considered in Mottershead's recent studies [10-15].

Follower force is a component of the disc to pad friction force acting normal to the disc surface as a result of tangential displacement. The follower force ensures the necessary coupling between the flexural and circumferential vibrations, because the follower force, being proportional to the friction force that acts in the plane of disc, is directed out of plane and thus it provides the feedback from circumferential oscillations to the flexural ones in a straightforward way.

Unlike Mottershead's three-dimensional simulation, the current study deals with two-dimensional problem, for this reason Mottershead's follower force formula was adapted for the 2-D case.

Recent mathematical models used by the researchers to simulate brake noise phenomenon are critically overviewed in current paper (see descriptions of these simulations in Chapter 7). Some of these simulations leave a lot of questions unanswered, some neglect important physical effects, some are using very complicated 3-D simulations, which are beyond this thesis work's competence. The intention of this work was to create a relatively simple mathematical model of the disc brake system that will give a precise insight into the disc brake squeal phenomenon.

The uniqueness of the current work is that it tries to consider all the possible forces, effects and nonlinearities (Stribeck effect, stick-slip friction, follower force) that may occur in automotive disc brake system using a simplified two-dimensional model.

The simulation code is written using Matlab and Simulink, which make it very interactive and easy to use. By changing the system's parameters in one easy step, the user can run the simulation with new constants and examine system's behavior under given conditions.

The last step of the current research is the analytical calculation of system's stability. Obviously, including Stribeck effect and the follower force into mathematical model makes it strongly nonlinear, which makes it complicated to study analytically using the S-plane techniques.

However, it is possible to linearize the system around some stable or unstable point, found from the simulation results and execute the calculations especially for that point using Lyapunov stability criterion.

The thesis work consisted of several stages:

- Literature overview (more then 30 papers on disc noise examined).
- Classification of all the scientific data available on disc noise and selection of the most adequate and up-to-date material.
- Creation of a comprehensive 2-D model that will include all the physical effects that are possibly influencing disc squeal.
- Simulation of the brake system model using Matlab, starting with the simplified cases and gradually adding more complicated effects, such as damping, Stribeck effect, follower force.
- Finding stable and unstable regions of the system. Changing system's parameters and studying their influence on system's stability.

CHAPTER 2

DISC BRAKE MECHANICS OVERVIEW

An automotive brake system can be divided into three main parts:

1. The rotor, as the name is indicating, is rotating with the wheel. It is the first part in the friction couple. Rotors made of gray cast iron have always dominated the market. The last couple of years, other materials have been introduced.
2. The brake pad is the second, stationary, part of the friction couple. During a brake application, the pad is pressed against the rotor with a hydraulic piston. The friction forces between the stationary pad and the rotating disc will turn the kinetic energy of the vehicle into heat.
3. The hydraulic system transfers and amplifies the brake force from the brake pedal to the hydraulic piston pressing the linings against the rotor. In modern brakes the hydraulic system also includes ABS-system.

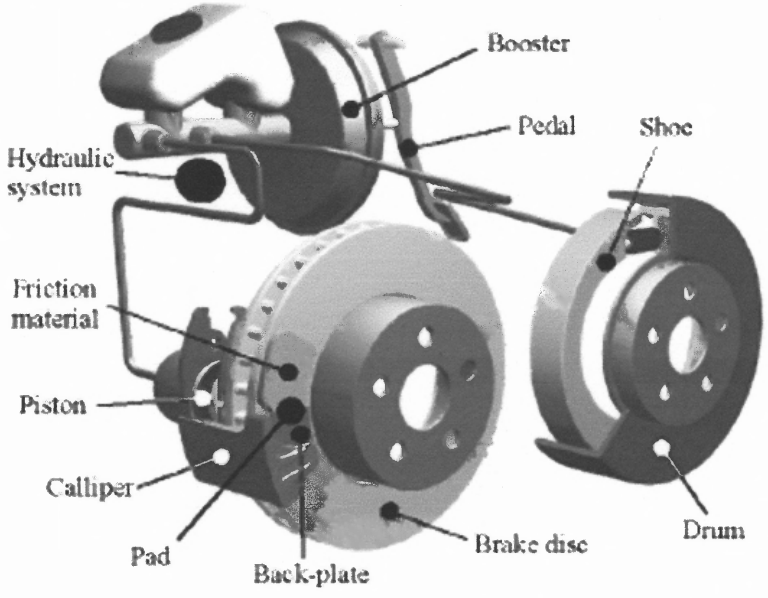

Figure 2.1 Disc brake system.

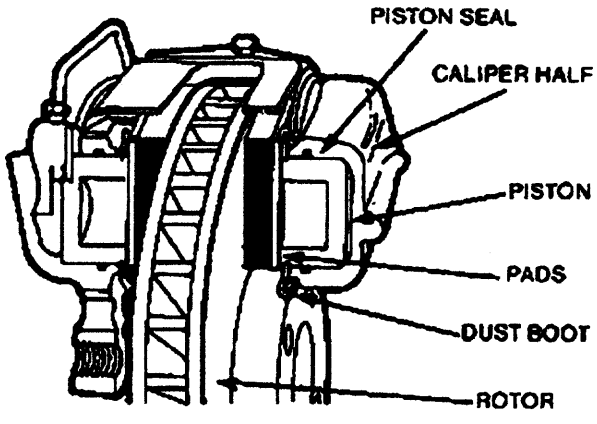

Cutaway - Typical Disc Caliper

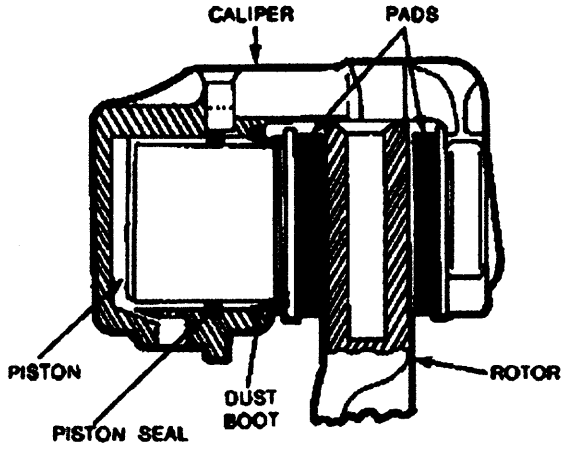

Disc Caliper Components

Figure 2.2 Disc/Pad assembly.

The disc and the pad are in the focus of the current study, for they are most probably the components responsible for disc squeal. The rotor disc is rigidly fixed to the wheel with bolts and is connected to the axle of a car. The pad is connected to the body of a car. In disc brake, the pads clamp the disc from opposite sides. The brake force from the hydraulic piston is distributed equally between the pads braking the disc. The friction force between the pad and the disc is perpendicular to the applied normal force on the pad. It may seem that because of this orthogonality the friction force does not affect the normal force, but the latest research indicates the presence of so-called follower friction load. The follower load hypothesis means that the tangential friction force follows the deformed surface of the disc (as a result of material waves) and changes its direction when the disc vibrates. As a result, the friction force has a transverse component affecting the normal force.

As the brake pads wear, the caliper automatically adjusts itself. Brake calipers consist of four major components: the dust boot, the seal, the piston, and the housing. Depending on its design, the caliper may have one, two, three, or four pistons, seals and

boots in a single housing. In either case, however, the operation is essentially the same. Calipers ride in anchor plates, which are either mounted to the suspension or frame. When the brakes are applied, hydraulic pressure causes the piston to move out of the caliper bore, and the opposing reaction slides the caliper in the anchor plate pushing the friction pads to the rotor with equal pressure

Since brake pads provide the friction necessary to stop the rotor, they must have heat resistance and physical strength. While that is true of all brake pads, each of the available types, semi-metallic or NAO, provides these properties in different degrees. Many vehicles today use semi-metallic brake pads to handle the higher operating temperatures, resulting from the changes in front brake rotors and downsized brake parts. With these changes, disc brake operating temperatures jump from 500 F up to 700+ F. Only the semi-metallic pads with an operating temperature range of 900+ degrees can work properly at that heat. NAO pads are designed for operating temperatures of 350 to 500 degrees. The ceramic variation is designed to care for noise and dusting problems.

CHAPTER 3

ROTOR DISC OSCILLATION MODES

Vibrating structures cause pressure waves in the surrounding media. These waves are known as sound and the tone a person hears depends on the frequency of the vibration. High frequencies are heard as high pitch tones and low frequencies as low pitch tones. Brake squeal has a main frequency between 1 and 20 kHz. Furthermore, brake squeal has a stable and dominating main frequency plus a number of overtones, resulting from different vibration modes of the brake assembly.

The modes describe the ways in which the system is allowed to vibrate easily. Frequencies corresponding to the nodes are called resonance frequencies and the phenomenon when a structure is easily vibrating is called resonance. Theoretically, at resonance the amplitude is only dependent on the damping of the system and the input energy. Equilibrium is reached when the input energy equals the energy absorbed by the damping.

According to the annular plate theory, disc rotor when being excited starts to oscillate both in normal and tangential directions. The experiments showed that the natural modes of the mechanically excited stationary brake system are qualitatively similar to the vibrational pattern observed on the operating brake system. Normal (flexural) direction resonances of the rotor disc exist throughout the disc squeal frequency range, starting with a 2 nodal diameter mode near 1 kHz through a 12 nodal diameter mode near 15 kHz. These resonances are known for their intensive sound propagation, and are considered to be the main cause for brake disc noise. The natural frequencies of

the rotor disc flexural resonances and their mode shapes for an arbitrary disc can be observed on Figure 3.1.

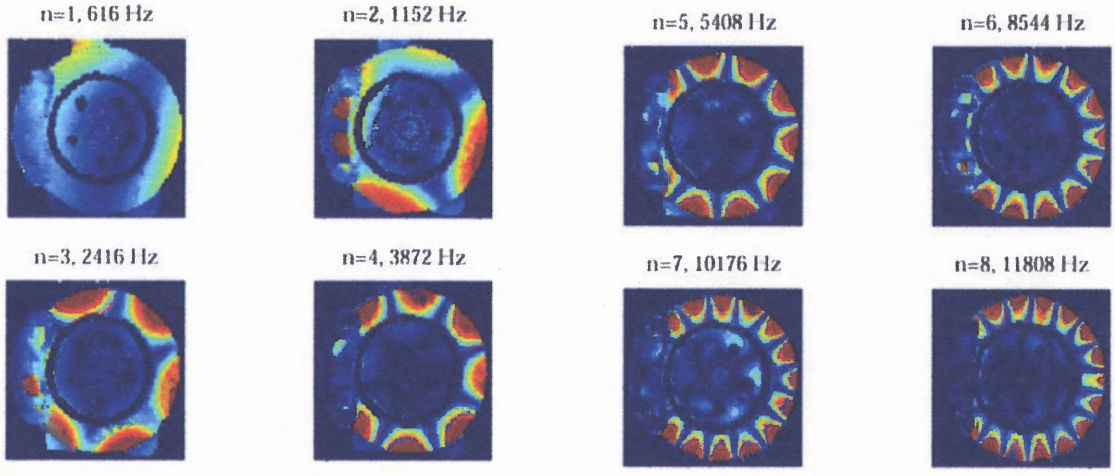

Figure 3.1 Rotor disc modes (Taken from McDaniel, Chen, Moore and Clarke 1999 [9]).

The flexural (out-of-plane) modes have much higher modal density then the circumferential (in-plane) modes. Usually, the first circumferential mode appears after 5 kHz. Circumferential modes can be viewed as a compression wave in the disc circumference, similar to a longitudinal mode of a solid bar Figure 3.2. When normal and circumferential resonances occur at the same frequency it is called modes coupling. Experimental observations previously made by researchers indicate that high frequency squeal is related to circumferential (in-plane) disc oscillations. On the other hand, both experiment and theory suggest that the audible noise is usually emitted by flexural (out-of-plane) oscillations.

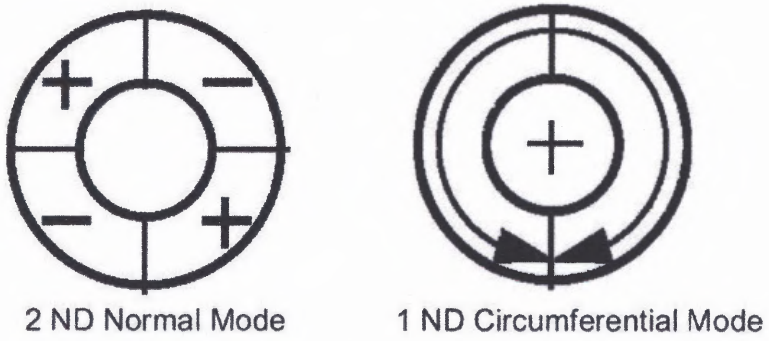

Figure 3.2 Disc modes shape.

CHAPTER 4

DISC BRAKE OSCILLATION TYPES

4.1 Rigid Body Oscillations

As the name implies, rigid body oscillations are those in which the vibrating masses move with little or no deflection. These are usually at vibrating frequencies well below these of brake squeal, and most below 600 Hz. Rigid body oscillations can be of very low frequency, so they can be seen or felt, but not heard. Brake roughness, judder and shudder are examples of these oscillations. Rigid body oscillations may have mechanical or thermal causes. Mechanical causes include such well-known phenomenon as Disc Thickness Variation.

DTV is caused by material transfer from the disc brake pads to the brake rotor due to light pad/rotor rubbing during off brake driving (e.g. highway cruising). Light contact starts at the location of maximum rotor run-out and develops slowly over thousands of miles. If a sufficient amount of DTV is generated, judder will be felt in the brake pedal or steering wheel when the brakes are applied.

Mechanical causes also include machining errors such as: thickness variation, ovality and runout. Uneven heating of brake rotors can temporarily cause or increase thickness variation and sometimes can produce a primary thermal buckling that wraps the rotor into a washboard with three or even five high spots per revolution.

Brake roughness is felt at wheel rotation speed, one torque pulse per revolution. DTV and drum eccentricity induce pulses at one per wheel revolution. Disc brake runout

and drum brake ovality produce two vibrations per revolution. Lug bolt and other wheel distortion can cause 4, 5 or even 6 pulses per wheel revolution.

Hum and moan are also caused by rigid body oscillations. These often occur in disc brake assemblies as the result of a dragging shoe that excites a caliper mount windup resonance. Rotor thermal distortion at highway speeds can also cause hum and moan.

4.2 Continuum Oscillations

These are the oscillations that cause brake squeal. For this report, squeal is the generic name for a friction-excited oscillation above 1000 hertz. The rigid body oscillations are very unlikely to be responsible for disc squeal, because in order to reach a 1000-hertz frequency at two or even six pulses per revolution, the wheel has to be rotating at a very high rate, and as well known, the squeal noise typically occurs at low vehicle velocities.

As the name "continuum" implies, the vibrating components flex to provide both spring and mass for the vibrations. Continuum oscillations are caused by positive mechanical feedback excitation from brake lining. Continuum oscillations typically happen when the system reaches the resonance frequency, corresponding to one of the natural modes of the disc. As it was mentioned before, the studies indicate that these are the circumferential vibrations that initiate the flexural ones to create the phenomenon of modes coupling, which most probably causes disc brakes squeal. The mechanisms that are responsible for this kind of oscillations are much more fugitive and complicated than the ones responsible for rigid body oscillations and include negative slope in the friction-velocity curve, the follower force and parametric resonance.

CHAPTER 5

BRAKE NOISE MECHANISMS

In this paragraph, various brake noise mechanisms will be discussed more closely. As it was mentioned earlier, disk brake squeal occurs when a system experiences large amplitude mechanical vibrations. The literature survey points on three major physical mechanisms that can cause self-excited vibrations in the car disc brakes.

5.1 Stribeck Effect and Stick-Slip Friction

Stribeck effect is a decrease of the dynamic friction coefficient with velocity that can lead to a negative damping coefficient, which provides the energy source of the break squeal. Stribeck effect causes the instability to occur in a bounded velocity range, like it is observed in practice. On the other hand, it is well known that the squeal is mostly generated by the out of plane vibrations of the disc while this instability causes oscillations in the plane of the disc. Thus, more complicated model seems to be necessary to account for excitation of flexural vibrations by the in-plane Stribeck effect. Such attempts have been undertaken by Pilipchuk, Ibrahim & Blaschke (2002), Quyang & Mottershead (2001b), Quyang et al. (1999) and Aviles et al. (1995) – see Chapter 7.

The variable friction coefficient can be modeled in a number of different ways having different degrees of complexity. For instance, Ouyang and Mottershead have adopted a relatively simple friction model for their simulation [14]:

$$\mu = \mu_s \cdot (1 - \upsilon/15) + 0.0002 \cdot \upsilon^2 \qquad [5.1]$$

Where μ_s is the static friction coefficient.

An example of stick-slip is a squeaky door hinge. Stick-slip consists of two phases, stick and slip. During the stick phase, the brake lining and cast iron move together, with no slippage at the interface. The stick time period is variable, depending on speed, load, and system stiffness. When slip begins, a noise burst occurs. This involves a half-cycle of motion at the rubbing surface. The sudden energy burst often produces a more sustained audible oscillation.

Stick-slip in brakes generally is confined to low speed rigid body vibrations, so have low frequencies. The noise bursts always start motion in one direction, and have peak amplitudes then. Many frequencies are excited at one time, so the time-domain waveform is complex. Vehicle speeds are normally less than 2 mph for brake stick-slip. It is possible for rounded particles within brake linings (such as glass beads) to undergo stick-slip within brake lining, when excited by rubbing surface. This stick-slip may occur at any vehicle speed, but still has very low rubbing speeds between the rounded particle and the brake lining matrix, where the stick-slip occurs.

Speaking of high frequency squeal, which is the most problematic of all the brake noises, most probably the Stribeck effect plays one of the key roles in squeal generation along with the follower force. The role of the Stribeck effect is to cause circumferential vibrations of the rotor disc that will in turn cause the flexural vibrations when amplified by the follower force.

5.2 The Follower Force

The second physical mechanism considered by Mottershead as a potential cause of unstable flexural vibrations of the disc is so called follower force. The follower force hypothesis assumes the friction force to be always directed tangentially along the surface. Flexural wave propagating along the surface subject to the friction will give rise to the component of force normal to the unperturbed surface. Obviously, follower force will oscillate together with surface slope that is shifted in phase by a fourth of period (90 degrees) relative to the amplitude oscillations in the wave. Thus, follower force is analogous to the viscous damping that is proportional to the velocity and so also shifted in phase by a fourth of period relative to the amplitude oscillations. Consequently, follower force can either damp or amplify oscillations depending on the sign of the damping coefficient.

It turns out that the action of the follower force depends on the direction of wave propagation relative to the direction of friction force: forward-traveling waves (against the friction force) are destabilized whereas backward-traveling ones are suppressed.

Thus, the stronger the friction force, the stronger the destabilizing action of the follower force. In simple models, the follower force appears as an asymmetry in the stiffness matrix proportional to the friction force. Note that without both follower force and viscous damping the symmetric stiffness matrix results in purely real spectrum for squares of frequencies of natural oscillations. However, this spectrum is no more necessarily real when stiffness matrix is not symmetric. In both cases, symmetric and asymmetric, the spectrum is defined as an eigenvalue problem of a real matrix that is equivalent to finding of roots of the characteristic polynomial with real coefficients.

As well known, polynomial with real coefficients can have complex roots only by complex conjugate pairs. Thus, oscillation modes with complex frequencies, if any, can appear only by pairs where one is exponentially decaying but the other exponentially growing, i.e., unstable in time. Consequently, appearance of a complex frequency unambiguously implies instability. On the other hand, since the number of roots of polynomial is fixed to its degree, emergence of a pair of complex conjugated roots implies disappearance of a pair of real roots. Since roots are expected to vary continuously with the coefficients of the equation, a pair of real roots has first to coalesce into duplet before it can further split up into complex conjugate pair in the course of development of instability. Such a type of instability developing via a coalescence of two frequencies is called flutter instability. Obviously, presence of close vibration frequencies in the brake system under the action of follower force poses a potential risk of development of flutter instability as it is often observed in practice. Note that in simple follower force model there is no dependence on the velocity that apparently contradicts practical observations of brake squeal appearance.

Follower force effect seems to be at the heart of the generalized theory of brake noise due to Nishiwaki (1993). For three different noise mechanisms he obtains similar simplified equations containing only inertial and stiffness effects with stiffness matrices containing an asymmetric component proportional to the friction force that is obviously due to the follower force effect.

5.3 Parametric Resonance

The third mechanism is the parametric resonance caused by rotation of the disc past sliding brake pads, that causes cyclic variation of system parameters rather than variation of externally applied load as it is the case for the usual resonance. In this case, unstable flexural (out of plane) vibrations of the disc can arise at some specific values of system parameters (typically rotation speed, stiffness and damping) even when friction between the disc and brake pads is absent. Normal reaction force alone between two components in cyclic relative motion is sufficient for this instability to appear. There are three types of parametric resonances possible in the rotating disc.

The first is the superharmonic resonance occurring when disc rotation rate becomes close to the circumferential speed of some flexural mode. Note that there is infinite number of such modes and so infinite number of critical speeds. Width of each unstable rotation rate range increases with the stiffness of the disc. Thus, originally this instability was referred to as the "stiffness instability."

Second type of parametric instabilities, called the "combination resonance", is expected to occur whenever either sum or difference of natural frequencies of two flexural modes coincides with the disc rotation speed multiplied by either sum or difference of circumferential nodal diameters of those modes. Thus, there is even greater number of possibilities for combination resonances than the superharmonic ones.

Third type of resonances has no simple functional relation between the speed of rotation and the natural frequencies of the disc. Obviously, for this instability to occur the rotation rate of the disc must be comparable to the frequency of flexural vibrations of the disc (about several kHz) that is quite high. Therefore, relevance of this instability to the

brake squeal generation is questionable. Moreover, practical observations show that squeal generation strongly depends on the friction and appears only at sufficiently low velocities whereas this instability appears independently of friction and only at sufficiently high speeds. Mathematically, parametric instabilities are described by quite complicated systems of Mathieu-Hill type-linear ordinary differential equations whose coefficients are in general periodic functions of time. Therefore, it may be quite complicated, if necessary, to incorporate adequately this type of instability into a simplified physical model.

As it was mentioned earlier, parametric resonance can occur when the disc rotation rate becomes close to the circumferential speed of some flexural mode. As it was mentioned before, the first flexural mode has around 1 kHz frequency. In a car it is very unlikely that a wheel will rotate at such frequency, that's why parametric resonance is not a mechanism that should be considered when simulating a realistic car brake model.

CHAPTER 6

DISC BRAKE NOISE SOLUTION TECHNIQUES

Current work focuses on high frequency squeal, because this group of noises is the most problematic one and no total solution has been found yet to eliminate high frequency squeal. The two other groups of noises can be successfully eliminated as described bellow.

6.1 Low Frequency Noise

Low frequency noise typically occurs in the frequency range between 100 and 1000 Hz. The noise is caused by friction material excitation at the rotor and lining interface. The energy is transmitted as a vibrational response through the caliper (brake corner) and couples with other chassis components. The typical failure mode occurs at deceleration of 5 to 20 $ft/\sec^2$, lining temperature of 150-250 $\circ F$ and vehicle speeds of 10-20 mph.

After conducting the experiment [4], a strong connection between sustained noise event and lateral caliper acceleration was found. Attempts to modify the vehicle response with various structural modifications were unsuccessful. The only practical solution was to reduce the forcing function. For that purpose, a new lining material needed to be found. A lining study was developed that pinpointed the major factors in the lining composition that reduced the propensity for noise. These factors were additional filler, abrasive and fiber, as well as a reduction in lubricant. Correcting these factors has solved the problem of low frequency noise.

6.2 Low Frequency Squeal

Low frequency squeal is generally classified as noise having a narrow frequency bandwidth in the frequency above 1000 Hz yet below the first circumferential mode of the rotor. The failure mode for this category of squeal can be associated with frictional excitation coupled with a phenomenon of "modal locking" of brake corner components. The typical failure mode occurs during low brake deceleration 4 to 6 $ft/\sec^2$, lining temperature of 30-40 $\circ F$ and vehicle speeds up to 5-10 mph.

After conducting the experiment [4] and capturing sound pressure data during a squeal event, it was found that the squeal was in the frequency range of 2500 to 2600 Hz. Structural dynamic measurements taken in the rotor and caliper indicated that both had resonances in the frequency range. The rotor resonance occurred at 2640 Hz in the 3rd node diameter mode. The caliper mode occurs at 2546 Hz and is a 1st bending about the bridge. This resonance coupling between the rotor and the caliper produces the squeal. The solution technique developed for this case was to decouple the caliper and rotor modes. As with any structural dynamic modifications, the damping, mass and/or stiffness of the rotor/caliper can be modified.

The simplest modification that could be made was to change the rotor material for gray cast iron. The goal of this modification was to reduce the amplitude of the rotor response by increasing the damping. After the "damped iron" rotor was used, the low frequency squeal was eliminated.

Frequency response measurements comparing gray iron versus "damped iron" rotor shows the shift down in frequency of approximately 400 Hz, therefore, the mode coupling is eliminated.

6.3 High Frequency Squeal

Unlike low frequency noise and low frequency squeal, high frequency squeal problem does not have an "absolute" solution yet. High frequency squeal is typically classified as a squeal occurring at frequencies above 5 kHz. Although there are many flexural (bending) modes of the disc brake rotor through the frequency range of squeal, the squeal frequencies are typically coincident with circumferential (longitudinal) modes. It is sought that high frequency squeal occurs as the result of cross coupling of a circumferential and flexural mode of the rotor or another mode of the brake system.

Experiments show that flexural vibrations of the rotor mostly cause the sound, but the correlation of the squeal occurance with the circumferential modes indicates that these are circumferential modes that trigger disc squeal. This fact supports the hypothesis of modes cross coupling. Then the question that needs to be answered is how do the circumferential vibrations cause the flexural ones. Despite these two vibrational modes being orthogonal to each other, the coupling mechanism between the modes is the follower force.

As it was mentioned earlier in the text, the follower force means that the tangential friction force follows the deformed surface of the disc and changes its direction when the disc vibrates. As a result, the follower force has a transverse component when the disc deforms during vibration.

Just like in the previous two cases, for a particular brake system there exist particular frequencies at which high frequency brake squeal will commonly occur. These frequencies typically remain constant for a particular brake rotor independent of the rest of the brake system. This fact supports the theory that disc rotor is a controlling element

responsible for squeal generation. Sample brake squeal data acquired with a dragging brake dynamometer is shown at the picture below [4]. From the Figure 6.1(a) it is obvious that squeal occurred at three distinct frequencies.

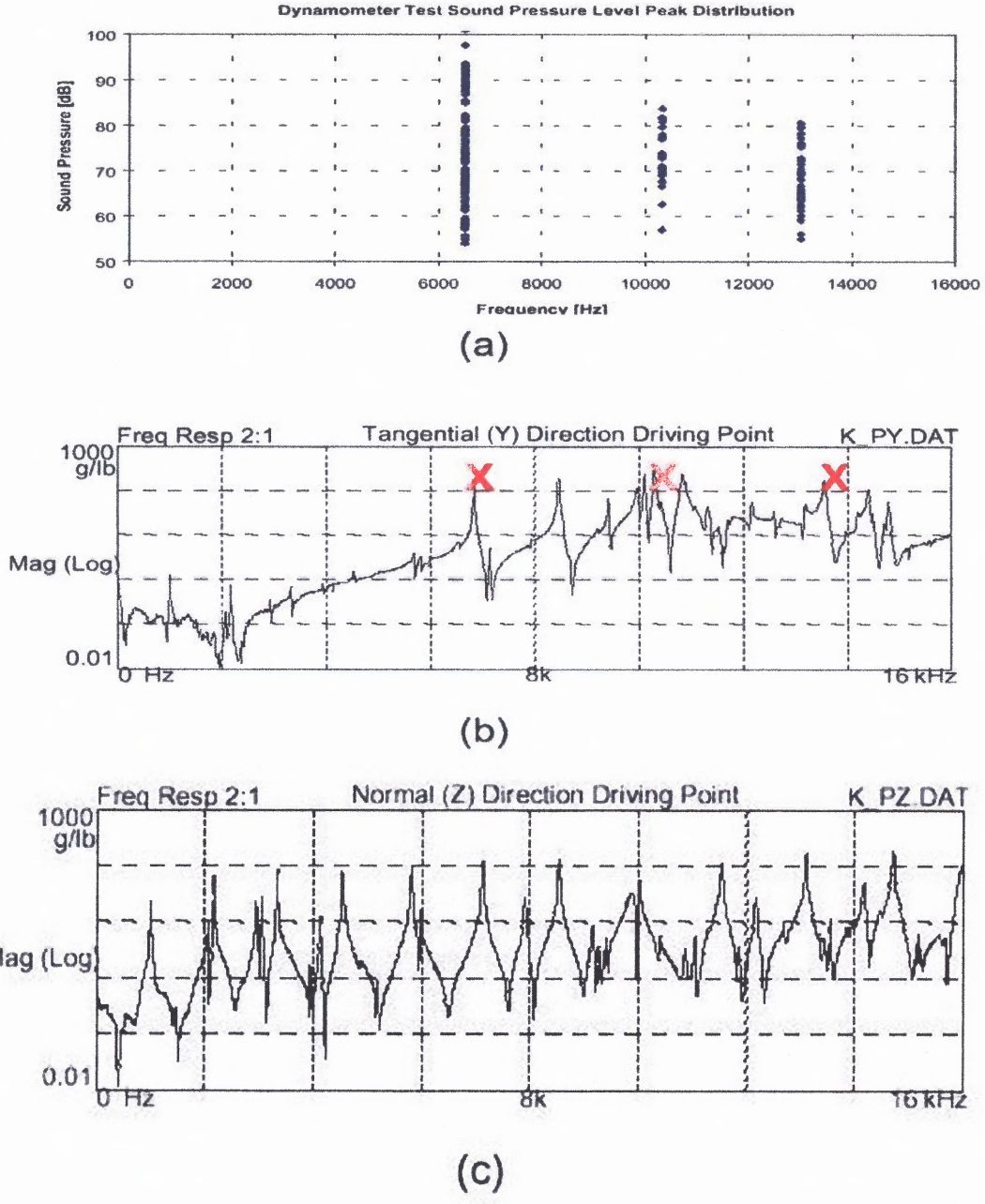

Figure 6.3 High frequency squeal as a result of modes coupling (Taken from Dunlap, Riehle and Longhouse 1999 [4]).

Frequency response function measurements of the rotor in tangential and normal directions are displayed in Figures (b) and (c). The first three circumferential modes of the rotor consisting of 1, 2 and 3 nodal diameters are identified by X's in Figure (b). It is obvious from the figure that circumferential modes are coincident to the squeal frequencies.

On the other hand, the presence of circumferential nodes does not itself guarantee the occurrence of brake squeal. For squeal to occur, it is expected that cross coupling of a circumferential and normal direction mode of the rotor or a circumferential mode of the rotor and another mode of the brake system must occur. In case of high frequency squeal, the vibration modes of the pad do not affect squeal occurrence, because the vibration frequencies of the rotor disc are much greater then these of the pad.

The objective of current study is to prove the above-mentioned experimental results analytically by creating a mathematical model of the disc brake system and simulating it in real time using Matlab software. Moreover, if the experimental study does not give the explanation to the modes cross coupling phenomenon, the mathematical modeling makes it possible to verify how the coupling mechanism works.

The disadvantage of the analytical modeling approach is that it does not allow measuring the noise level of the system. The only thing that can be found from current simulation is the unstable vibration, but it is impossible to suggest with a high degree of accuracy that these vibrations will produce sound.

CHAPTER 7

MATHEMATICAL MODELS OVERVIEW

Before building a mathematical model for this thesis work, it would be useful to overview the existing analytical and experimental models. For the analytical models implementation, the mathematical software such as Matlab, Simulink or FEM packages can be used. For the experimental models - laser Doppler velocimetry (LDV), laser vibrometers and electronic speckle pattern interferometry (ESPI) are used.

Here is a short overview of the mathematical and experimental models, which have been created by different researchers, placed in a chronological order:

Chan, Mottershead and Cartmell (1994) considered the parametric resonances in a stationary classical annular disc excited by a rotating mass-spring-damper system together with frictional follower load. Using the method of multiple scales, they find instabilities associated with subcritical parametric resonance and other instabilities associated with backward wave modes with nodal diameters (non-zero circumferential wave numbers). The later are shown to be driven by friction and thus to be rotation-speed-independent.

Aviles et al. (1995) introduced a simple model based on both velocity and temperature dependent friction coefficient to model the judder in disc brakes at high speeds. The authors mostly focus on the low frequency (100-500 Hz) circumferential caliper vibrations (so called brake groan) resulting from the velocity and temperature dependent friction coefficient.

Quyang et al. (1999) assumed the static friction coefficient to be higher than the dynamic one in his study of the in-plane vibration of a slider-mass driven around the surface of a flexible disc. The disc is considered as an elastic annular plate and the slider has flexibility and damping in the circumferential (in-plane) and transverse directions. Due to the friction force between the disc and the slider system, the slider oscillates in the stick-slip mode in the plane of the disc. The transverse vibrations induced by the slider change the normal force on the disc, which in turn changes the in-plane oscillation of the slider. The obtained results indicate that normal pressure and rotating speed can drive the system into instability. The rigidity and damping of the disc and transverse stiffness and damping of the slider tend to suppress the vibrations whereas the in-plane stiffness and damping of the slider do not always have a stabilizing effect.

El-Butch & Ibrahim (1999) consider seven-DOF (degree of freedom) multi-body model of brake system including disc, pad, caliper and piston, where the first three components have both translational and rotational DOF, whereas the latter only translational DOF. Equations of motion are obtained using the Lagrangian approach with generalized forces to include follower forces, which are the only potential source of the instability in the model. The authors claim that according to their model the position of the piston is of substantial importance though it is not clear how this position is taken into account in the model.

Mahajan, Hu & Zhang (1999) describe three CAE-based brake squeal analysis methods implemented on disc-type brakes in a vehicle program at Ford.

The first method was the nonlinear transient analysis based on the FEM modeling of a realistic brake system comprising the rotor, the caliper, the lining with baking plates, and the anchor bracket guiding the caliper through pins. The outputs of the model were the time responses of different mode vibrations after the start of braking event. Advantage of the code was the sophisticated handling of the frictional contact able to capture accurately the rotor-pad interface geometric nonlinearities.

The second method was normal modes analysis that was used to investigate uncoupled free vibration modes only of the primary brake components: the rotor and the pads. This approach relies upon the assumption of a likely coupling of close modes due to the friction. Rotor and pad/backing plate modes that are close each to other are identified as likely to couple.

The third method was the complex eigenvalue method using the model very similar to the one used in the Nonlinear Transient Analysis method. The friction in this model is introduced as coupling between the degrees of freedom along the normal and tangential directions at each node in the rotor/pad contact interface. The critical part of this method is the inclusion of coupling terms in the system stiffness matrix that leads to the asymmetric form of the system stiffness matrix. All three methods, when applied for optimization of brake pad design, showed a good potential for the application to the automotive brake system development. The transient method provided good comparison with test data while the normal modes method provided a cost-efficient way of driving certain design changes.

Chen et al. (2000) presents results of experimental investigation using LDV and phase shifting pulsed ESPI to visualize vibrations of brake disc and pad/caliper assembly during the squeal generation process. It is found, that the key to the squeal generation is the modal coupling between the disc and pad/caliper assembly. It is shown in a case study, that squeal generation is associated with coupling of the fifth flexural disc mode with the pad-bending mode. The authors also demonstrate that using mass loading/damping can decouple the modes between the disc and pad/caliper assembly vibration by which the squeal is eliminated.

Chung et al. (2001) analyses brake stability problem in the modal domain by searching vibrations as superposition of free-oscillation modes of separate brake elements. Interaction between the disc and pads is described by means of the generalized coordinates defined as relative normal and tangential displacements at the disc/pad interface. In accordance to the geometry (follower force) instability hypothesis, relative tangential displacement between the rubbing surfaces gives rise to the normal force perturbation that is source of the instability appearing as an asymmetry in the stiffness matrix proportional to the friction force. The authors consider frictional stiffness asymmetry as a small perturbation that allows obtaining a simple approximate expression for the perturbed frequency spectrum of oscillations. This solution is further used to define the coupling strength between various pairs of natural modes. The coupling strength provides a measure of how fast two modes will approach or move apart when the friction force increases from zero. This criterion allows identifying potentially unstable pairs of modes.

Shi et al. (2001) describes state-of-art complex eigenvalue analysis at GM to predict brake rotor out-of-plane mode coupling with rotor's tangential vibrations (responsible for high frequency squeal). In general, they find a good agreement between the theoretical predictions and experimental findings. The major problems are related to insufficient knowledge of material constants (elasticity and damping) and to complexities in modeling contact interfaces.

Quyang & Mottershead (2001a) investigated the instability of the forward and backward traveling waves in the transverse vibration of a stationary disc induced by the friction in a rotating mass-spring-damper system. The authors consider combination resonances across the whole speed range and model the friction force as a follower force. They find regions of instability for combination resonances and the instability of the associated traveling waves at the subcritical speeds. In addition to the already well-known facts that the friction alone destabilizes the backward traveling waves in the speed-independent resonances and that the damping of the rotating system is destabilizing in the subcritical speed range, it is found that the friction modeled as a follower force is the most destabilizing factor among the system parameters.

Quyang & Mottershead (2001b) introduced the velocity-dependent friction with the Stribeck effect into the moving load problem for the vibration of car disc brake. The authors claim that by solving corresponding eigenvalue problem, a bounded region of instability is obtained for the rotating speed of the disc versus the friction coefficient at the disc/pads interface, which is compatible with the observed squeal phenomenon of a car disc brake.

Quyang & Mottershead (2001c) is concerned with suppression of parametric vibrations in discs under rotating frictional loads. The authors investigate the parametric resonances of a stationary disc excited by a rotating frictional load and influenced by series of mass-spring-damper systems with or without friction. The genetic algorithm is used to reduce and even eliminate the dynamic instability caused by the rotating friction as a follower force on the disc surface. It is found that if the mass-spring-damper systems involve no or low friction, they can reduce or suppress the dynamic instability of friction induced parametric resonances when correctly located, but they have, at best, no effect when the level of friction is high.

Hendricks et al. (2002) conducted experimental investigation of low frequency squeal (1.6 kHz) using spectral and acoustic holography techniques. It was found that the low frequency squeal is mostly emitted by the pad to disc interface. The squeal generation strongly correlates with pad properties whereas influence of the disc is very weak. The most important parameter influencing squeal frequency is the braking pressure while rotating speed has less importance.

Pilipchuk, Ibrahim & Blaschke (2002) take into account Stribeck effect by considering velocity-dependent friction coefficient, which, however, is smoothed about zero velocity to render this dependence artificially continuous. In addition, the authors assume the friction force acting on the pad to be concentrated along its trailing edge due to the moment arising from the friction force, and thus to cause redistribution of normal forces that seems to be similar to the effect of a follower force. Eventually, they consider only in-plane disc vibrations while transverse ones are completely ignored by arguing that the contact forces from both sides of the disc are equal.

CHAPTER 8

MATHEMATICAL MODEL

8.1 Mass-Spring-Damper System of the Disc Brake

The study and prevention of unstable vibrations is very important to the vehicle brakes industry and there is a need for a model that will predict unstable squeal-noise dynamics with reasonable accuracy. Dynamic measurements from systems with dry friction are notoriously difficult to obtain, not only because the data from displacement transducers tend to be very noisy, but also because the system can change significantly with wear on the surface. However, the existence of the traveling waves on the surface of the disc is thought to be relatively easy to confirm, and it is one of the motivations for the present theoretical study.

Current study considers two degrees of freedom (circumferential and transverse) model to describe the rotating mass-spring-damper system of the disc brake (Figure 8.1).

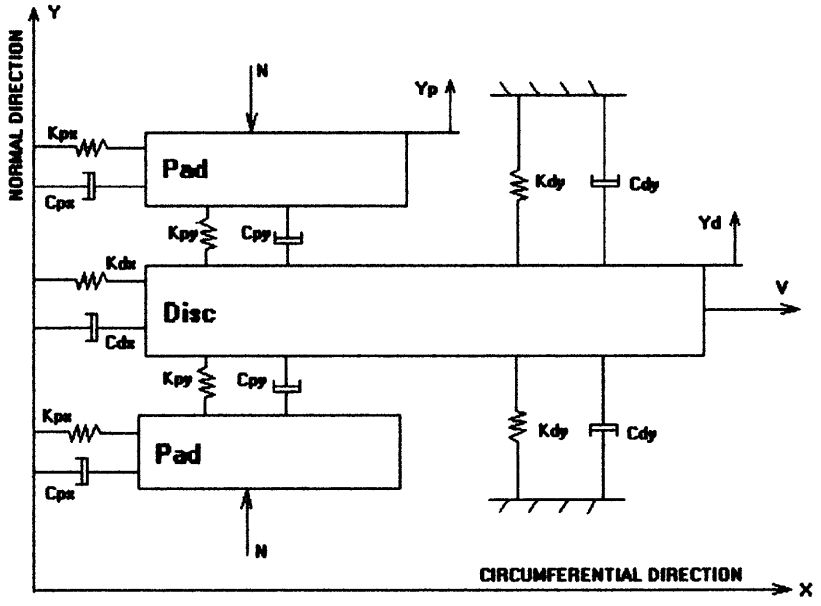

Figure 8.1 Mass-spring-damper system of the disc brake.

Due to the symmetry, it is sufficient to study half-body diagram, consisting of the disc and the upper pad - Figure 8.2.

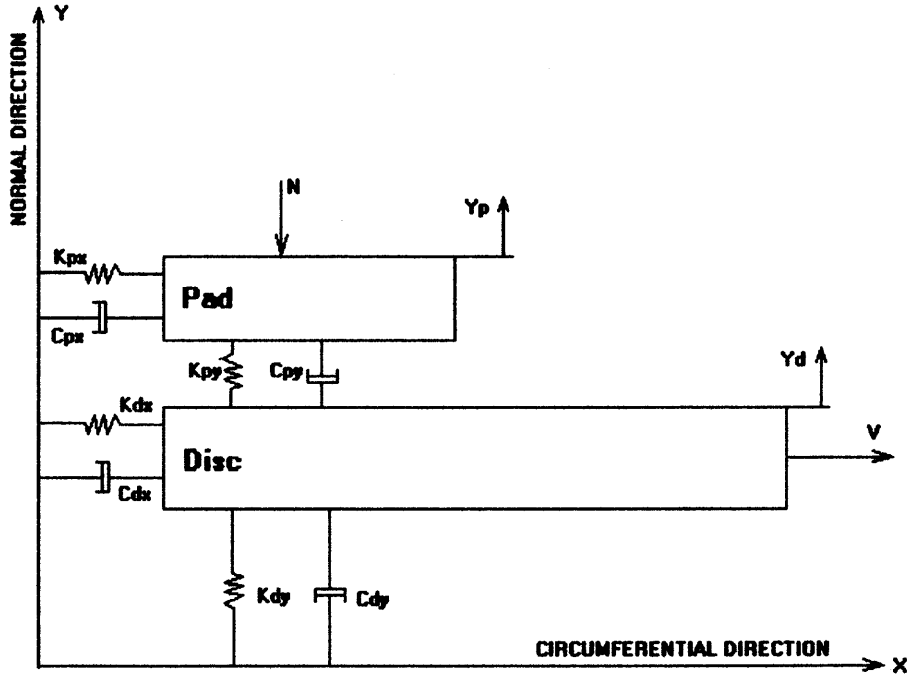

Figure 8.2 Half-body model.

During a brake application, the pad is pressed against the rotor with force N. Material properties of the braking pad surface as well as stiffness and damping of the rotor disc relative to the chassis are the first candidates to be studied when trying to understand the mechanisms responsible for disc squeal. Spring and damper coefficients of the disc and the pad for both normal and circumferential directions are included in the system. Their approximate values are calculated in Chapter 9.

In Figure 8.3 the free body diagram of the disc is presented. The forces that act on the disc surface are the reaction force and the friction force. The same forces but with opposite signs are acting on the bottom surface of the pad.

As shown on the Figure 8.3, the disc, as well as the pad, have a local coordinates

systems attached to them. Therefore, x_d and x_p in [8.1, 8.2], as well as y_d and y_p in [8.3, 8.4] are the deviations of the local coordinate systems of the pad and the disc relative to the global coordinate system of the brake disc assembly. Note that the rotational velocity of the disc V is measured relative to the global coordinate system.

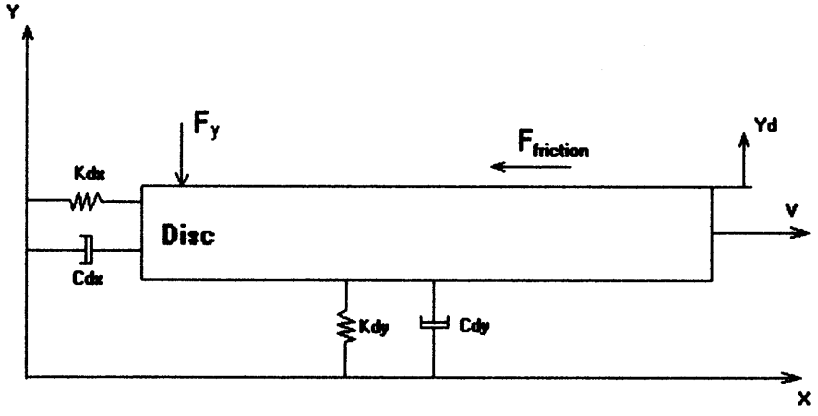

Figure 8.3 Free body diagram of the disc.

System's equations for the circumferential direction of motion:

$$m_d \cdot \ddot{x}_d = -k_{d,x} \cdot x_d - c_{d,x} \cdot \dot{x}_d - F_{friction} \qquad [8.1]$$

$$m_p \cdot \ddot{x}_p = -k_{p,x} \cdot x_p - c_{p,x} \cdot \dot{x}_p + F_{friction} \qquad [8.2]$$

Where:

x_d - Circumferential deviation of the disk from its state of uniform rotation with constant velocity V.

x_p - Circumferential deviation of pad from its initial position before brake application.

$k_{d,x}, c_{d,x}$ - Circumferential stiffness and damping of the disk.

$k_{p,x}, c_{p,x}$ - Circumferential stiffness and damping of the pad.

m_d - The mass of the disk.

m_p - The mass of the pad.

System's equations for the normal direction of motion are:

$$m_d \cdot \ddot{y}_d = -k_{d,y} \cdot y_d - c_{d,y} \cdot \dot{y}_d - F_y \qquad [8.3]$$

$$m_p \cdot \ddot{y}_p = F_y - N \qquad [8.4]$$

Where:

y_d - Deviation of disk from its normal equilibrium position.

y_p - Deviation of pad from its normal equilibrium position.

$k_{d,y}, c_{d,y}$ - Normal stiffness and damping of the disk.

$k_{p,y}, c_{p,y}$ - Normal stiffness and damping of the pad.

N - Normal force acting on the pad.

F_y - Normal force acting on the disk.

V – The velocity of the disk rotation.

Obtaining the equations for F_y and $F_{friction}$:

The normal force N acting on the pad is translated to the disk's surface. The reaction force on the disc surface can be found from the following relation of disk/pad displacements and velocities:

$$F_y = k_{p,y}(y_d - y_p) + c_{p,y}(\dot{y}_d - \dot{y}_p) \qquad [8.5]$$

From the definition of the friction force:

$$F_{friction} = f \cdot F_y \qquad [8.6]$$

In order to take the Stribeck effect into consideration, the friction coefficient has to be velocity-dependant. In the literature different approximations of velocity-

dependant coefficient exist. In this work a relatively simple approximation from Mottershead's paper [12] will be used:

$$f(\upsilon) = f_s(1-\upsilon/15)+0.0002\upsilon^2 \qquad [8.7]$$

For $f_s = 0.1$ a curve displayed in Figure 8.4 can be obtained:

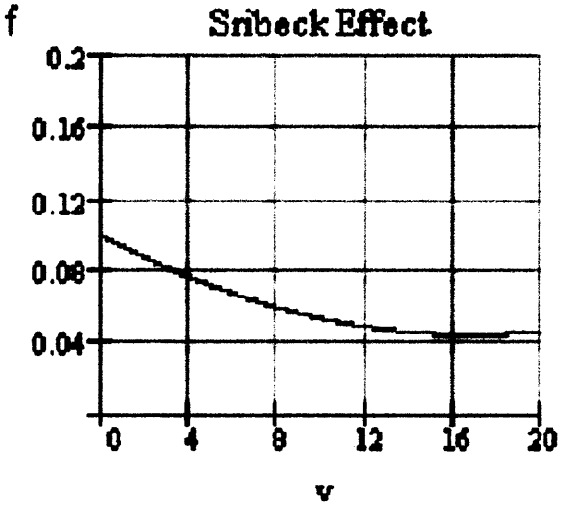

Figure 8.4 Velocity-dependant friction coefficient.

The graph of the velocity-dependant friction coefficient clearly shows that the coefficient of friction changes from 0.1 (equal to f_s) when velocity is zero, to approximately 0.04 when velocity is equal to 16 m/sec. The simulation showed that when the disc rotation velocity is smaller than Uc (16 m/sec) and the Stribeck curve has a negative slope, this may cause instability in the system, while the velocities greater than Uc will never lead to system's instability and therefore, can no be a disc noise source.

The velocity in [8.7] is the disk relative to pad sliding. It can be found from:

$$\upsilon = V + \dot{x}_d - \dot{x}_p \qquad [8.8]$$

8.1 Follower Force Hypothesis

Another factor, apart from the Stribeck effect, that may cause the system to become unstable is the follower force. From definition, the follower force is component of friction force as the result of flexural displacement. The friction force follows the deformed surface of the disc and changes its direction when disc vibrates; therefore follower force acts in direction normal to the sliding plane, which is Y.

The follower force was discussed in at least two papers by Mottershead [10, 11]. The original expression of the follower force given by Mottershead is:

$$F_{follower} = F_{friction} \cdot \frac{dw}{rd\theta} \qquad [8.10]$$

Where dw is the flexural displacement and $rd\theta$ is the circumferential distance, that is the product of disc radius and circumferential angle. Figure 8.5 shows the graphical explanation of the follower force phenomenon.

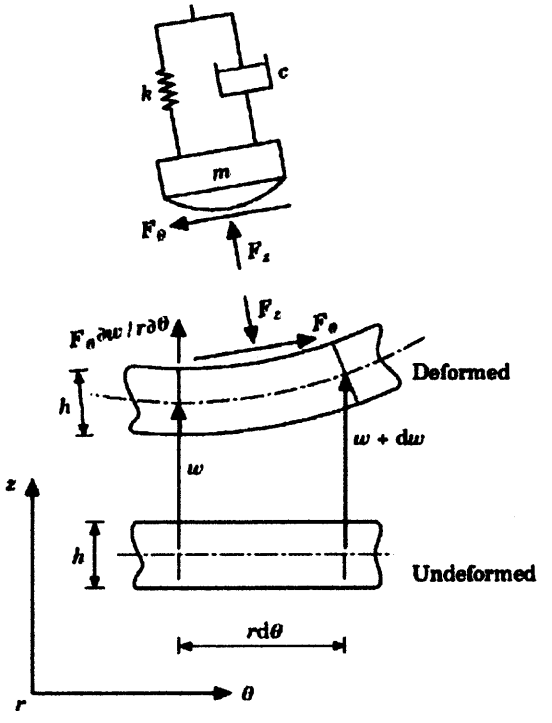

Figure 8.5 Follower force acting on deformed disc surface (Taken from Mottershead and Quyang 1999 [12]).

Our model is too simple to include the follower force representation given in Mottershead's paper in its exact form. It would require considering a system with spatial dependence, namely, force distribution over the disk and pad surfaces. This would result in partial differential equations. The only thing that can be done to consider the follower force in current model is to take an approximate integral version of the follower force, which involves the basic features of the local follower force.

There are two such basic features, which appear from the definition of the follower force. Namely, follower force is the normal component of the friction force appearing in the result of bending (inclination) of the contact surface. Thus, the two basic conclusions following from this definition are:

- The follower force is proportional to the friction force.
- The follower force is proportional to the inclination angle of the bent surface.

Since we consider the normal oscillations as amplitude of a flexural wave, the inclination angle in flexural wave is proportional to the amplitude of the wave y_d. Therefore, in the most general form, follower force may be written as:

$$F_{follower} = \alpha \cdot y_d \cdot F_{friction} \qquad [8.11]$$

Where α is some proportionality coefficient that relates the product of friction force and normal displacement to the follower force. This may be regarded as a phenomenological definition of the follower force similar to the definition of the friction force via product of normal pressure and friction coefficient.

The follower force causes asymmetry in the stiffness of the brake system and therefore it represents a potential destabilizing effect. However, this asymmetry turns out

to be too weak to cause a real instability in the system. According to the definition of the follower force [8.11], the constant alpha has a dimension of inverse distance (1/m).

Therefore, this constant can be expected to have a typical size of ~0.1 (m) and to be equal to ~10 (1/m). The effective stiffness coefficient (proportionality constant to the deformation) related with the follower force is $\alpha \cdot F_f \approx \alpha \cdot N \cdot f \approx 10^3$ while the real disk and pad stiffness coefficients are much larger (~1.e7~1.e9). Therefore, unrealistically large values of alpha are necessary to get a noticeable effect of the follower force on the oscillations.

Consequently, it seems unrealistic to include the follower force effect in a two-dimensional model like the one presented in the paper.

Chapter 11 contains the Simulation Variables Table, which shows all the parameters that were used during simulations. Note that only the last three simulations (38, 39, and 40) have Alpha not equal to zero, meaning that these simulations included follower force effect. It can be also seen from the Figures 16 and 17 in Appendix A that the follower force effect did not cause instability in the system as it could be expected.

CHAPTER 9

PHYSICAL PARAMETERS

According to SAE paper [19] the masses of the disk and the pad are:

$m_d = 1.5kg$ $\qquad$ $m_p = 0.36kg$

To evaluate disk stiffness an inverse approach can be adopted. Namely, it is possible to take the experimentally observed natural frequencies of disk vibrations and use the chosen mass m_d to evaluate the corresponding stiffness. As known, linear frequency of harmonic oscillations is $f = \frac{\sqrt{k/m}}{2\pi}$, or substituting for k_d:

$$k_d = 4m_d(\pi f)^2 \qquad [9.1]$$

We know that frequency of flexural oscillations is about several kHz, while frequency of circumferential oscillations is typically above 5 kHz.

Thus, for $m_d = 1.5kg$ and f=1 kHz the formula results in $k_{d,y} \approx 1.5 \cdot 10^7 [N/m]$.

While for f=5 kHz substituting into [9.1] results in $k_{d,x} \approx 3.7 \cdot 10^8 [N/m]$.

As to the damping constant *c*, then according to the above-mentioned paper, it can be obtained from the real part of the oscillation growth rate, gamma. If oscillation amplitude is written in complex form: $A = e^{\lambda t}$ where λ is complex growth rate and *t* is time, the angular frequency of oscillations is given by the imaginary part of the growth rate, and the real part characterizes the damping or amplification of oscillations gamma: $\gamma = \mathrm{Re}[\lambda]$. Gamma is the inverse of the characteristic time of oscillation damping (the time over which amplitude reduces/grows by e=2.73). The range of gamma is 1-3[1/s].

Since the damping constant c is multiplied by velocity to obtain force, its dimension is [kg/s]. Thus, using simple dimensional arguments it is possible to evaluate the damping coefficient as:

$$c_d = m \cdot \gamma \qquad [9.2]$$

Therefore, for the disk it is possible take c in a range of 1 to 5 [kg/s].

For the pad things are a bit different, because natural frequencies are not well known. However, in this case the approach of the above-mentioned paper [19] can be adopted for direct evaluation of pad stiffness from its Young's modulus E~ 0.8 GPa (according to Mottershead's data) using following formula:

$$k_p = \frac{E \cdot S}{h} \qquad [9.3]$$

Where S is pad contact area and h is its thickness. Taking thickness $1cm$ and contact area $42cm^2$ for $E = 1GPa$ results in $k_{p,y} = 4.2 \cdot 10^9 [N/m]$.

For tangential direction taking into account that the shear modulus $G = \frac{1}{2(1+\nu)}E$ is by a factor of $2(1+\nu) = 2.5$ ($\nu = 0.25$ Poisson ration for pad) smaller than Young's modulus, the pad shearing stiffness can be evaluated as $k_{p,x} = k_{p,y}/2.5 = 1.7 \cdot 10^9 [N/m]$. The real part of pad normal frequency seems to be absolutely unknown. However, it is possible to take it in the range of $\gamma_p = 1 - 10[1/s]$ and to evaluate the damping coefficient similarly as before $c_p = m_p \cdot \gamma_p \approx 0.3 - 3[kg/s]$.

CHAPTER 10

MATLAB AND SIMULINK PROGRAM CODE

For the purpose of current research work, the Matlab and Simulink software seems to be the most appropriate and convenient one. The printout of the program code can be found in Appendix B.

The program code represents an open-loop system describing disc brake system's basic equations and principles [8.1-8.9]. Open-loop system is a system that does not have any feedback or controller responsible for error correction. In the real disc brake system, the only feedback is the pressure on braking pedal: when the driver hears disturbing noise he may reduce the pressure on the pedal. There is no other control system preventing disc squeal in a car yet. In modern cars, the ABS system is often installed. In prevents disc brakes from locking, by reducing the pressure on the pad N, but not from squeal noise.

Program's main page consists of a 'Subsystem' block, the integrator and the measuring tools – scopes and spectral density analyzer (specially made for this purpose). The scopes provide the time-scale measurements of displacements, velocities and other signals. Spectral density analyzer contains a Matlab program inside (see Appendix B).

The spectral analyzer plots the frequency spectrum graph from which it can be seen at what frequencies the high-amplitude noise occurs. Actually, it plots two graphs. The first graph shows the part of the time signal that is being analyzed. The second graph is the frequency spectrum, where the frequency is measured in Hz and amplitude in meters per second square units, or Joule per kilogram units. There are two parameters to define the sample signal in the first window. The first parameter is the sample time,

which is the step by which signal is sampled. It must be short enough to capture the highest relevant frequency in the signal.

The second relevant parameter is the number of point for FFT, which together with the time step defines the length of the time signal to be analyzed.
This sample time must be long enough to contain at least several periods of the relevant lower frequency oscillations. Additional parameter is the number of points after which FFT is repeated. The last parameter is 'Length of Buffer'. Buffer is just as intermediate storage that has to be large enough.

Double-clicking the 'Subsystem' block shows a table with system's parameters, such as stiffness, damping, masses and other coefficients, that can be changed by the user before running the simulation.

Looking under 'Subsystem' mask shows the subsystem block diagram. It consists of two main blocks – 'Tangential' and 'Normal'. The 'Tangential' block is responsible for calculating tangential acceleration, friction force and the flag state. The 'Normal' block calculates flexural acceleration and the normal force F_y acting on the disc. Note that F_y is then transmitted to 'Tangential' block's input, while 'Normal' block uses the friction force output from the 'Tangential' block for the follower force calculation. In this way a real time continuous interaction between this two blocks is achieved.

The system has eight inputs and nine outputs. The ninth output is the flag. The flag indicates the state of the system, whether it is in slip mode, when the disc slides past the pad, or in stick mode, when the pad and the disc move together as a single body.
To define flag's state, there are two test blocks in 'tangential' block– 'slip test' and 'stick test'. The stick test is using a relatively simple criterion: when disc to pad velocity

$\upsilon = V + \dot{x}_d - \dot{x}_p$ becomes zero, the flag state changes to '1' symbolizing stick mode of the system. The stick test is located in the 'Friction' block, where the friction coefficient is calculated. This block has the disc and the pad velocities on its input and calculates the relative velocity v using the above-mentioned formula. This velocity is used in evaluating the velocity-dependant friction coefficient. Stick test is executed by using a single Hit Crossing block, which registers input signal's passing through zero, which changes the output and consequently the flag to "1" value.

When the flag is '0' and the system is in slip mode, the friction coefficient is calculated using Stribeck effect simplified formula, for instance Mottershead's approximation. The Mottershead's formula $f = f_s(1-\upsilon/15)+0.002\upsilon^2$ was rewritten in a more convenient form:

$$f = f_0 + f_1\left[(u-u_c)^2 - u_c^{\,2}\right]^2 / 2u_c \qquad [10.1]$$

Where $f_0 = f_s$, u=v, f_1 is the friction velocity coefficient found to be equal to 1/15 and u_c is equal to 16.7(m/s) when comparing [10.1] equation's coefficients to Mottershead's formula. It is also possible to neglect Stribeck effect, substituting zero f_1 coefficient in 'Subsystem' mask.

The slip test criterion is based on the following principle: total force action on the pad is compared with maximum friction force, as the slip velocity tends to zero. The stick persists as long as the total force on the pad (inertia + elasticity + damping) is smaller then the friction force. During the stick phase, the pad and the disc move together in tangential direction as a solid body. The friction force is equal to the sum of all other

forces acting on the pad, as long as this total does not exceed $f_s \cdot F_y$, which is the criterion for transition to the slip state. Without this, equilibrium stick state would be impossible.

In another word, the friction force serves two purposes. First, during the slip phase, when slip velocity v is nonzero and, consequently $|v| > 0$, the friction force is directed against the slip velocity and therefore, it is multiplied by sign (v) (see the 'friction coefficient' block). In the stick phase defined by v=0, the maximal friction force corresponding to v=0 is needed to detect transition from stick to slip.

The 'normal' block is a relatively straightforward one. It does not contain any sub blocks and it only serves the purpose of calculating $\ddot{y}$ and F_y from $y, \dot{y}$ and F_f.

From formulas [8.3] and [8.4] after dividing both sides of the equation by *m*, it is possible to obtain $\ddot{y}$ for both the disc and the pad.

The 'Tangential' block, calculating the tangential acceleration of the disc and the pad using formulas [8.1, 8.2], the friction force and the flag state, is more complicated then the 'normal' block. It contains several sub blocks discussed earlier ('Slip Test', 'Friction & Stick Test', 'Friction Coefficient' and 'Stribeck Effect'). It also contains three switches separating slip and stick modes. The threshold on every switch is 0.5 ('1' represents stick mode and '0' is for slip mode).

CHAPTER 11

SIMULATING WITH DIFFERENT PARAMETERS

As it was stated before, the purpose of this work is to study the influence of system's parameters on disc squeal development. The simulation variables such as wheel velocity, pad pressure force, damping, friction coefficients and alpha (follower force constant) were changed from one simulation to another in order to learn about system's behavior.

In course of simulations, it is logical to start with the simplest case and then to advance to more complicated ones. At the last stages all the physical effects such as Stribeck effect, the follower force and the stick-slip friction were included in the simulation.

Simulation results are illustrated with two types of graphs: time-scale and frequency power spectrum. Each set of variables from Table 11.1 is represented by three graphs. The first graph is the time scale representation of disc's normal and tangential velocities. The second graph is the power spectrum of the normal disc oscillations. The third graph is the power spectrum of the tangential disc oscillations.

The reason the velocities graph is used is that from the spectral point of view it is not important whether to plot displacements or velocities, but velocities contain no permanent signal, which is not the case for displacements. Namely, for displacements there will be also signal at zero velocity. For example, friction force causes some mean tangential deformation of the disk. Thus, displacement oscillations will not occur about zero level, which is the initial undeformed state, but rather about some permanent nonzero deformed state. After decay of initial oscillations, which is the case when the

system has enough damping, the application of braking force results in some steady non-zero deformations (offset of the equilibrium state). Conversely, velocity oscillations always occur around zero level, because in all cases equilibrium state, regardless whether it is undeformed or deformed, corresponds to the zero equilibrium velocity. As to the squeal, it is caused by vibrations rather than by the steady part of the deformation. Therefore, this steady part of the displacement is not important.

Below is the computer simulation variables table. The Table 11.1 contains 40 sets of variables describing mathematical model's behavior. Of course, many other variable values were tried while running the computer simulation, but these 40 sets are chosen to be the characterizing ones.

Among those 40 sets another 16 sets were picked to be included in the thesis print-up. The 'Figure' column contains the numbers of these figures, which can also be found in Appendix A. The values of variables are also printed on each figure for convenience.

Simulations 1-5 are representing the case when a static disc is being excited by the pad force application. Simulations 6-14 neglect velocity dependent friction and the follower force and concentrate on disc/pad damping values. Simulations 15-20 study the influence of the variable force and wheel rotation velocity on systems stability, read conclusions to find out how exactly this parameters affect the system. Simulations 21-37 are the most essential ones, most of the conclusions made about the model are based on these simulations and have to do with the damping values and the Stribeck effect influence.

Table 11.1 Simulation Variables Table

Num	Alpha	V	N	f1	f0	Uc	Cdx	Cpx	Cdy	Cpy	Figure
1	0	0	500	0	0.5	16.7	0	0	0	0	1
2	0	0	500	0	0.5	16.7	0	0	10	0	2
3	0	0	500	0	0.5	16.7	0	0	1	0	
4	0	0	500	0	0.5	16.7	0	0	10	10	
5	0	0	500	0	0.5	16.7	0	0	0	10	3
6	0	1	500	0	0.5	16.7	0	0	0	0	4
7	0	1	500	0	0.5	16.7	0	0	10	0	
8	0	1	500	0	0.5	16.7	0	0	100	0	5
9	0	1	500	0	0.5	16.7	1	0	0	0	
10	0	1	500	0	0.5	16.7	10	0	0	0	6
11	0	1	500	0	0.5	16.7	100	0	0	0	
12	0	1	500	0	0.5	16.7	10	10	0	0	7
13	0	1	500	0	0.5	16.7	10	10	0	10	
14	0	1	500	0	0.5	16.7	10	10	10	10	
15	0	1	500	0.06	0.5	16.7	0	0	0	0	
16	0	10	500	0.06	0.5	16.7	0	0	0	0	8
17	0	20	500	0.06	0.5	16.7	0	0	0	0	9
18	0	1	2000	0.06	0.5	16.7	0	0	0	0	10
19	0	10	2000	0.06	0.5	16.7	0	0	0	0	
20	0	20	2000	0.06	0.5	16.7	0	0	0	0	
21	0	1	500	0.06	0.5	16.7	0	0	10	0	
22	0	1	500	0.06	0.5	16.7	0	0	100	0	
23	0	1	500	0.06	0.5	16.7	10	0	0	0	
24	0	1	500	0.06	0.5	16.7	10	10	0	0	
25	0	1	500	0.06	0.5	16.7	100	0	0	0	11
26	0	1	500	0.06	0.5	16.7	100	100	0	0	12
27	0	1	500	0.06	0.5	16.7	0	1	0	0	
28	0	1	500	0.06	0.5	16.7	0	10	0	0	
29	0	1	500	0.06	0.5	16.7	0	100	0	0	
30	0	1	500	0.06	0.5	16.7	1	100	0	0	
31	0	1	500	0.06	0.5	16.7	10	100	0	0	
32	0	1	500	0.06	0.5	16.7	100	100	0	0	
33	0	1	500	0.06	0.5	16.7	100	100	10	0	
34	0	1	500	0.06	0.5	16.7	100	100	100	0	
35	0	1	500	0.06	0.5	16.7	100	100	100	10	
36	0	1	500	0.06	0.5	16.7	100	100	100	100	13
37	0	1	500	0.06	0.5	16.7	0	100	100	100	14
38	-1000	1	500	0.06	0.5	16.7	0	100	100	100	15
39	-10000	1	500	0.06	0.5	16.7	0	100	100	100	
40	-1E+05	1	500	0.06	0.5	16.7	0	100	100	100	16

CHAPTER 12

SIMULATION RESULTS

In order to study system's behavior, it is more convenient to start with the most simplified cases and gradually increase the level of complexity. The first simulation (Appendix A, Figure 1) considers a static system V=0 that is being activated by normal force application N=500. The Stribeck effect, follower force and system's damping are neglected: Alpha=0, fl=0, Cdx=Cpx=Cdy=Cpy=0. Looking at time-scale disc velocity plot (Figure 1a), there are harmonic oscillations in normal direction and no oscillations in tangential direction, as it should be expected. The frequency spectrum for the normal oscillations shows a peak amplitude signal of 0.7 $[J/kg]$ at around 450 Hz frequency.

Therefore, in this case pad hits the disk and excites purely normal oscillations (there are no tangential oscillations excited because there is no friction force when disk is not rotating). Normal oscillations contain two frequencies that are just the natural frequencies of the disk and pad where the latter is considerably higher. In addition, it is visible that the amplitude of pad is much smaller than that of the disk. It means that the pad being much stiffer with respect to normal compression/extension than the disk with respect to the normal bending effectively oscillates together with disk as a solid body exercising only small-amplitude and high frequency oscillations with its natural frequency.

The next step is to add normal damping (Cdy and Cpy). The damping does not change the natural frequency of oscillations, but reduces their amplitude. The Figure 2c

represents the case when Cdy=10 is added, here the peak amplitude is 0.4[J/kg]. In contrast to the previous case, oscillations now become decaying, though the effect of disk damping is much stronger than that of the pad because the later is effectively oscillating as solid body without significant deformations and therefore it does not experience damping which is proportional to the deformation speed.

The next step is to add some rotational velocity to the system V=1[m/sec]. Note that tangential oscillations are exited only when the disk is rotating and there is nonzero friction acting. In this case the oscillations with at least two natural frequencies can be observed. In addition to the natural tangential frequencies, there also appear normal oscillations frequencies, because of the friction force, which is varied by the oscillations of the normal pressure N. Thus, normal oscillations induce additional tangential ones by modifying the friction force through the normal pressure variations. All these oscillations are decaying sooner or later depending on the damping coefficients. Thus there is no squeal.

The third step of experiment is to activate the Stribeck effect. In order to take Stribeck effect into consideration, f1 has to be changed to 0.06 value as it was calculated earlier. In this case, growing tangential oscillations can appear. First of all, this requires rotation speed to be low enough (smaller than Uc) see Figure 8.

For rotation speeds larger than Uc, tangential oscillations are always decaying (Figure 9). When tangential oscillations are unstable, they grow until stick-slip effect sets in that limits further increase of oscillations. It means that in the velocity of unstable tangential oscillations attain the speed disk rotation where they become limited by stick/slip. Instability can be suppressed by increasing tangential damping coefficients.

Depending on the magnitude of damping coefficients, it can happen that unstable tangential oscillations develop for both the disk and pad or only one of them, if one coefficient is larger ant other is smaller than the critical, or none of them, if both damping coefficients are large enough.

Increasing normal brake pressure also enhances the instability. Comparing Figure 10 where N=2000 with the analogous simulation (same velocity and damping coefficients) with N=500, both the time-scale graph and the power spectrum plot point at significant instability increase for the first case.

The last step is to include the follower force, in other words to define Alpha (Figures 15, 16). Here it is necessary to use some guesswork, because the only thing known about Alpha is that it has to be negative value. After running the simulation with different values of Alpha, it became clear that follower force is too weak to influence the oscillations. Actually, the system is very stiff and the unrealistically large values of the follower force constant is needed in order the follower force to become comparable to the dominating elastic forces. See Conclusions for the complete simulation results analysis.

CHAPTER 13

CONCLUSIONS

Probably the main result is that unstable tangential oscillations can develop in the brake system due to the unstable Stribeck effect. Critical parameter for this instability is the wheel rotation speed V. This instability can develop only when the rotation speed becomes smaller than some critical threshold velocity Uc, in current case it was equal to 16.7 [m/s].

When the rotation speed is lower than critical threshold, tangential vibrations can develop depending on tangential damping and on the normal pressure N. Increased damping has a stabilizing effect, whereas increased friction destabilizes tangential oscillations. Note that this instability never develops when the rotation speed is higher than the critical threshold Uc.

This conclusion can be explained by the following argument. Friction force acting from pad to the disk is: $F = -F_y \cdot f(V + d\dot{x})$ where $d\dot{x} = \dot{x}_d - \dot{x}_p$ is the velocity difference between the disk and pad oscillations. In the equilibrium state, when there are no oscillations, $F_y = N$ (normal pressure force is transferred from the pad to the disk without changes). On the other hand, in the equilibrium $d\dot{x}$ =0, because both $\dot{x}_d$ =0 and $\dot{x}_p$ =0. Further let's consider a small deviation from this equilibrium, when $d\dot{x}$ is nonzero but still small compared to the rotation speed. Using Taylor series expansion: $f(V + d\dot{x}) = f(V) + f'(V)d\dot{x} + O(d\dot{x})^2$ where f (V) is the equilibrium value of the friction coefficient at the sliding velocity V, and f' (V) is the derivative of the friction

coefficient with respect to the velocity at the sliding velocity V. $O(d\dot{x})^2$ are second order terms, which are much smaller than the first two terms when the velocity difference is small, which is the case under consideration here. Thus, for small perturbations of the sliding velocity the Stribeck effect results in the additional friction force which proportional to the perturbation of the sliding velocity.

On the other hand, there already is such a force in the equations, which is proportional to the velocity through the damping coefficients C. From current simulations, application of damping results in decay of oscillations. Thus, Stribeck effect is expected to have a similar influence on the oscillations. We can call this damping coming from Stribeck effect "effective damping". However, Stribeck effect is different from the normal damping in one important way, namely, the sign of the effective damping coefficient depends on the sign of the derivative f ' (V). Thus, if the sliding velocity is sufficiently slow, and the friction coefficient decreases with increasing velocity (in other words the fiction coefficient graph Figure 8.4 has a negative slope) then f ' (V) is negative, which means that the sign of damping associated with Stribeck effect is opposite to the normal damping Cx. Consequently, in this case Stribeck effect will cause oscillation amplification, namely, instability, rather than damping of the oscillations.

Only for sufficiently large velocities, where the effective friction coefficient increases with velocity and the f (V) graph is having a positive slope (f ' (V) > 0), the Stribeck effect damping force will act like a normal damping with positive coefficient suppressing the oscillations. Actually, system stability will depend on the total damping coefficient, which is the sum of the physical damping and the damping due to the

Stribect effect with effective damping coefficient N*f ' (V) (proportionality coefficient at the velocity). Of course, all these assumptions refer only to system's stability in tangential direction, the fact that tangential oscillations can cause flexural ones will be discussed later in the text.

For a system to be stable the resulting damping coefficient must be positive:

$$Cx + N^{*}f'(V) > 0 \qquad [12.1]$$

Thus, at low velocities with f ' (V) < 0, increase of brake pressure N always reduces the effective damping and can drive system to instability, provided that physical damping is not large enough. On the other hand, the increase of physical damping always increases stability. At large velocities with f ' (V) > 0, damping is always positive and there is no instability, no matter how large is the pad normal force N.

Note that at small sliding velocities f ' (0) = -fl = -1 /15 according to Motteshead's formula. The application of a typical normal brake force that is equal to N=500-2000 (N) would result in destabilizing damping coefficient of N*f ' (0) ~30-100, that considerably exceeds previously made estimates of physical damping coefficients for the disk and the pad. Thus, a considerable addition may be required to suppress the instability related with Stribeck effect.

In the case of the instability, tangential oscillations increase until stick/slip effect sets in. This happens when velocity of tangential oscillations reaches the velocity of disk's rotation. In this way the stick/slip effect actually limits the amplitude of unstable oscillations which otherwise would grow unbounded in current model. Note that for velocity of V=1 [m/s] and at high frequency of oscillations (about 5 kHz) the amplitude of harmonic oscillations is still relatively small: $a = V / 2\pi f \approx 0.003(mm)$

It is interesting to note that in case of absent or small physical damping of the disk and the pad the unstable oscillations start to develop for both friction couple elements, but despite of the identical negative damping acting on the disk and the pad as a result of Stribeck effect, pad oscillations develop faster, because the pad has smaller inertia than the disk. Thus, the velocity of the pad oscillations reaches the velocity of disk rotation first and the slip/stick oscillations set in so limiting further increase of pad oscillations.

An interesting effect takes place at this point. Namely, the disk oscillations start to decay rather than increase. Therefore, the pad oscillating with much higher natural frequency while experiencing stick/slip transitions suppresses unstable disk oscillations. This seems to be an unobvious effect related to non-linear stick/slip oscillations of the pad, which deserve an additional study.

Even more interesting things happen when trying to stabilize tangential pad oscillations by adding more damping to the pad. It is indeed possible to suppress pad oscillations in this way, however at the price of destabilizing disk oscillations. Thus, increased pad damping can have an adverse of effect on the disk stability. In order to stabilize the disk itself, much more additional damping is necessary. Therefore, allowing unstable pad oscillations may be a way to avoid the development of disk oscillations.

If the follower force mechanism is not included, then the tangential oscillations do not influence normal ones. Thus, without the follower force, normal oscillations always decay according to their damping coefficients, regardless of the development of tangential oscillations. Note that normal oscillations do influence the tangential ones through the variation of normal force Fy. As a result, it is possible to observe frequencies of normal oscillations in the spectra of tangential ones, but not the other way.

The most valuable conclusions obtained from current simulation are:

- Unstable tangential oscillations can develop in the brake system due to the unstable Stribeck effect.
- Normal oscillations do influence the tangential ones through the variation of normal force Fy.
- Tangential instability never develops in the system when the rotation speed is higher than the critical threshold Uc.
- When the rotation speed is below the critical level the unstable tangential oscillations may arise, especially when braking pad pressure N is high.
- Stick/slip effect actually limits the amplitude of unstable oscillations.
- Decreasing pad's damping may stabilize disc's unbounded vibrations.
- The follower force effect is not sufficient to enable the coupling mechanism between tangential and normal oscillations.
- Tangential oscillations do not influence normal ones.

APPENDIX A

SIMULATION FIGURES

Appendix A contains the simulation figures referring to the parameter sets from Table 11.1. Each parameter set is represented by three figures: the time-scale graph of tangential and normal vibrations (Figures 1a-16a), the tangential frequency power spectrum (Figures 1b-16b) and the normal frequency power spectrum (Figures 1c-16c). On top of each graph the values of simulation parameters are shown.

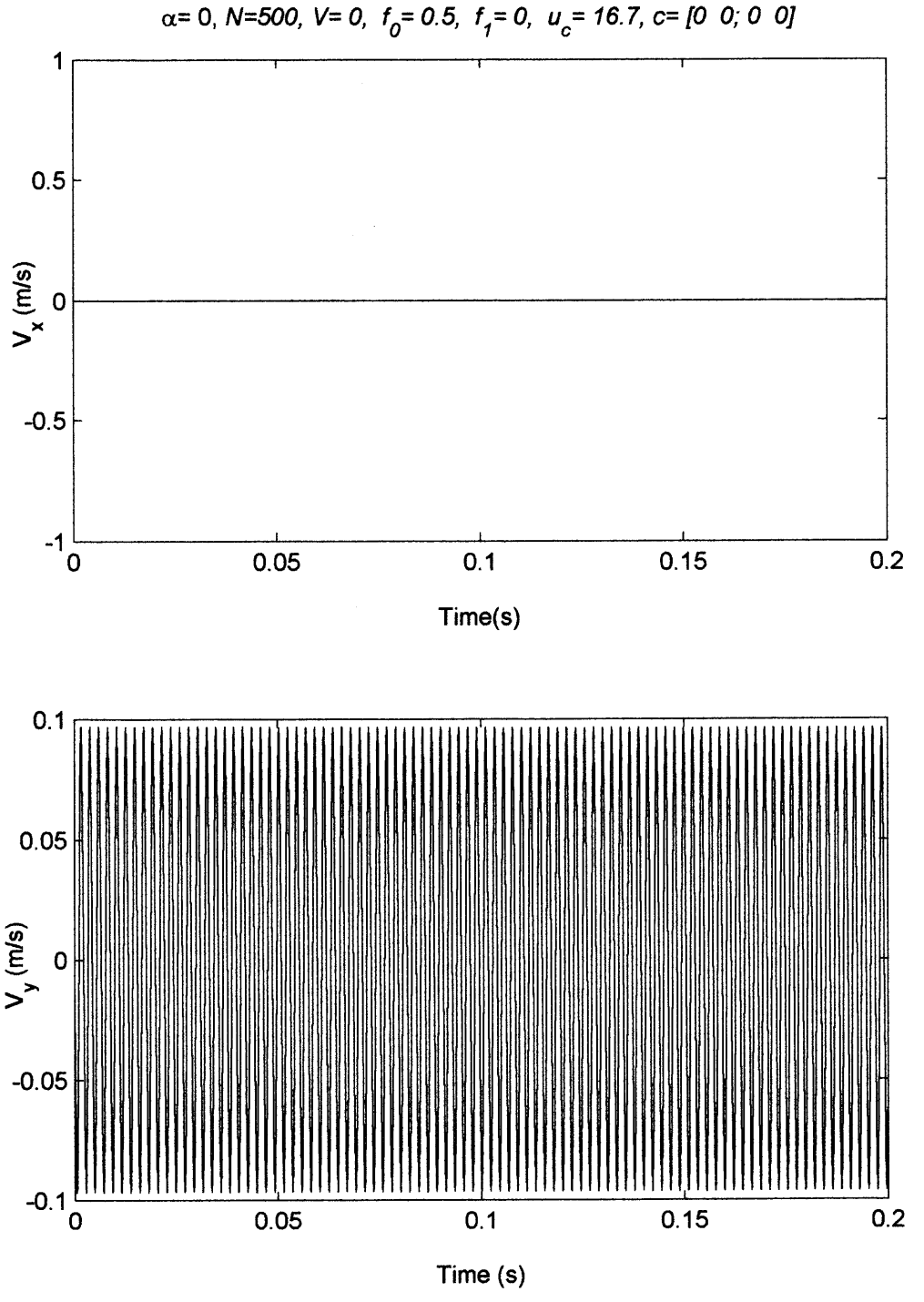

Figure 1a

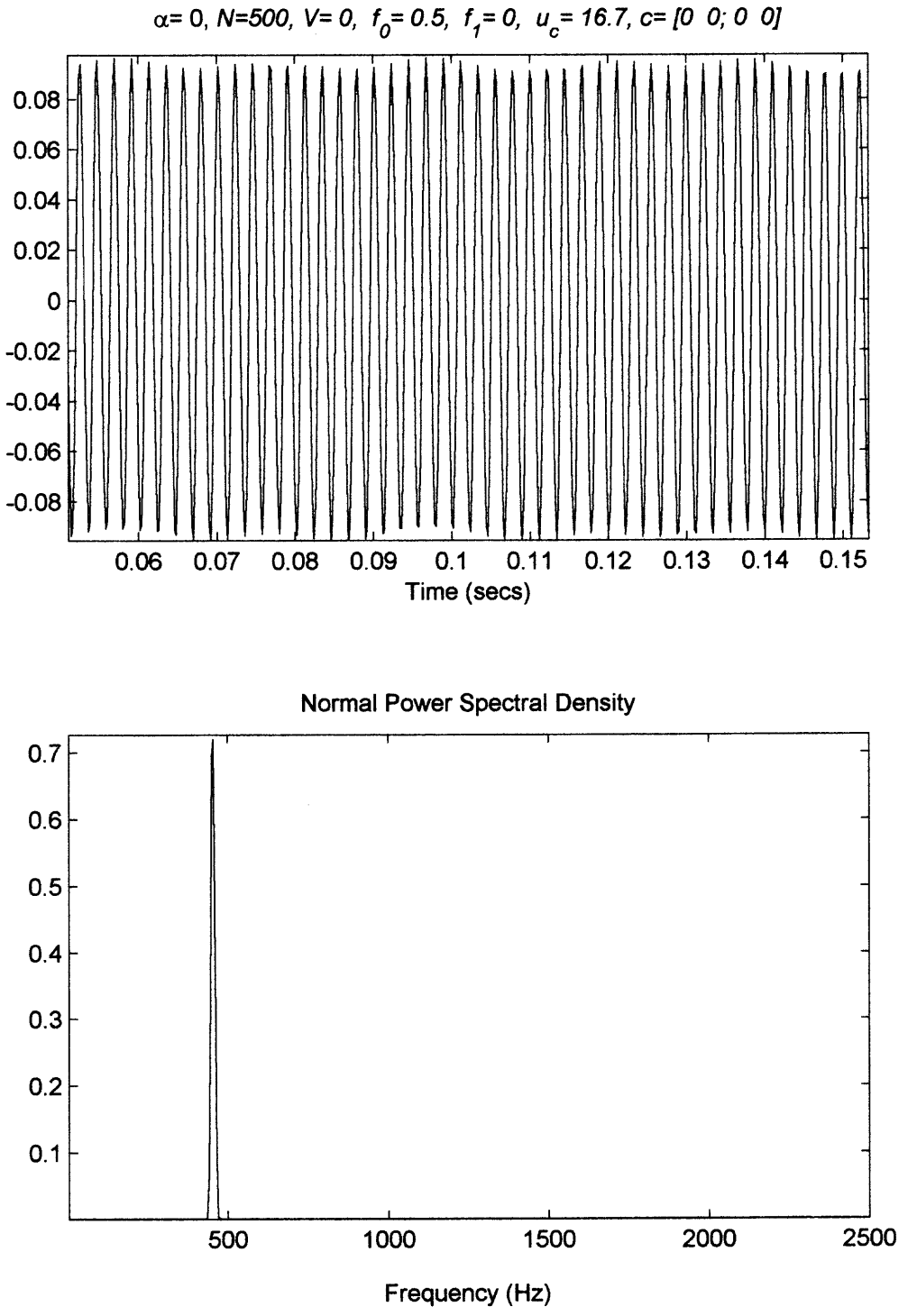
α= 0, N=500, V= 0, f0= 0.5, f1= 0, uc= 16.7, c= [0 0; 0 0]
0.08
0.06
0.04
0.02
0
-0.02
-0.04
-0.06
-0.08
0.06 0.07 0.08 0.09 0.1 0.11 0.12 0.13 0.14 0.15
Time (secs)
Normal Power Spectral Density
0.7
0.6
0.5
0.4
0.3
0.2
0.1
500 1000 1500 2000 2500
Frequency (Hz)

Figure 1c

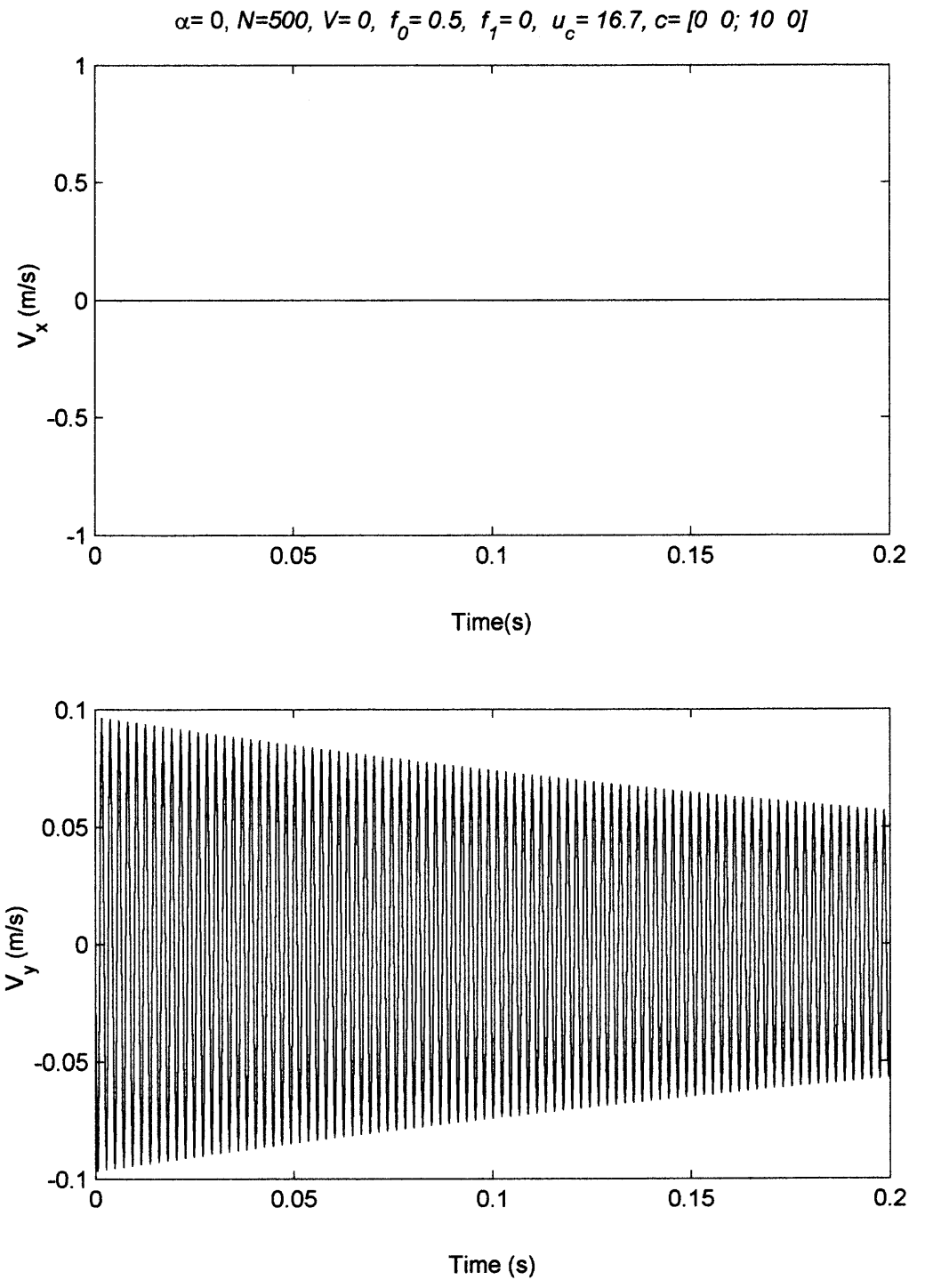

Figure 2a

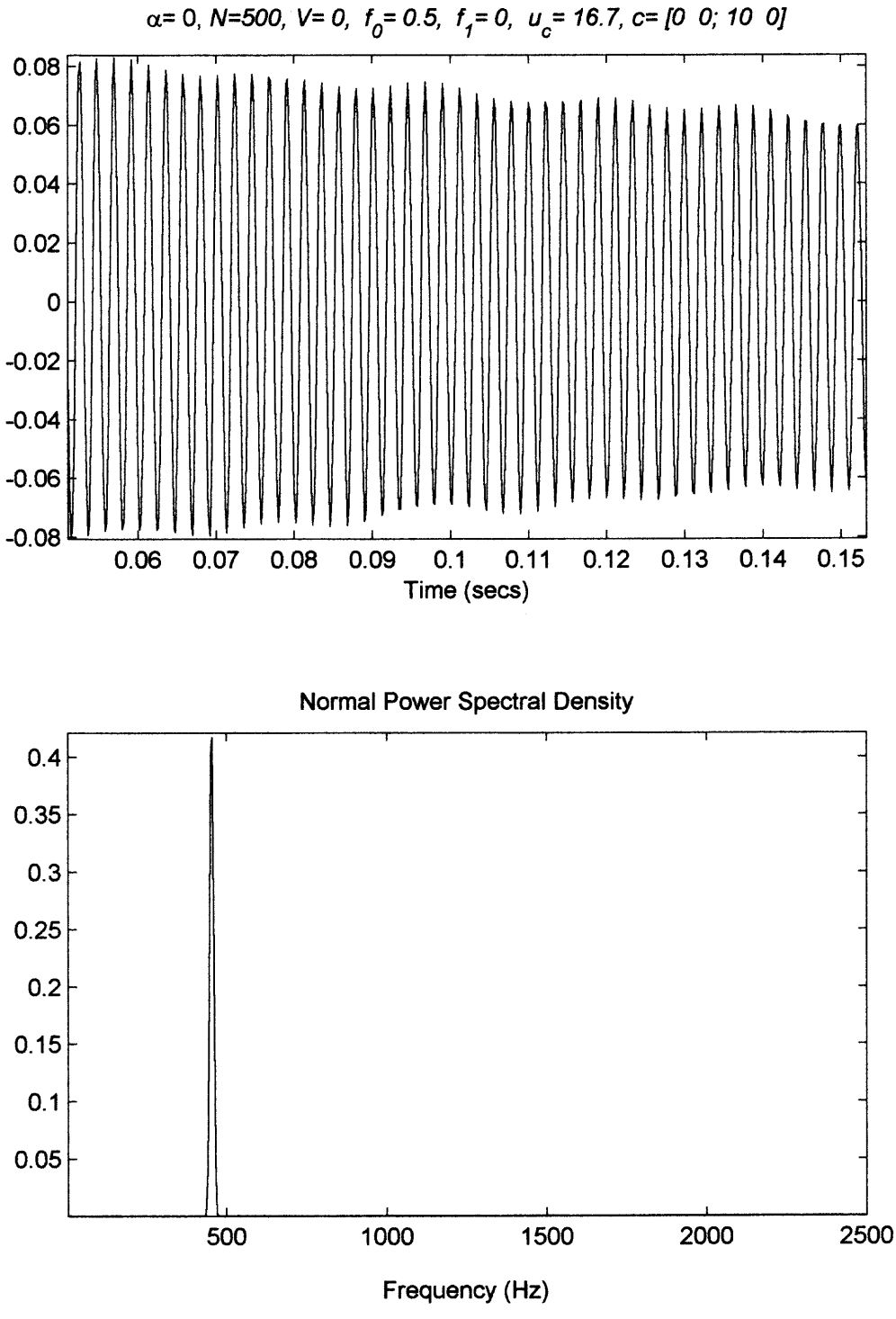
α= 0, N=500, V= 0, f0= 0.5, f1= 0, uc= 16.7, c= [0 0; 10 0]
0.08
0.06
0.04
0.02
0
-0.02
-0.04
-0.06
-0.08
0.06 0.07 0.08 0.09 0.1 0.11 0.12 0.13 0.14 0.15
Time (secs)
Normal Power Spectral Density
0.4
0.35
0.3
0.25
0.2
0.15
0.1
0.05
500 1000 1500 2000 2500
Frequency (Hz)

Figure 2c

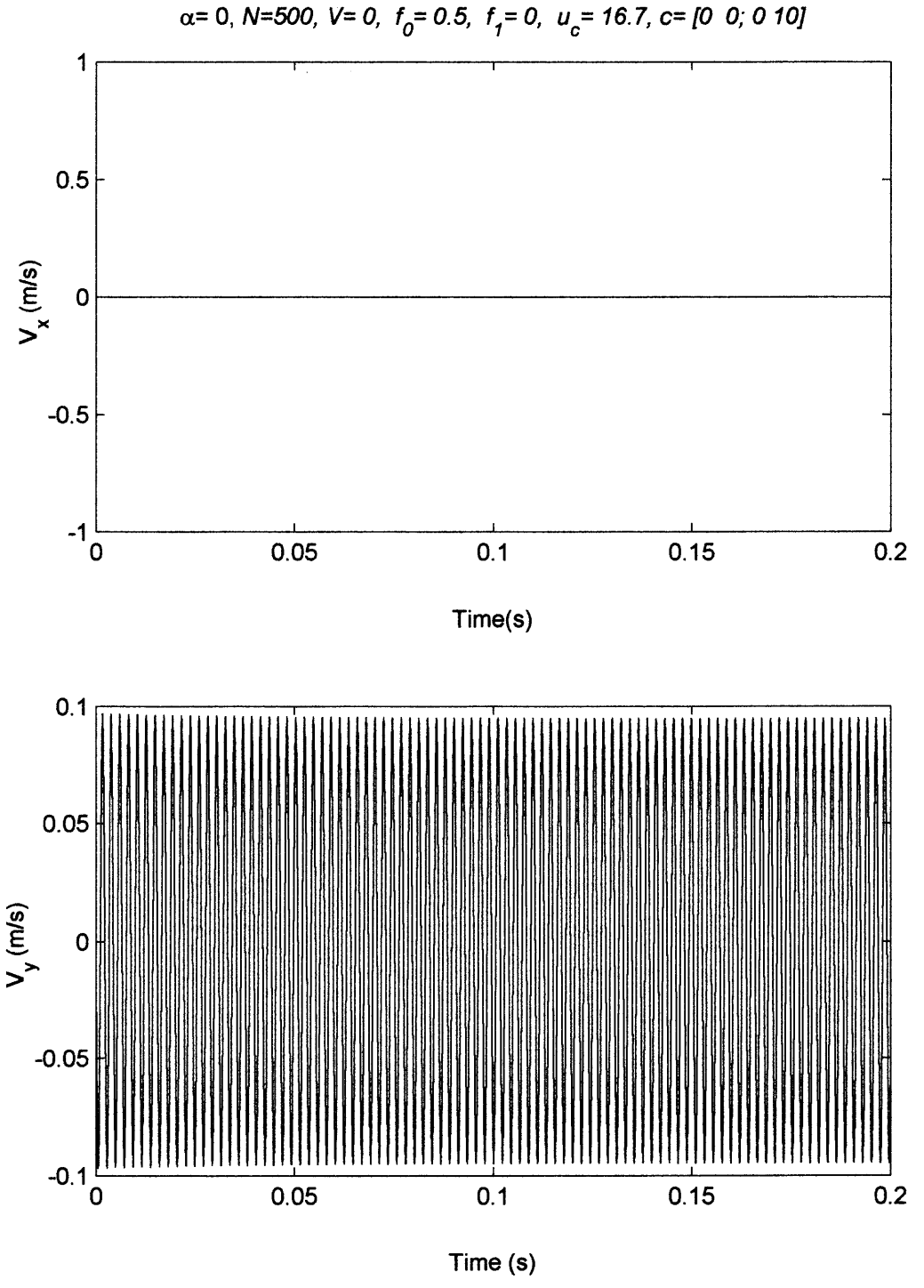

Figure 3a

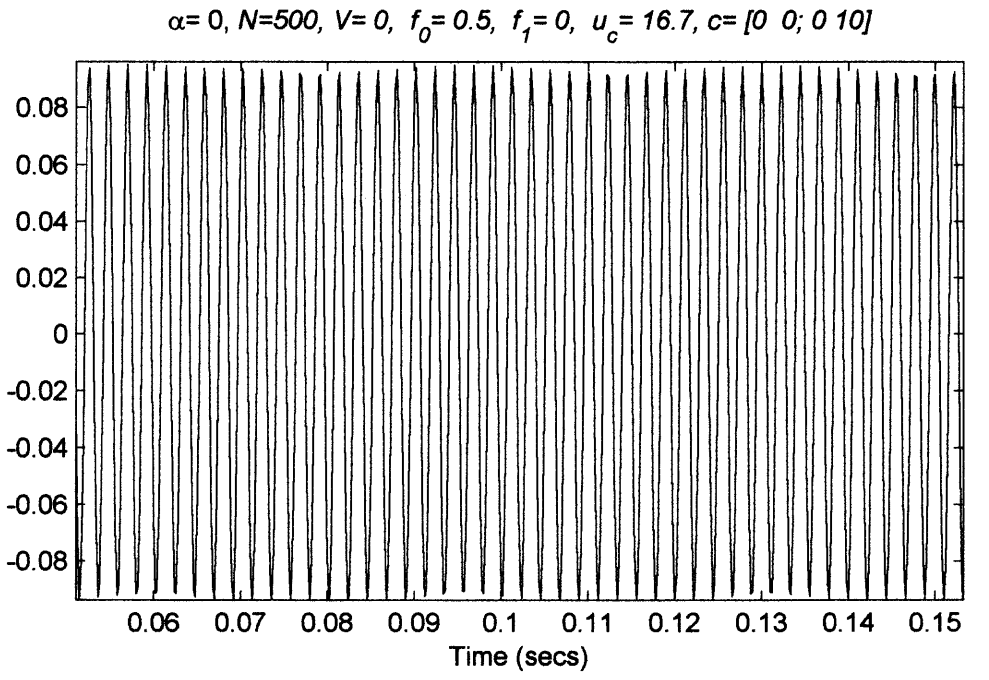
α= 0, N=500, V= 0, f0= 0.5, f1= 0, uc= 16.7, c= [0 0; 0 10]
0.08
0.06
0.04
0.02
0
-0.02
-0.04
-0.06
-0.08
0.06 0.07 0.08 0.09 0.1 0.11 0.12 0.13 0.14 0.15
Time (secs)

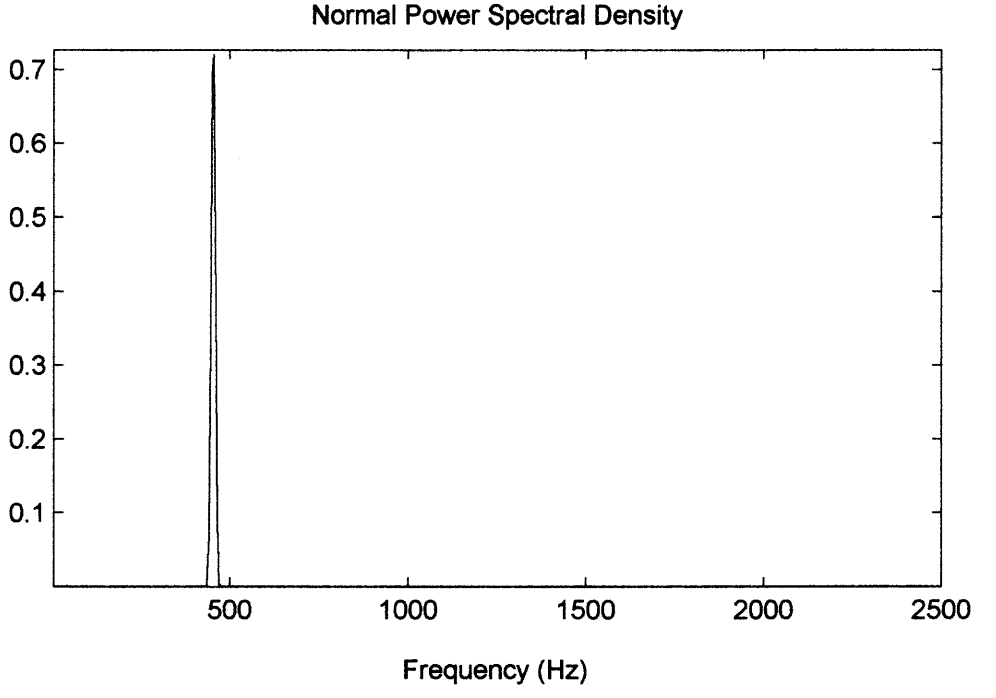
Normal Power Spectral Density
0.7
0.6
0.5
0.4
0.3
0.2
0.1
500 1000 1500 2000 2500
Frequency (Hz)

Figure 3c

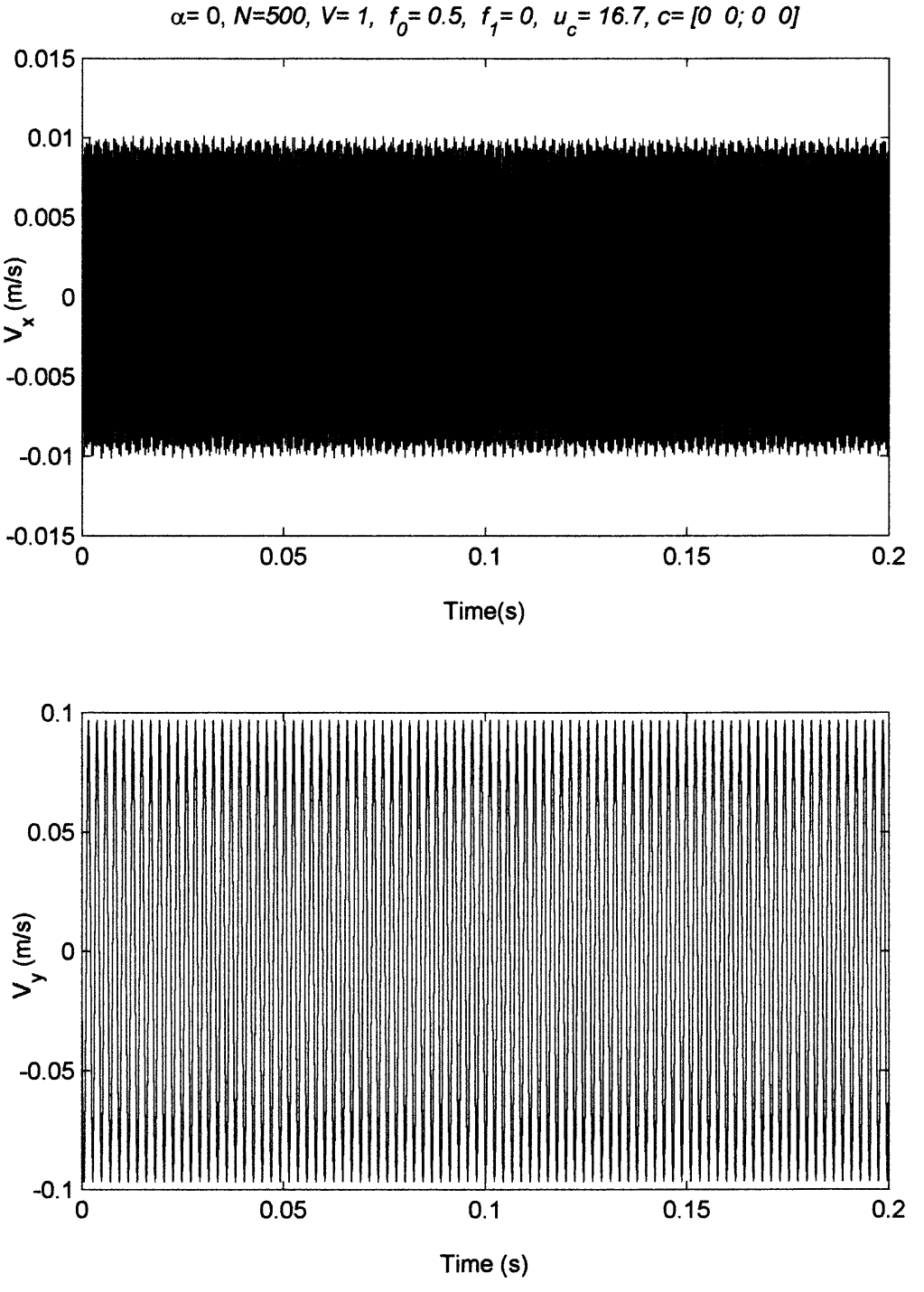
α= 0, N=500, V= 1, f0= 0.5, f1= 0, uc= 16.7, c= [0 0; 0 0]
0.015
0.01
0.005
0
-0.005
-0.01
-0.015
Vx (m/s)
0
0.05
0.1
0.15
0.2
Time(s)
0.1
0.05
0
-0.05
-0.1
Vy (m/s)
0
0.05
0.1
0.15
0.2
Time (s)

Figure 4a

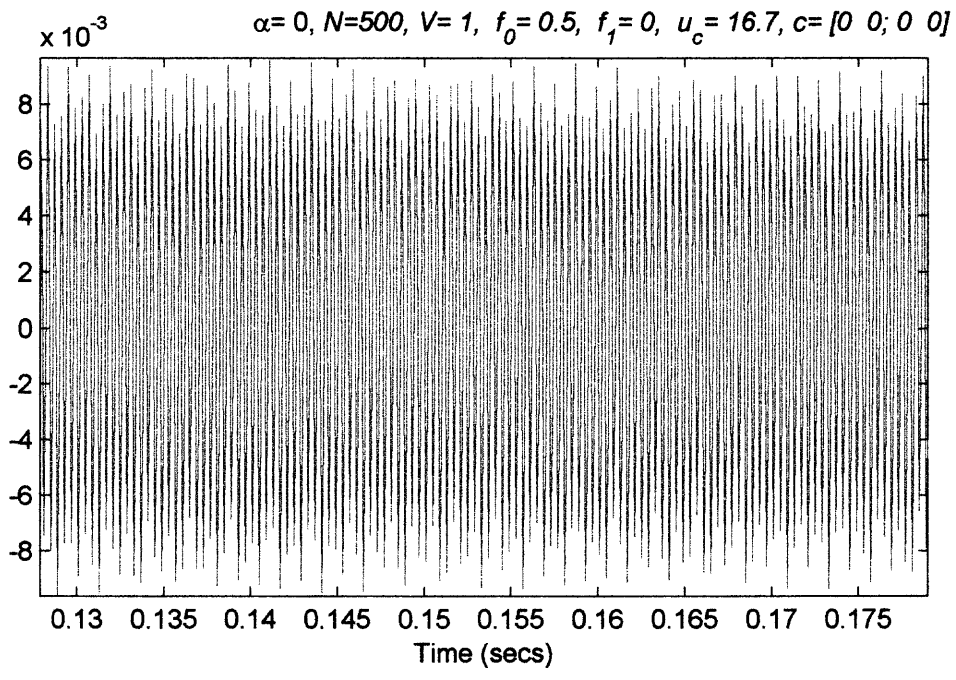
α= 0, N=500, V= 1, f0= 0.5, f1= 0, uc= 16.7, c= [0 0; 0 0]
x 10-3
8
6
4
2
0
-2
-4
-6
-8
0.13 0.135 0.14 0.145 0.15 0.155 0.16 0.165 0.17 0.175
Time (secs)

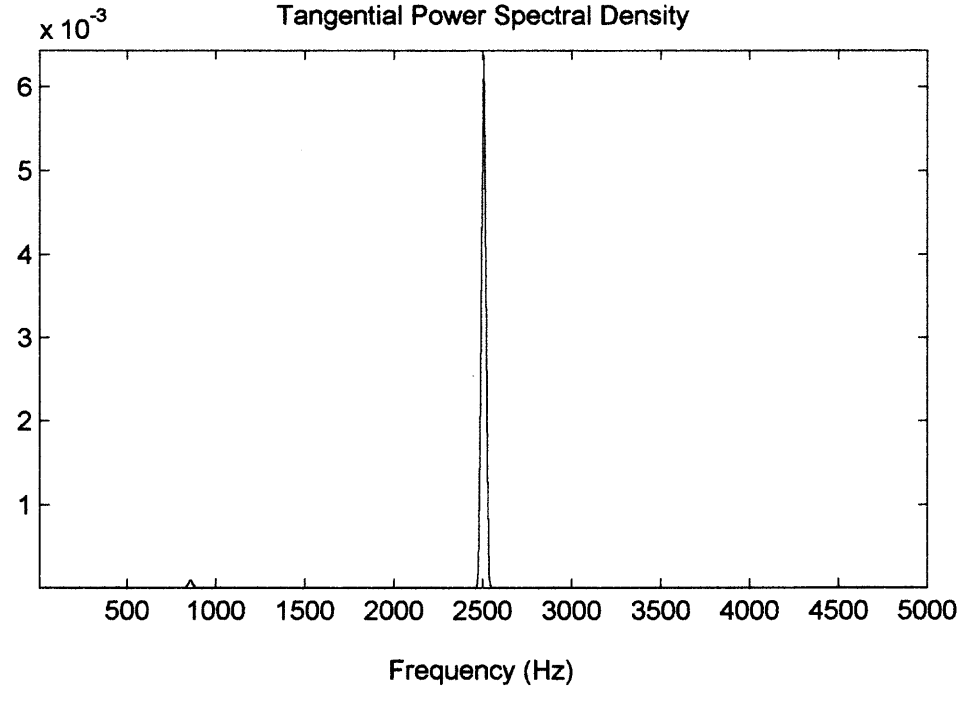
Tangential Power Spectral Density
x 10-3
6
5
4
3
2
1
500 1000 1500 2000 2500 3000 3500 4000 4500 5000
Frequency (Hz)

Figure 4b

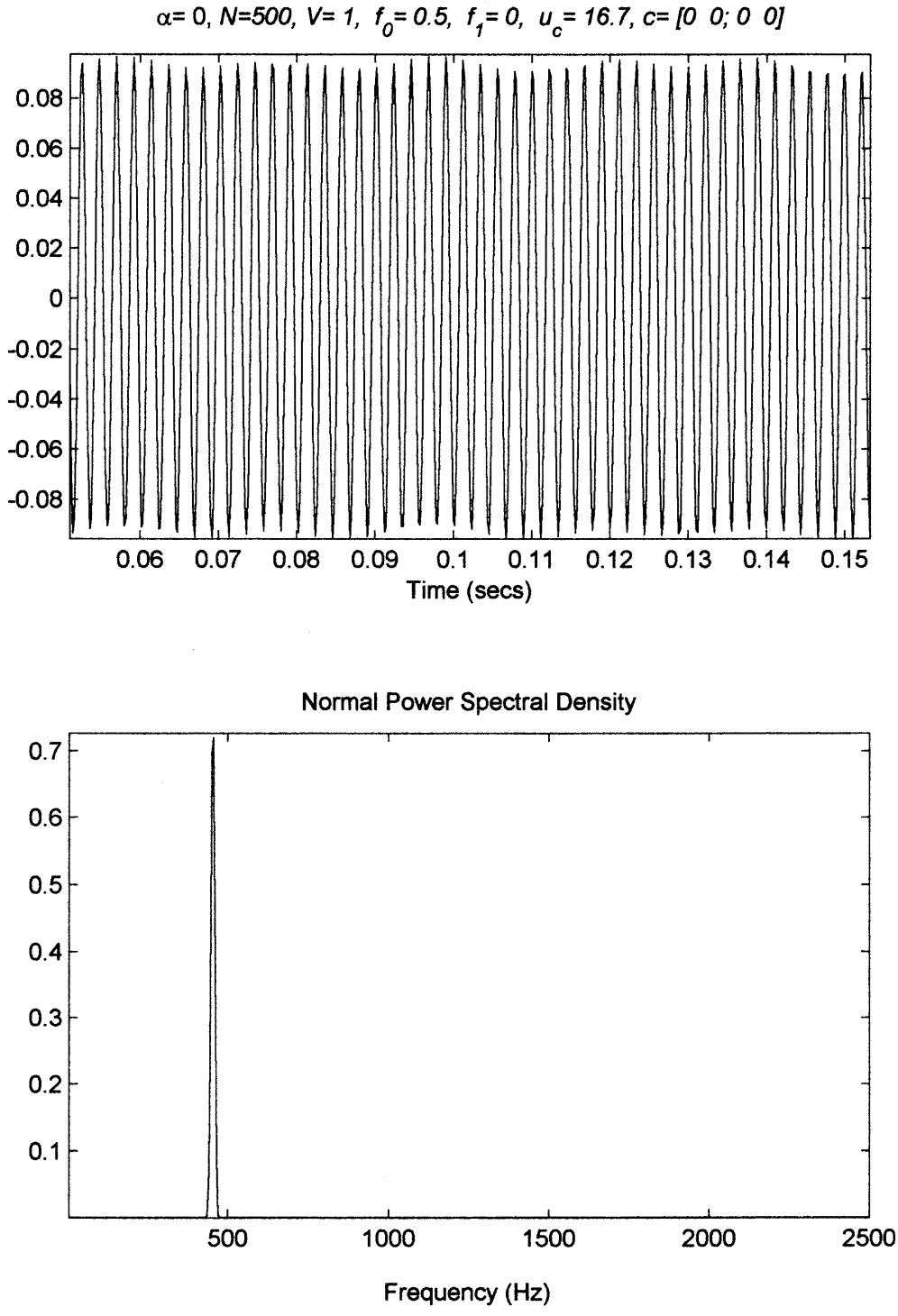
α= 0, N=500, V= 1, f0= 0.5, f1= 0, uc= 16.7, c= [0 0; 0 0]
0.08
0.06
0.04
0.02
0
-0.02
-0.04
-0.06
-0.08
0.06 0.07 0.08 0.09 0.1 0.11 0.12 0.13 0.14 0.15
Time (secs)
Normal Power Spectral Density
0.7
0.6
0.5
0.4
0.3
0.2
0.1
500 1000 1500 2000 2500
Frequency (Hz)

Figure 4c

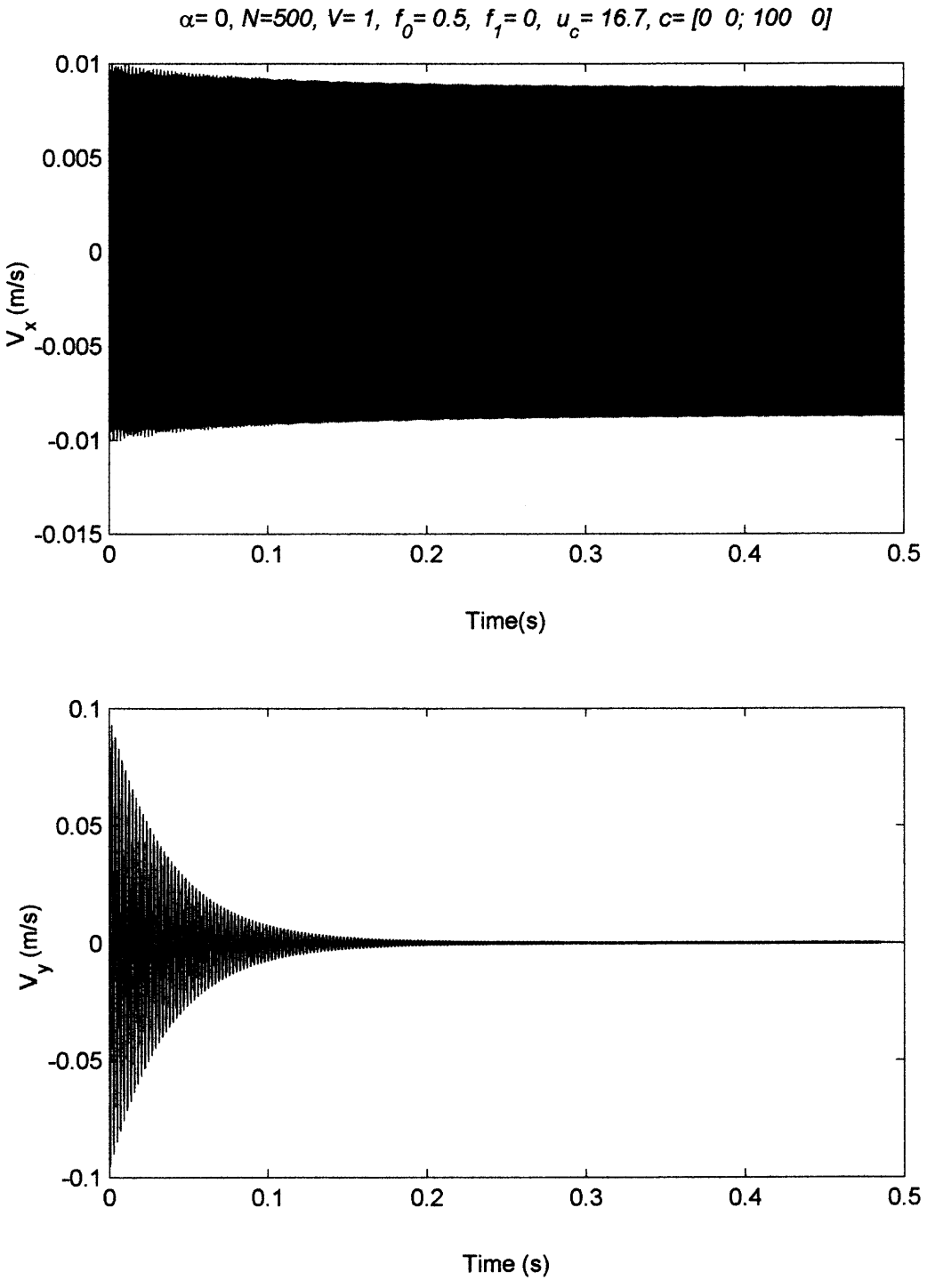
α= 0, N=500, V= 1, f0= 0.5, f1= 0, uc= 16.7, c= [0 0; 100 0]
0.01
0.005
0
-0.005
-0.01
-0.015
Vx (m/s)
0
0.1
0.2
0.3
0.4
0.5
Time(s)
0.1
0.05
0
-0.05
-0.1
Vy (m/s)
0
0.1
0.2
0.3
0.4
0.5
Time (s)

Figure 5a

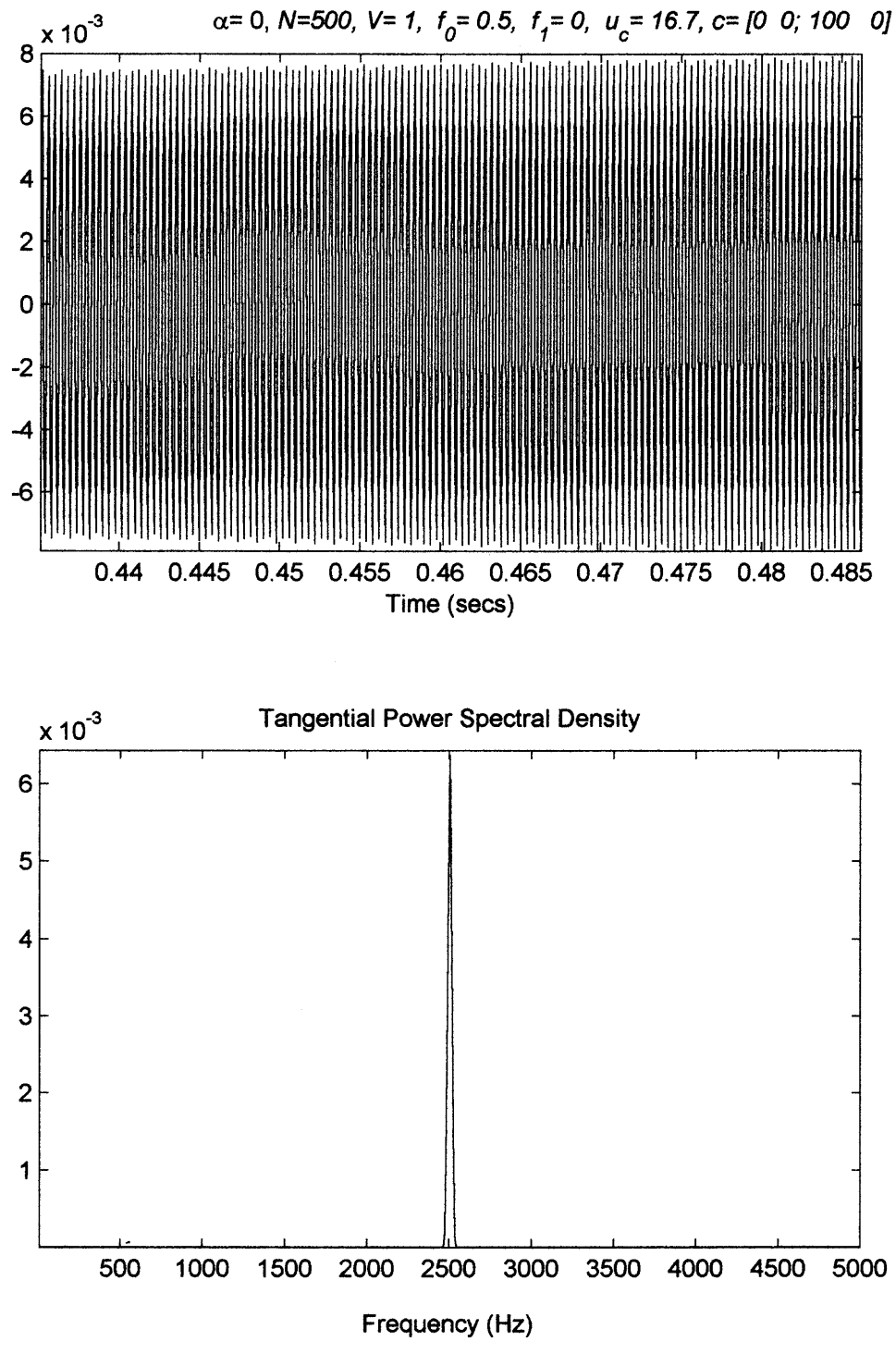
α= 0, N=500, V= 1, f0= 0.5, f1= 0, uc= 16.7, c= [0 0; 100 0]
x 10-3
8
6
4
2
0
-2
-4
-6
0.44 0.445 0.45 0.455 0.46 0.465 0.47 0.475 0.48 0.485
Time (secs)
Tangential Power Spectral Density
x 10-3
6
5
4
3
2
1
500 1000 1500 2000 2500 3000 3500 4000 4500 5000
Frequency (Hz)

Figure 5b

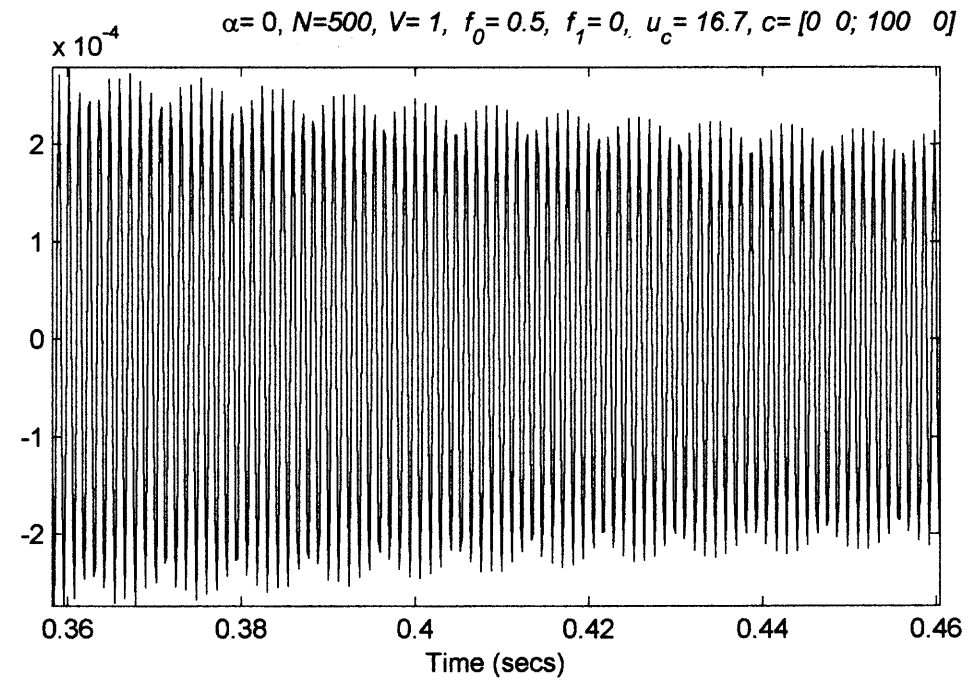
α= 0, N=500, V= 1, f0= 0.5, f1= 0, uc= 16.7, c= [0 0; 100 0]
x 10^-4
2
1
0
-1
-2
0.36
0.38
0.4
0.42
0.44
0.46
Time (secs)

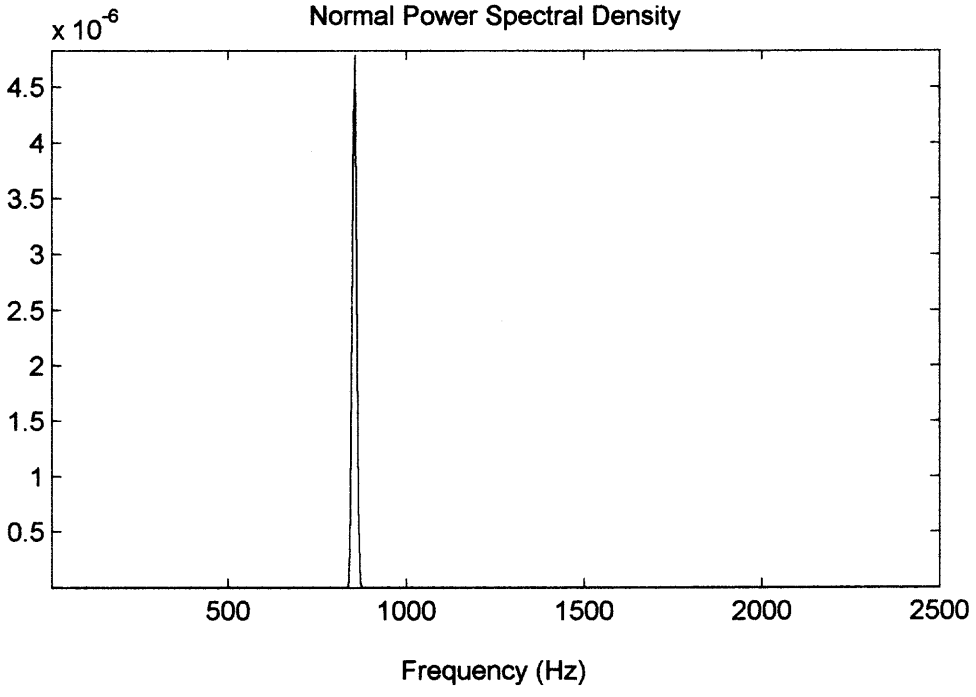
Normal Power Spectral Density
x 10^-6
4.5
4
3.5
3
2.5
2
1.5
1
0.5
500
1000
1500
2000
2500
Frequency (Hz)

Figure 5c

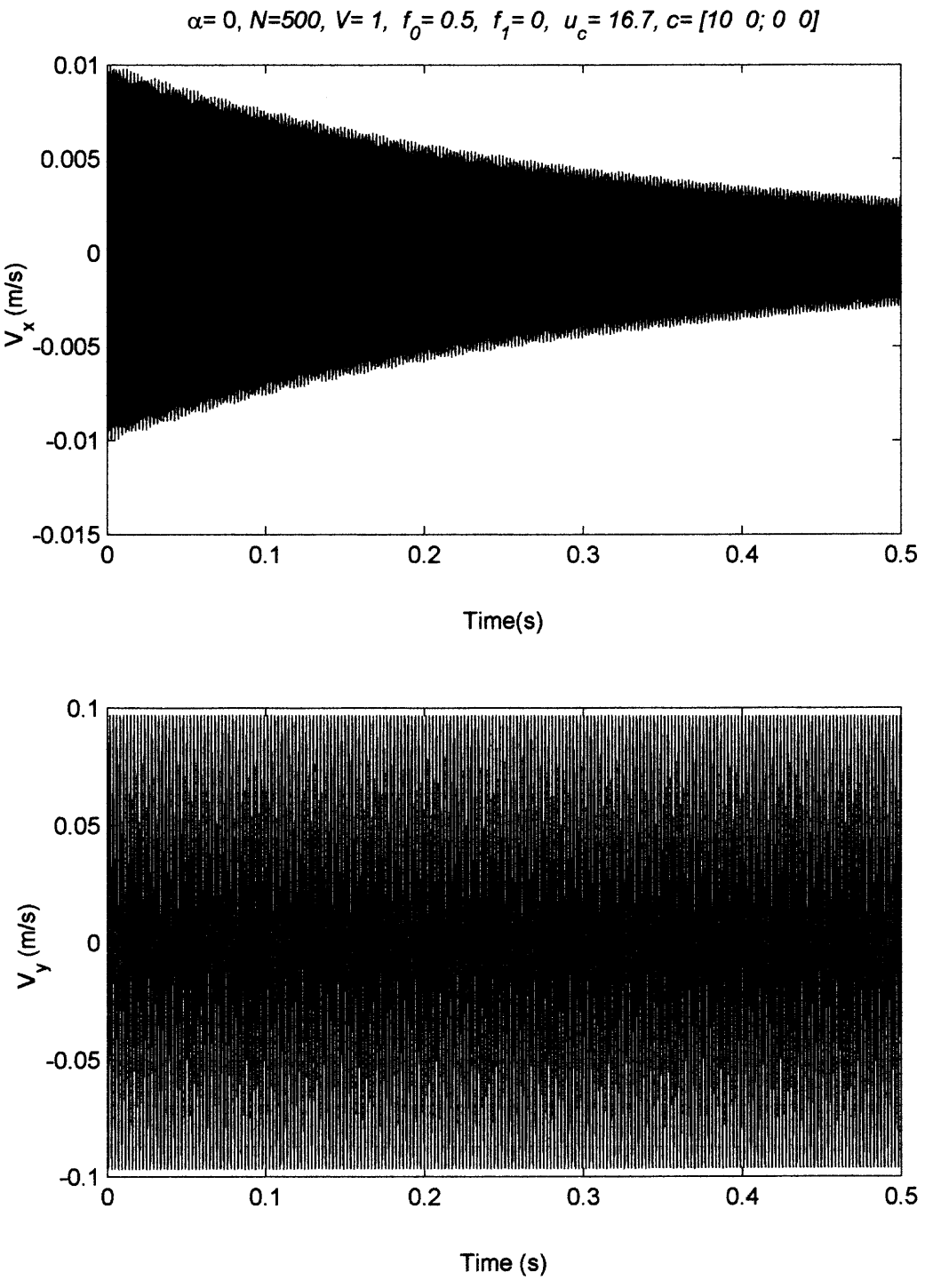
α= 0, N=500, V= 1, f0= 0.5, f1= 0, uc= 16.7, c= [10 0; 0 0]
0.01
0.005
0
-0.005
-0.01
-0.015
Vx (m/s)
0
0.1
0.2
0.3
0.4
0.5
Time(s)
0.1
0.05
0
-0.05
-0.1
Vy (m/s)
0
0.1
0.2
0.3
0.4
0.5
Time (s)

Figure 6a

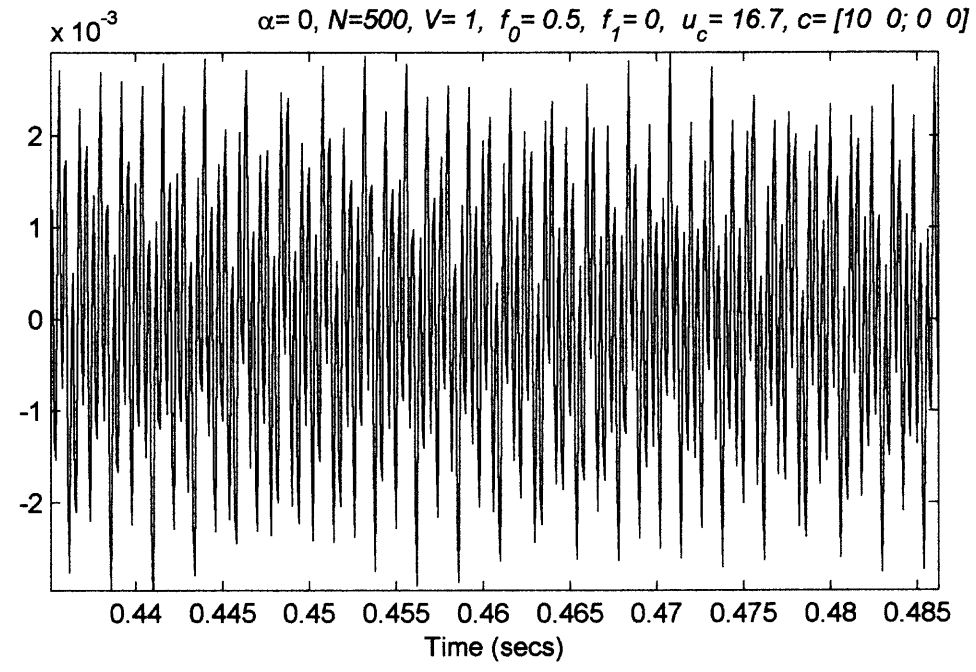
x 10^-3
α= 0, N=500, V= 1, f0= 0.5, f1= 0, uc= 16.7, c= [10 0; 0 0]
2
1
0
-1
-2
0.44 0.445 0.45 0.455 0.46 0.465 0.47 0.475 0.48 0.485
Time (secs)

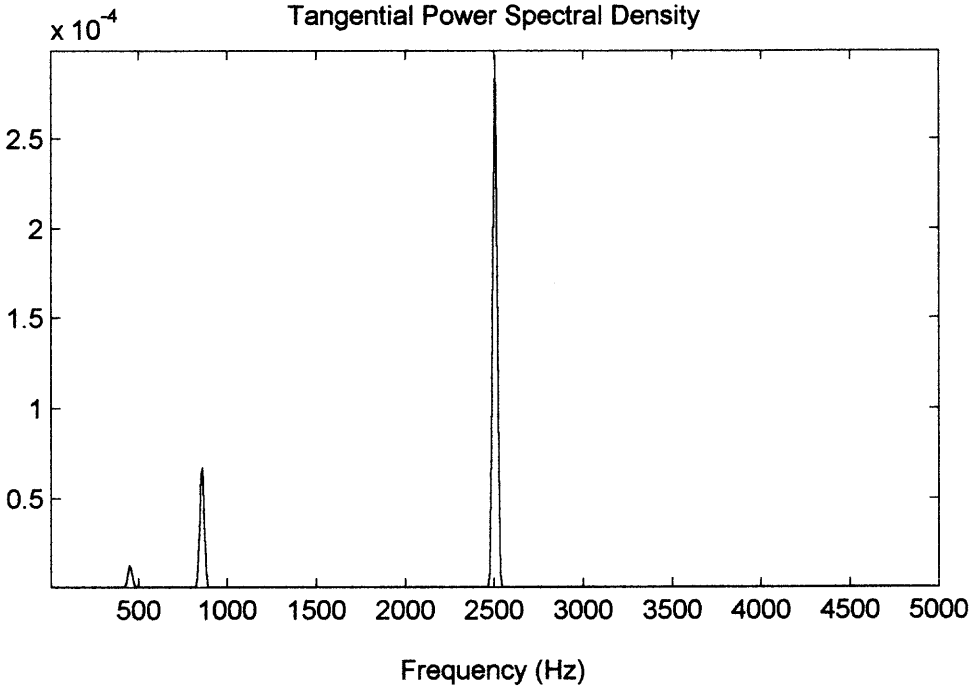
x 10^-4
Tangential Power Spectral Density
2.5
2
1.5
1
0.5
500 1000 1500 2000 2500 3000 3500 4000 4500 5000
Frequency (Hz)

Figure 6b

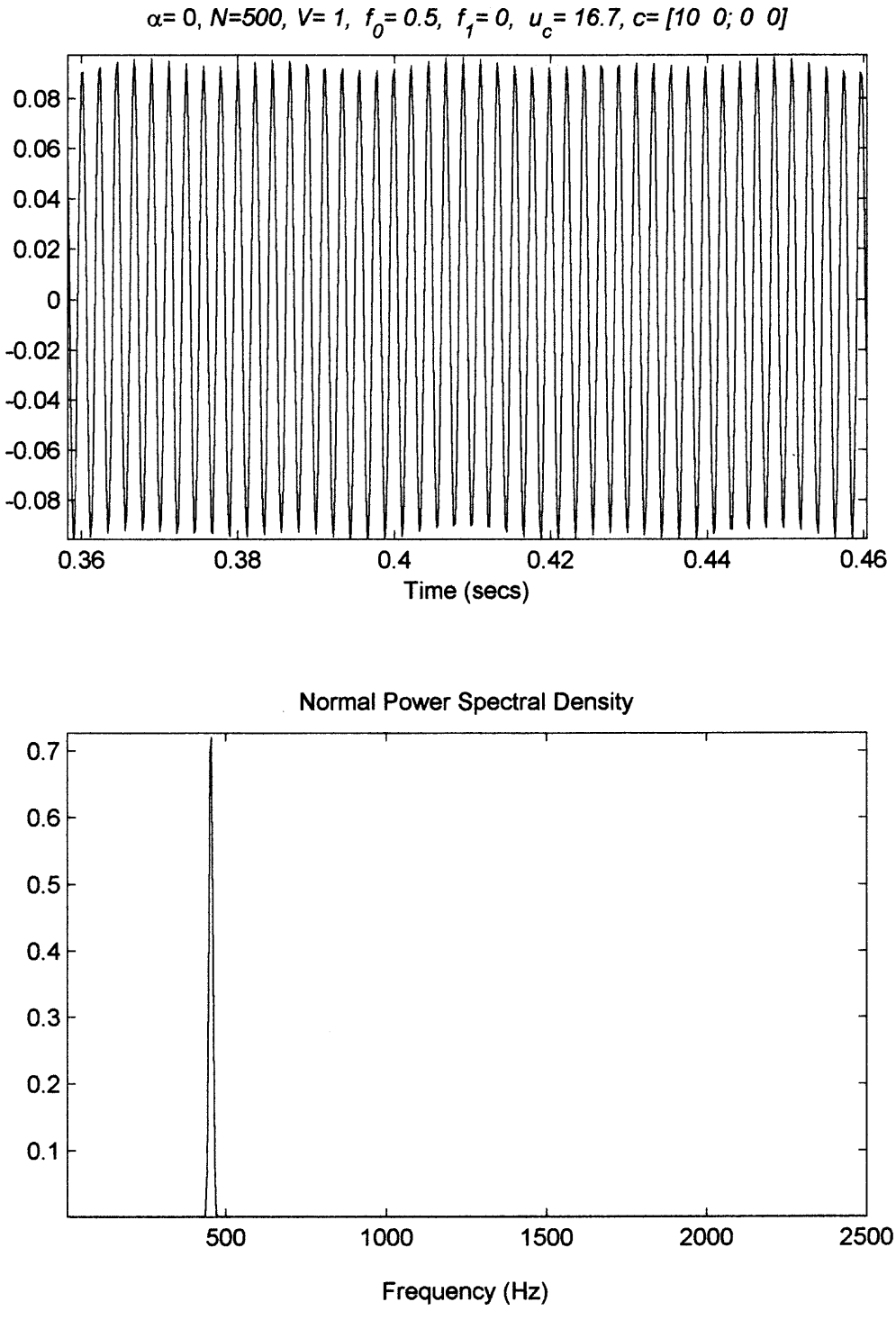
α= 0, N=500, V= 1, f0= 0.5, f1= 0, uc= 16.7, c= [10 0; 0 0]
0.08
0.06
0.04
0.02
0
-0.02
-0.04
-0.06
-0.08
0.36
0.38
0.4
0.42
0.44
0.46
Time (secs)
Normal Power Spectral Density
0.7
0.6
0.5
0.4
0.3
0.2
0.1
500
1000
1500
2000
2500
Frequency (Hz)

Figure 6c

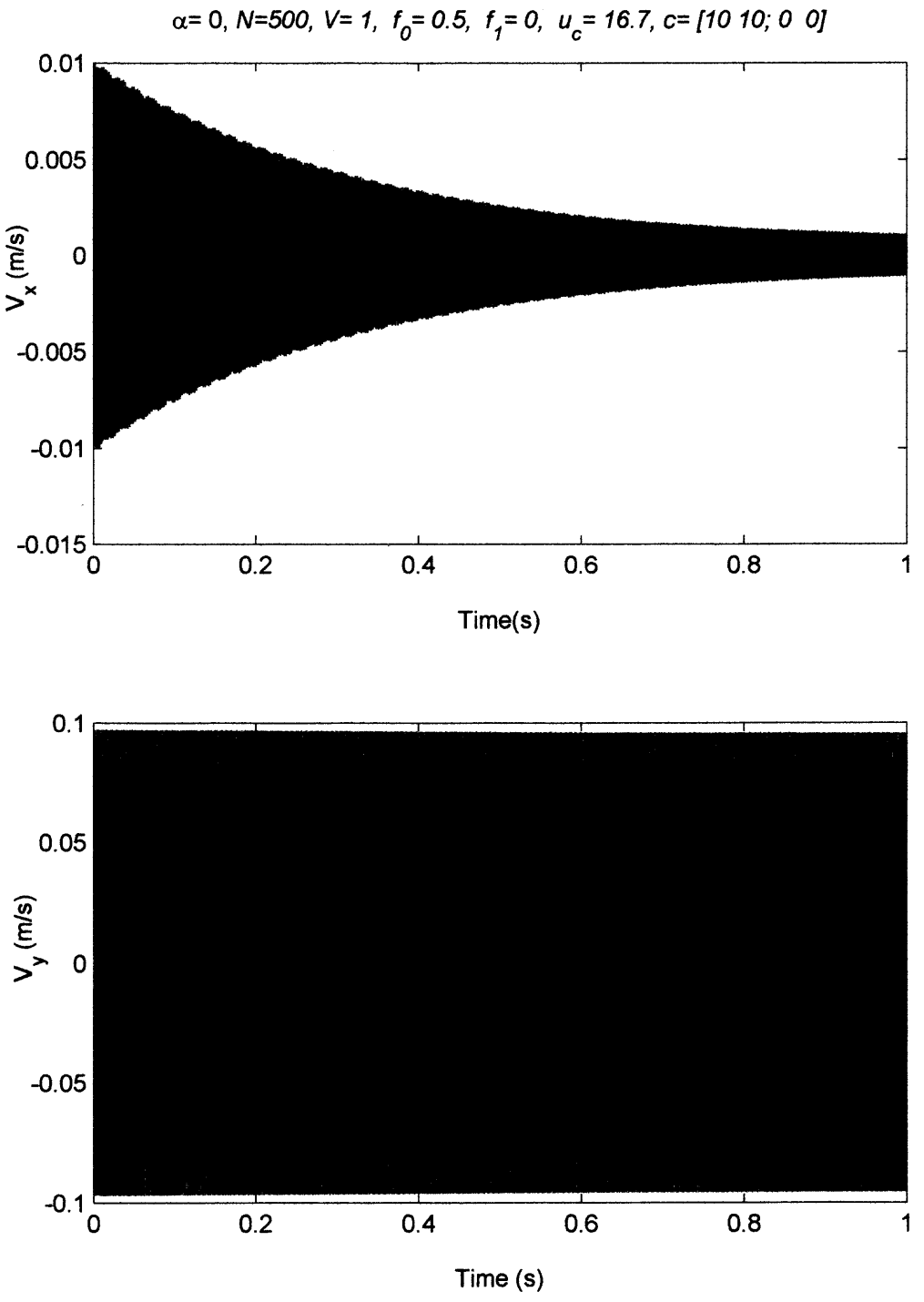
α= 0, N=500, V= 1, f0= 0.5, f1= 0, uc= 16.7, c= [10 10; 0 0]
0.01
0.005
0
-0.005
-0.01
-0.015
Vx (m/s)
0
0.2
0.4
0.6
0.8
1
Time(s)
0.1
0.05
0
-0.05
-0.1
Vy (m/s)
0
0.2
0.4
0.6
0.8
1
Time (s)

Figure 7a

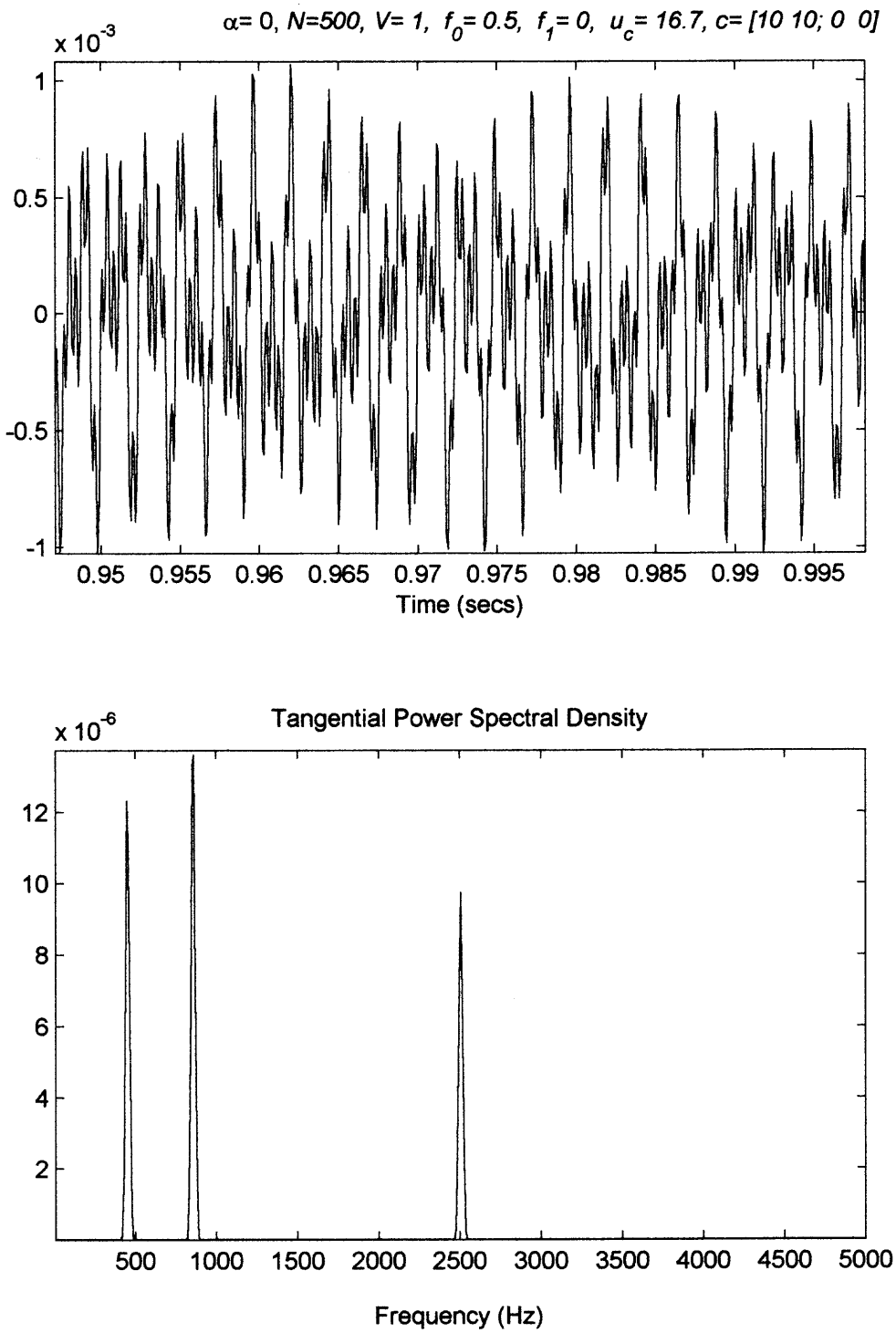
α= 0, N=500, V= 1, f0= 0.5, f1= 0, uc= 16.7, c= [10 10; 0 0]
x 10^-3
1
0.5
0
-0.5
-1
0.95 0.955 0.96 0.965 0.97 0.975 0.98 0.985 0.99 0.995
Time (secs)
Tangential Power Spectral Density
x 10^-6
12
10
8
6
4
2
500 1000 1500 2000 2500 3000 3500 4000 4500 5000
Frequency (Hz)

Figure 7b

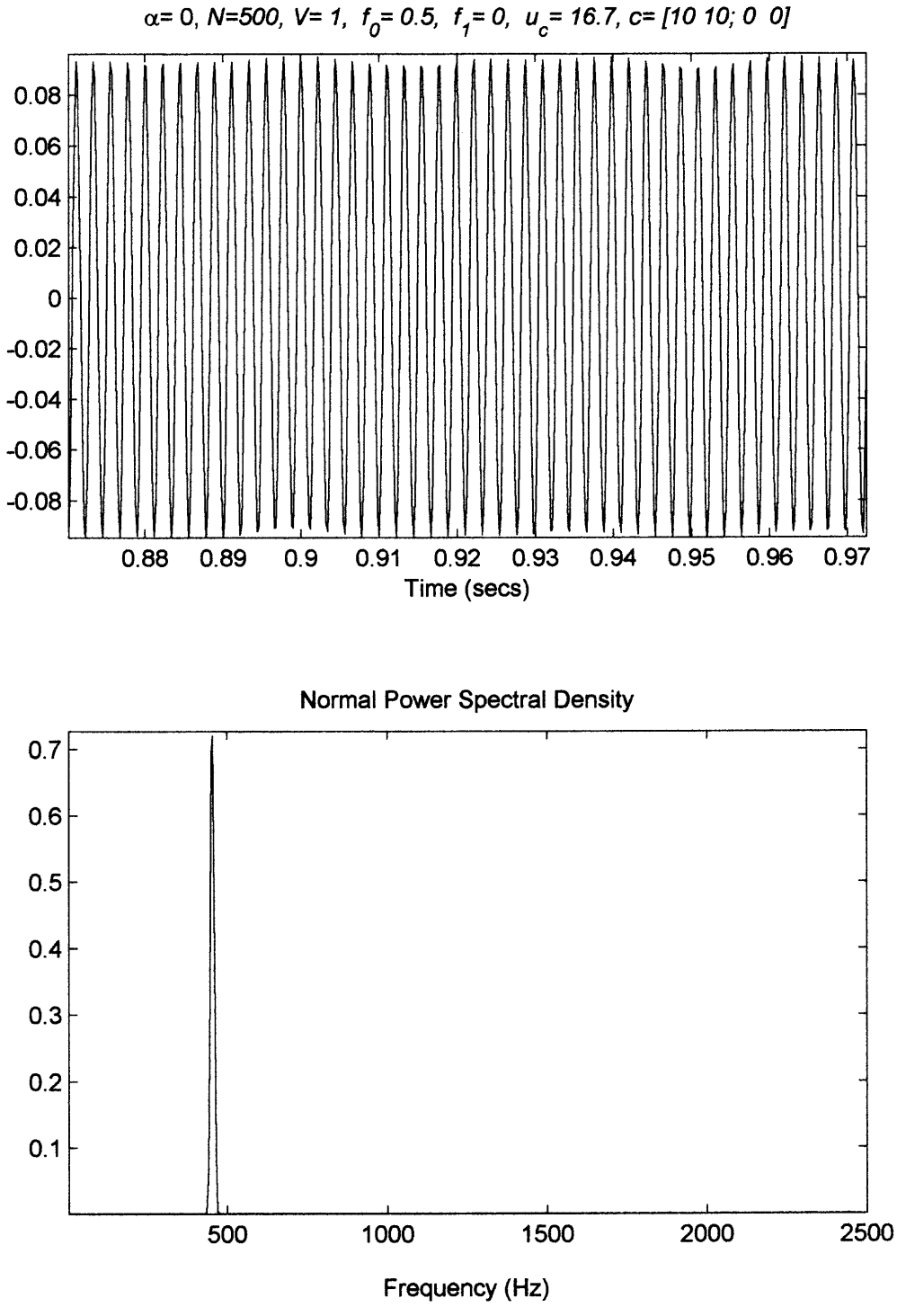
α= 0, N=500, V= 1, f0= 0.5, f1= 0, uc= 16.7, c= [10 10; 0 0]
0.08
0.06
0.04
0.02
0
-0.02
-0.04
-0.06
-0.08
0.88
0.89
0.9
0.91
0.92
0.93
0.94
0.95
0.96
0.97
Time (secs)
Normal Power Spectral Density
0.7
0.6
0.5
0.4
0.3
0.2
0.1
500
1000
1500
2000
2500
Frequency (Hz)

Figure 7c

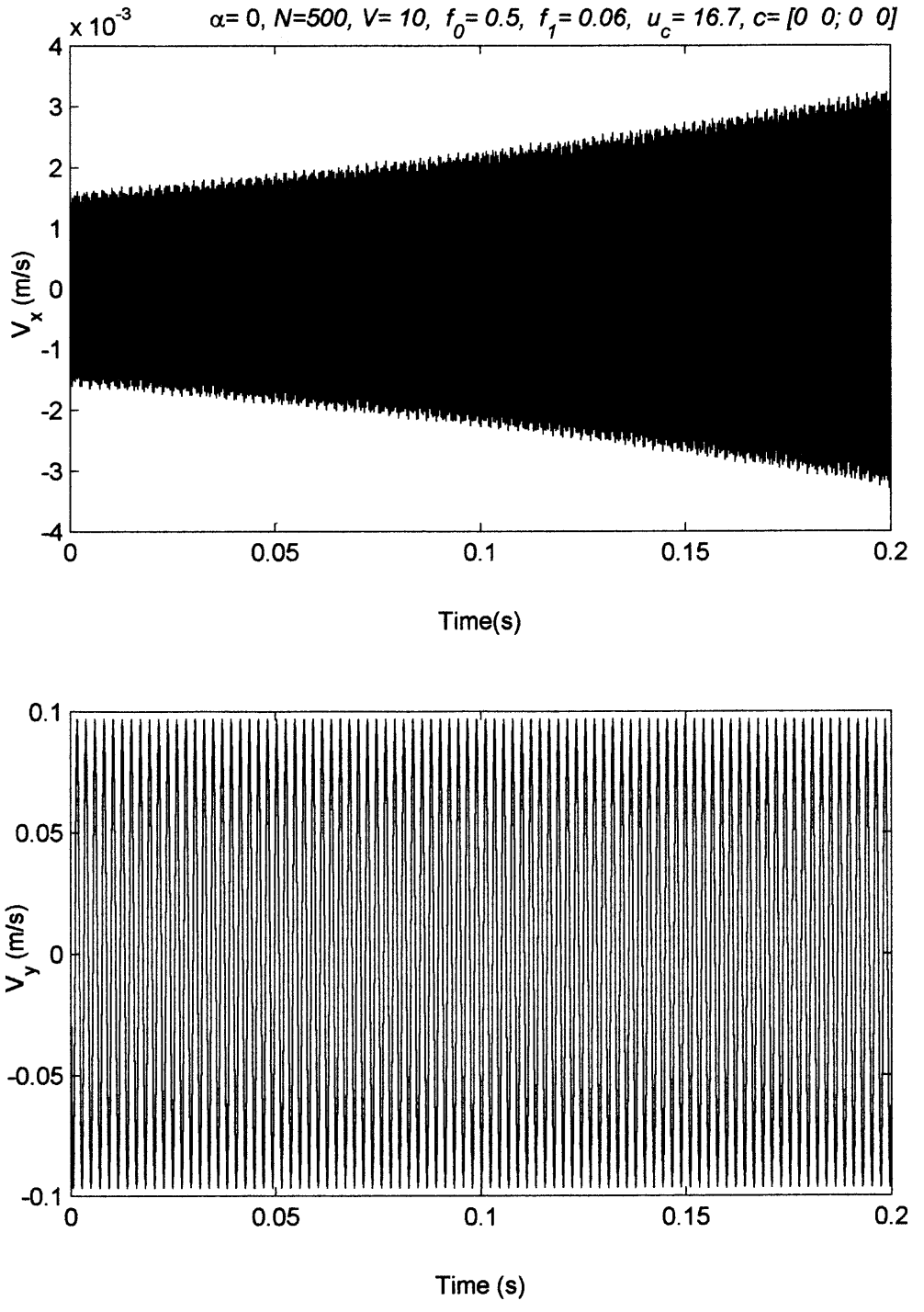
x 10^-3
α= 0, N=500, V= 10, f0= 0.5, f1= 0.06, uc= 16.7, c= [0 0; 0 0]
Vx (m/s)
Time(s)
Vy (m/s)
Time (s)

Figure 8a

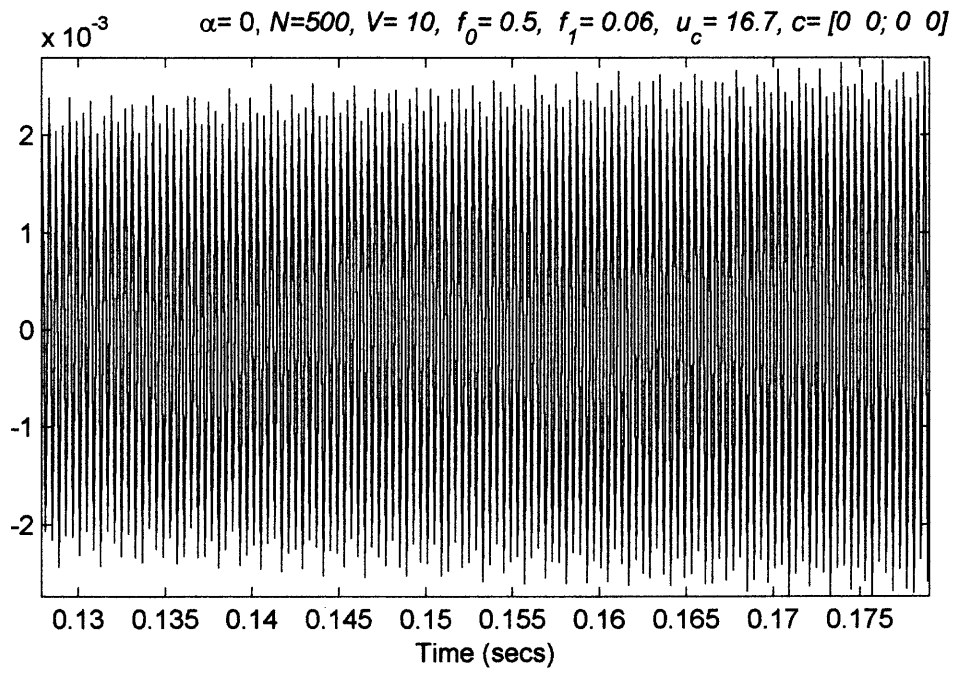
α= 0, N=500, V= 10, f0= 0.5, f1= 0.06, uc= 16.7, c= [0 0; 0 0]
x 10-3
2
1
0
-1
-2
0.13 0.135 0.14 0.145 0.15 0.155 0.16 0.165 0.17 0.175
Time (secs)

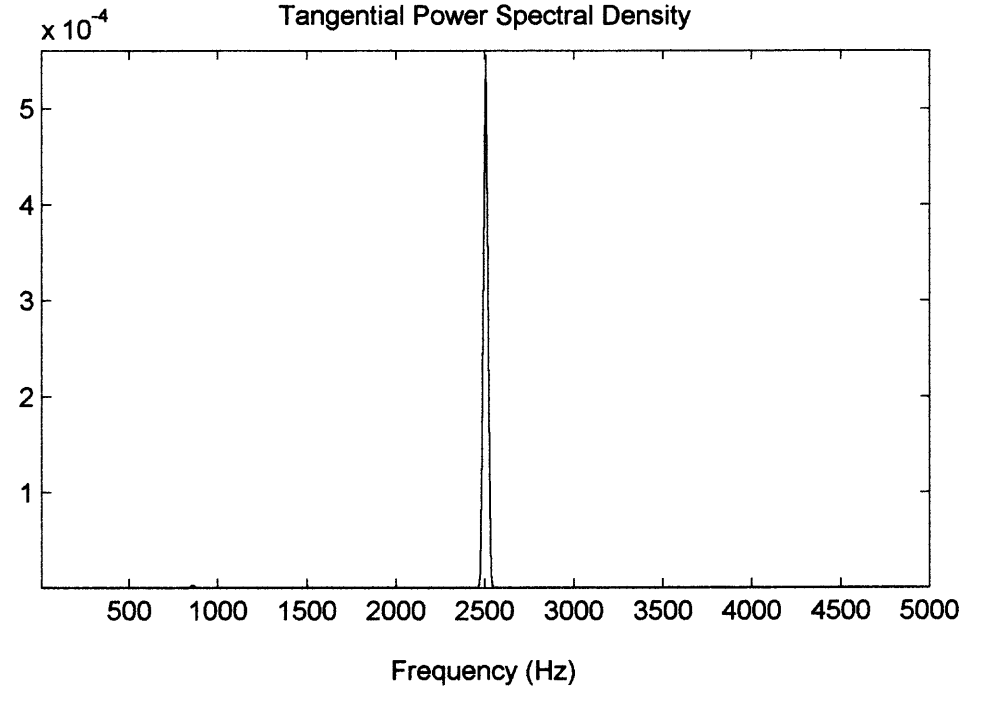
Tangential Power Spectral Density
x 10-4
5
4
3
2
1
500 1000 1500 2000 2500 3000 3500 4000 4500 5000
Frequency (Hz)

Figure 8b

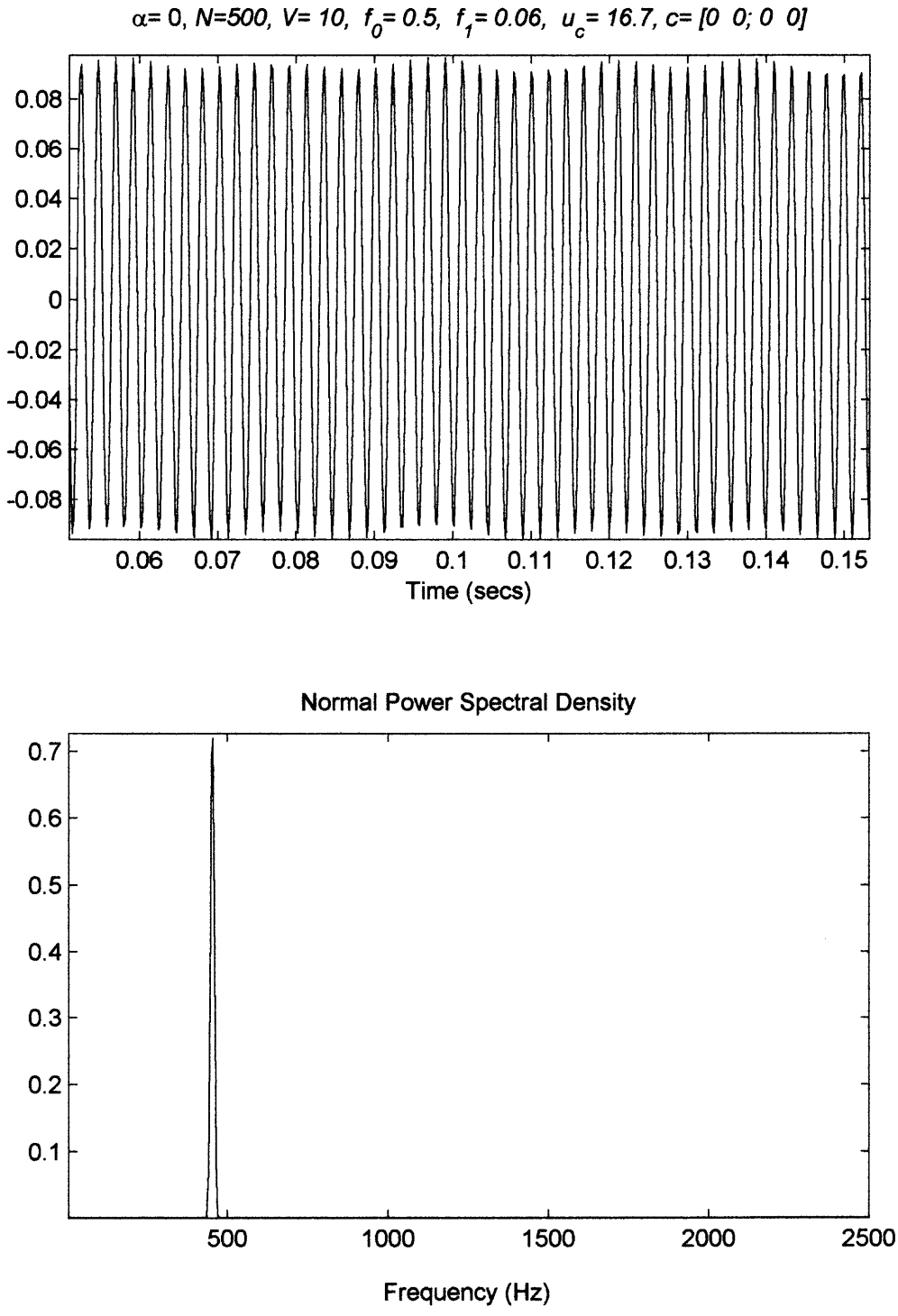
α= 0, N=500, V= 10, f0= 0.5, f1= 0.06, uc= 16.7, c= [0 0; 0 0]
0.08
0.06
0.04
0.02
0
-0.02
-0.04
-0.06
-0.08
0.06 0.07 0.08 0.09 0.1 0.11 0.12 0.13 0.14 0.15
Time (secs)
Normal Power Spectral Density
0.7
0.6
0.5
0.4
0.3
0.2
0.1
500 1000 1500 2000 2500
Frequency (Hz)

Figure 8c

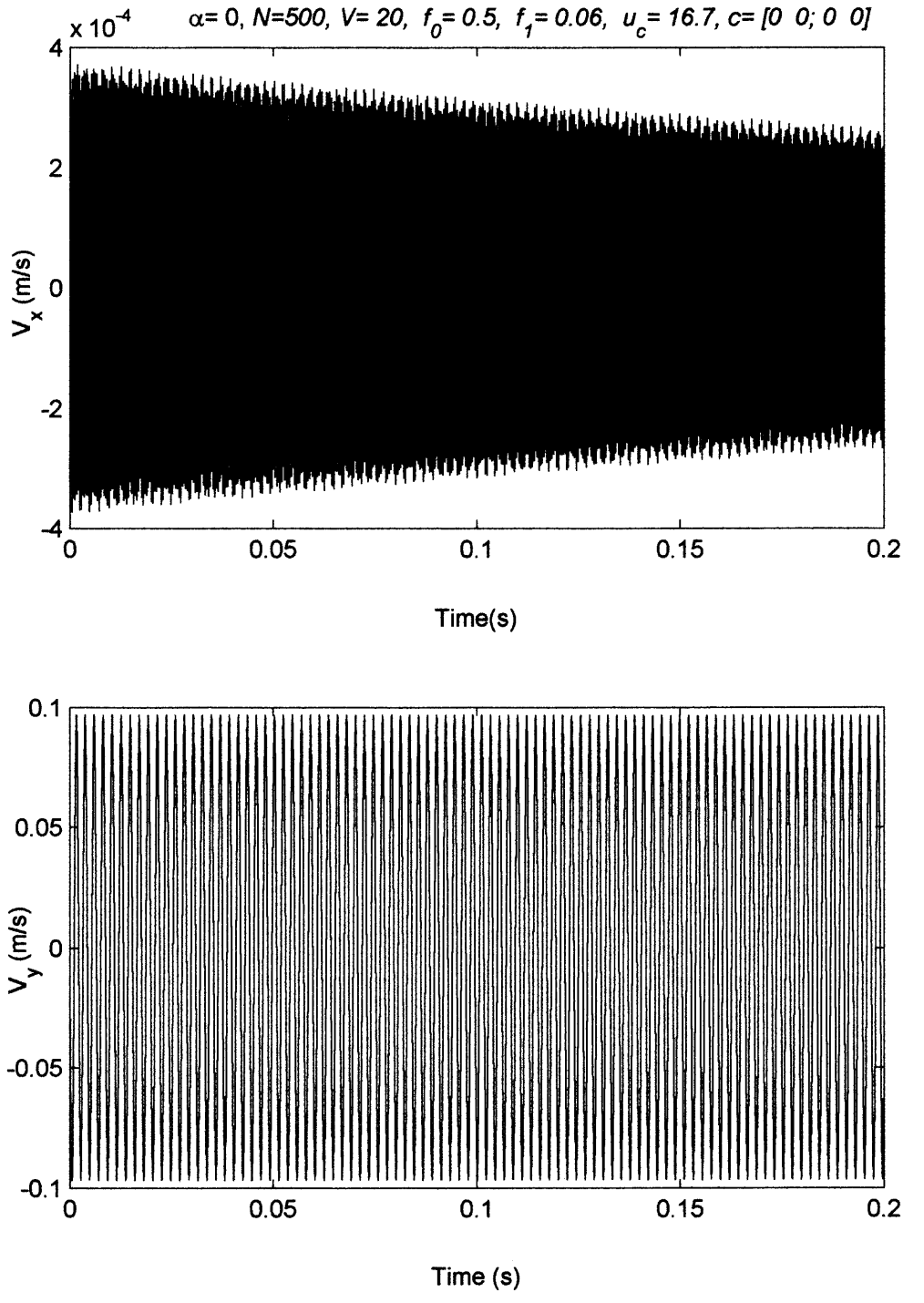
α= 0, N=500, V= 20, f0= 0.5, f1= 0.06, uc= 16.7, c= [0 0; 0 0]
x 10^-4
4
2
0
-2
-4
Vx (m/s)
0
0.05
0.1
0.15
0.2
Time(s)
0.1
0.05
0
-0.05
-0.1
Vy (m/s)
0
0.05
0.1
0.15
0.2
Time (s)

Figure 9a

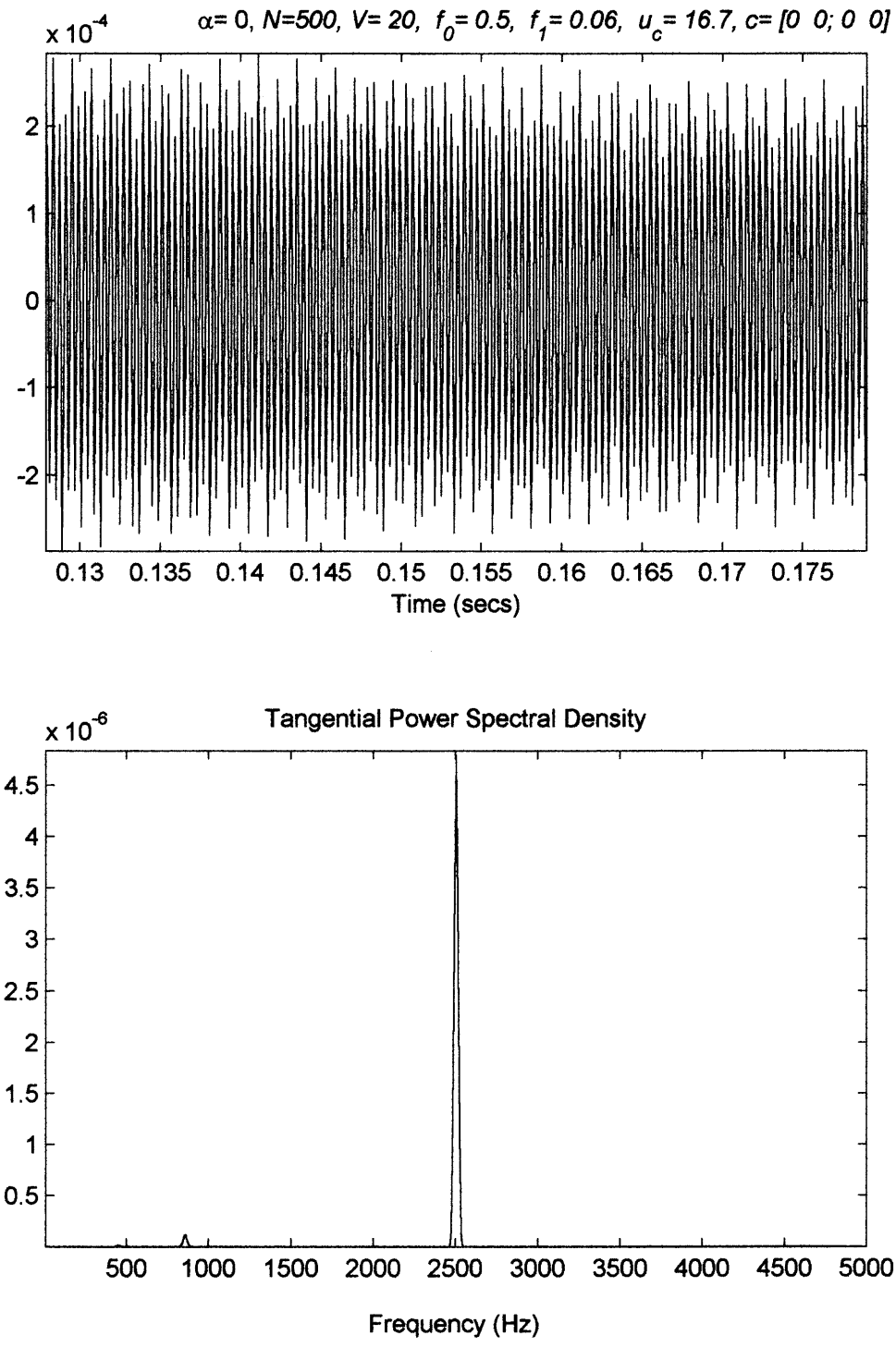
α= 0, N=500, V= 20, f0= 0.5, f1= 0.06, uc= 16.7, c= [0 0; 0 0]
x 10^-4
2
1
0
-1
-2
0.13 0.135 0.14 0.145 0.15 0.155 0.16 0.165 0.17 0.175
Time (secs)
Tangential Power Spectral Density
x 10^-6
4.5
4
3.5
3
2.5
2
1.5
1
0.5
500 1000 1500 2000 2500 3000 3500 4000 4500 5000
Frequency (Hz)

Figure 9b

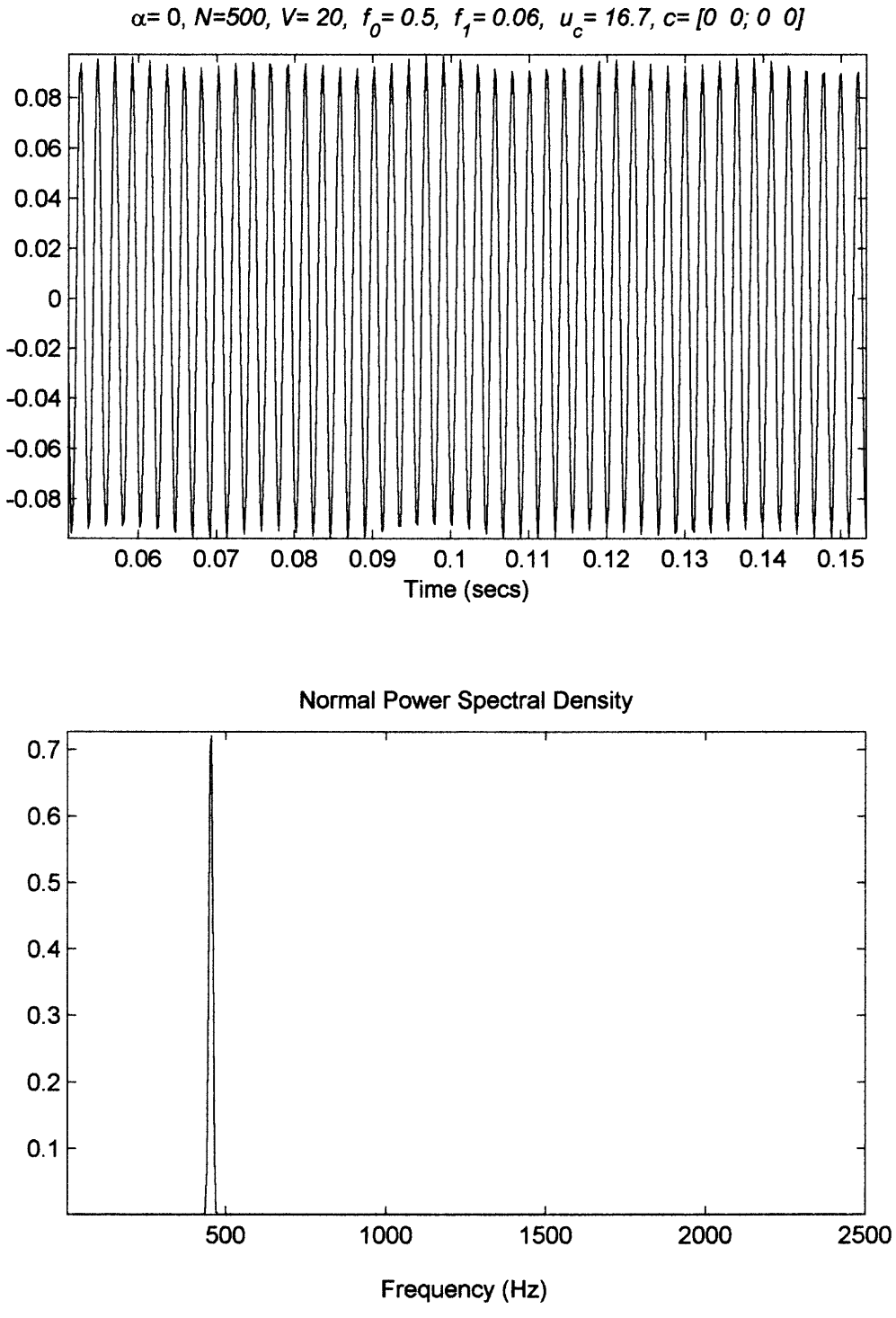
α= 0, N=500, V= 20, f_0= 0.5, f_1= 0.06, u_c= 16.7, c= [0 0; 0 0]
0.08
0.06
0.04
0.02
0
-0.02
-0.04
-0.06
-0.08
0.06 0.07 0.08 0.09 0.1 0.11 0.12 0.13 0.14 0.15
Time (secs)
Normal Power Spectral Density
0.7
0.6
0.5
0.4
0.3
0.2
0.1
500 1000 1500 2000 2500
Frequency (Hz)

Figure 9c

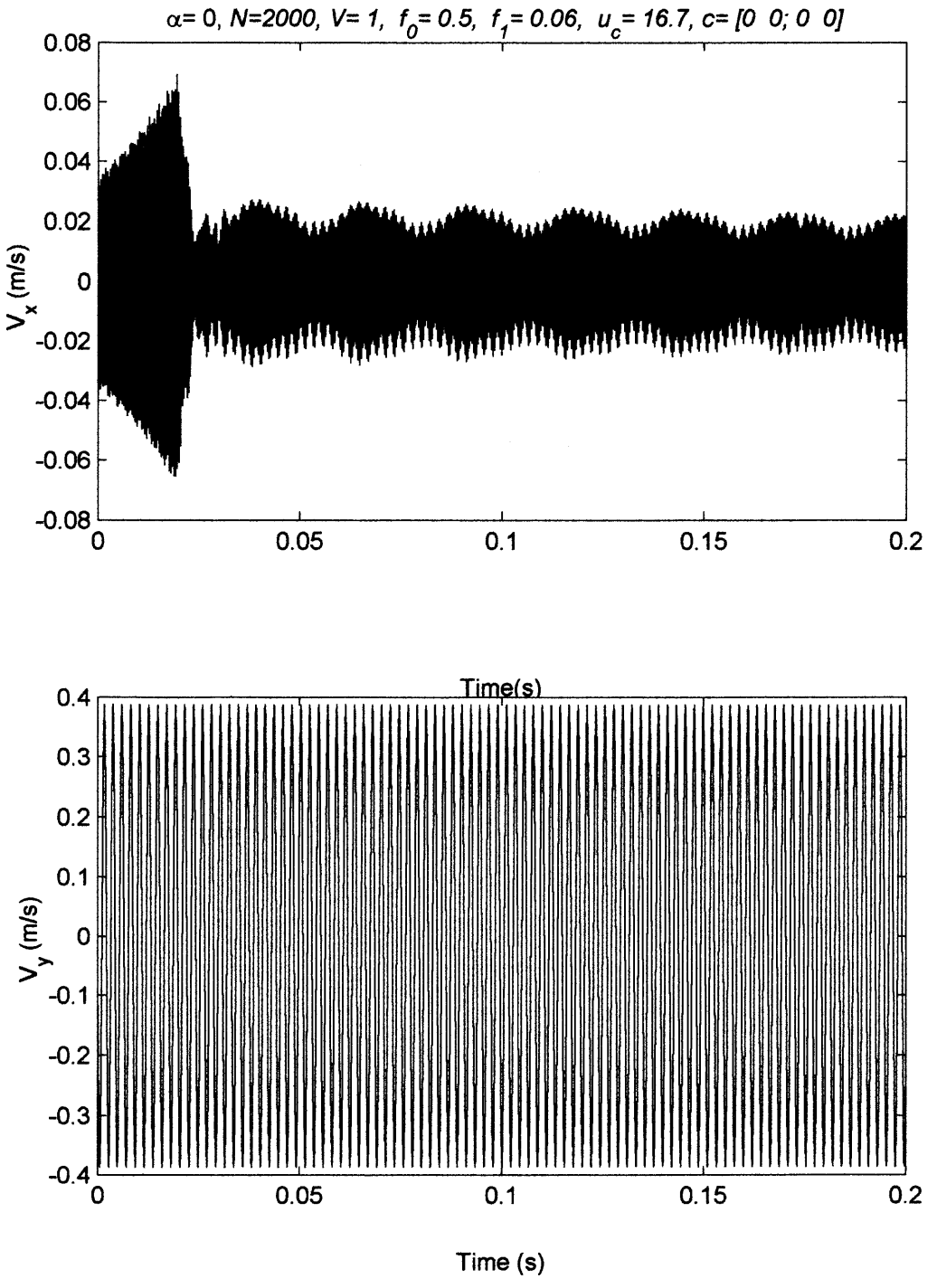

Figure 10a

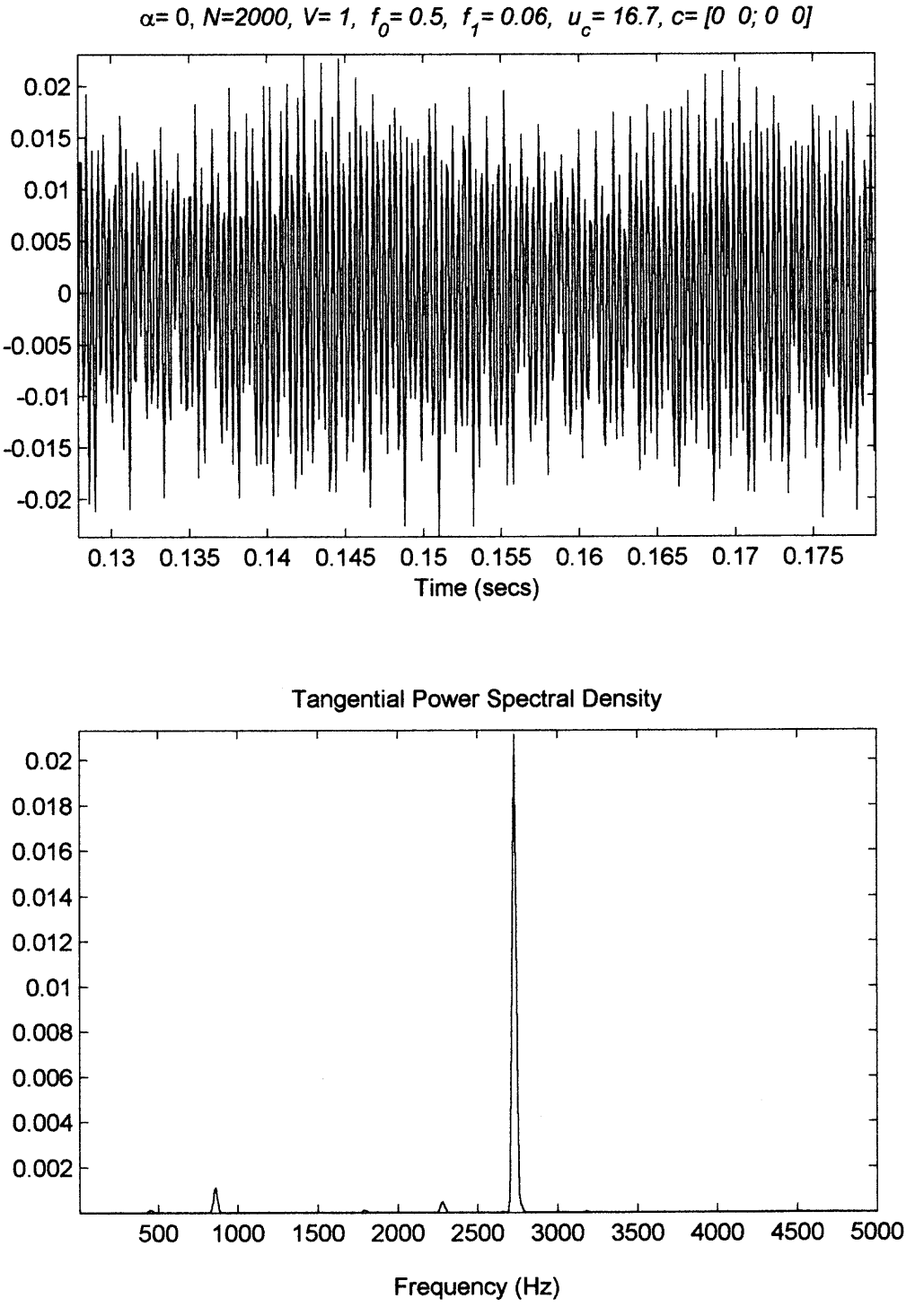
α= 0, N=2000, V= 1, f0= 0.5, f1= 0.06, uc= 16.7, c= [0 0; 0 0]
0.02
0.015
0.01
0.005
0
-0.005
-0.01
-0.015
-0.02
0.13 0.135 0.14 0.145 0.15 0.155 0.16 0.165 0.17 0.175
Time (secs)
Tangential Power Spectral Density
0.02
0.018
0.016
0.014
0.012
0.01
0.008
0.006
0.004
0.002
500 1000 1500 2000 2500 3000 3500 4000 4500 5000
Frequency (Hz)

Figure 10b

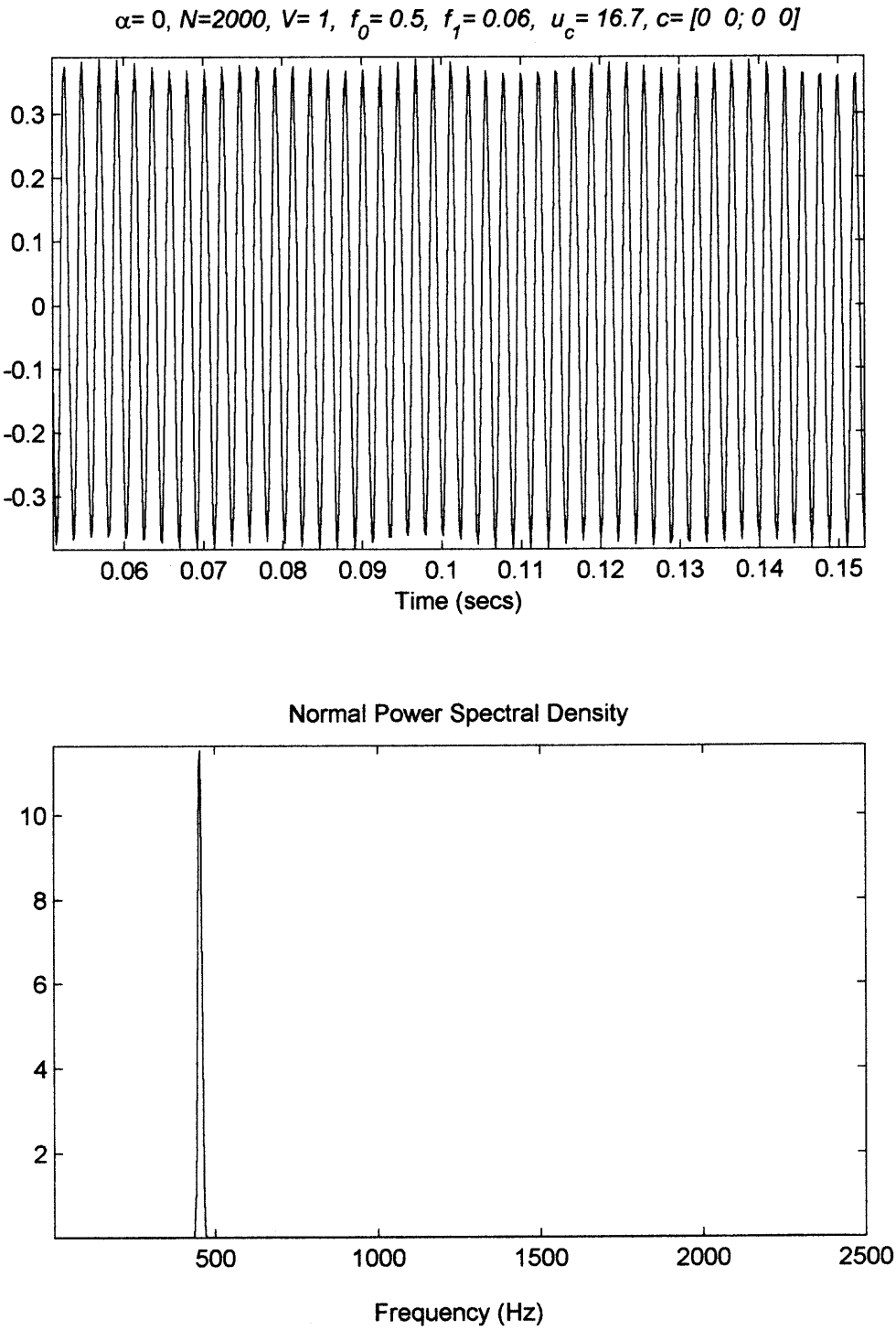
α= 0, N=2000, V= 1, f0= 0.5, f1= 0.06, uc= 16.7, c= [0 0; 0 0]
0.3
0.2
0.1
0
-0.1
-0.2
-0.3
0.06 0.07 0.08 0.09 0.1 0.11 0.12 0.13 0.14 0.15
Time (secs)
Normal Power Spectral Density
10
8
6
4
2
500 1000 1500 2000 2500
Frequency (Hz)

Figure 10c

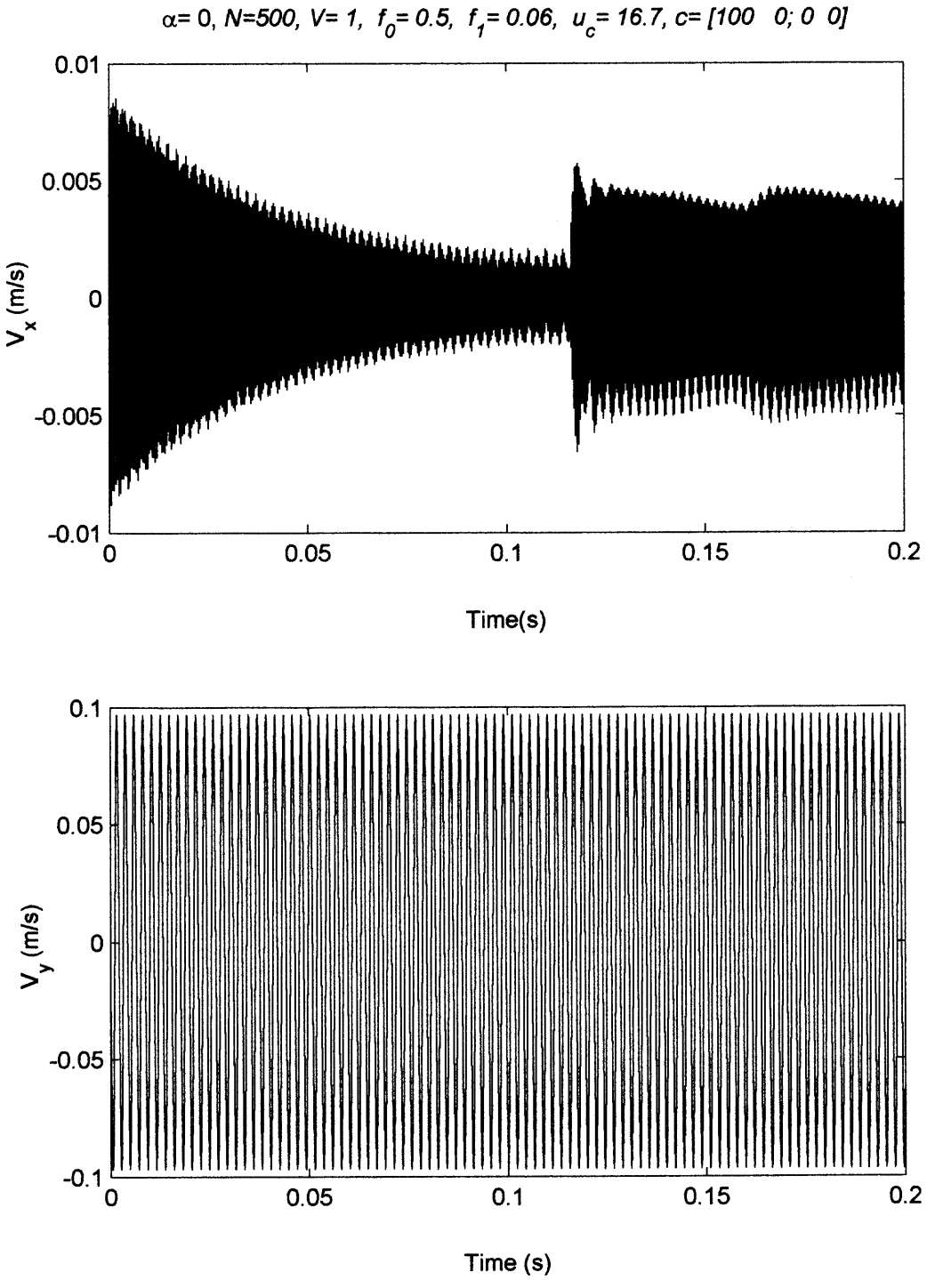
α= 0, N=500, V= 1, f0= 0.5, f1= 0.06, uc= 16.7, c= [100 0; 0 0]
0.01
0.005
0
-0.005
-0.01
Vx (m/s)
0
0.05
0.1
0.15
0.2
Time(s)
0.1
0.05
0
-0.05
-0.1
Vy (m/s)
0
0.05
0.1
0.15
0.2
Time (s)

Figure 11a

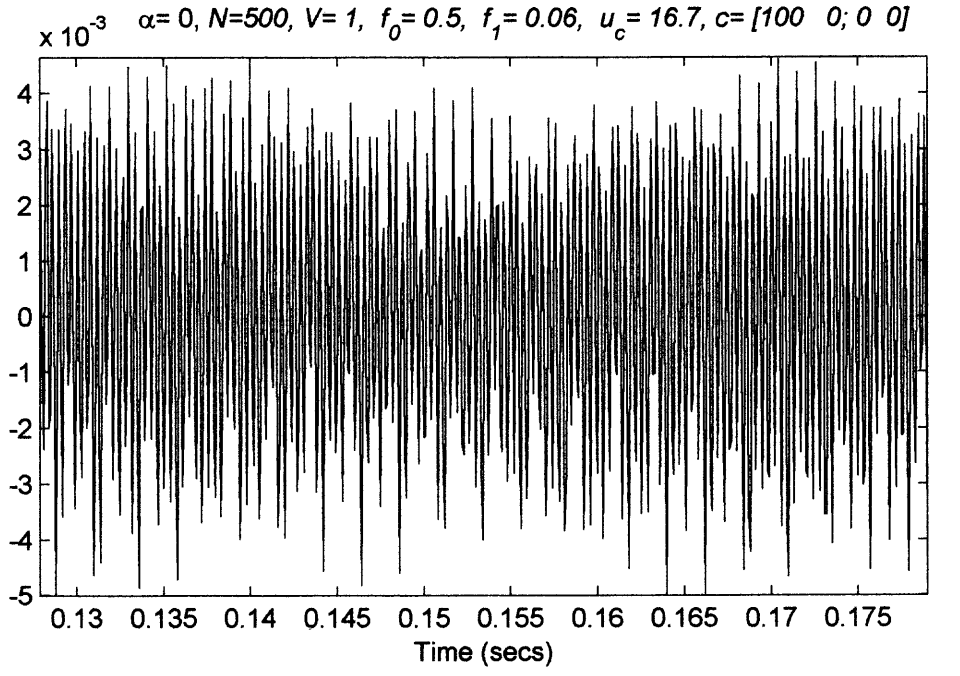
x 10^-3
α= 0, N=500, V= 1, f0= 0.5, f1= 0.06, uc= 16.7, c= [100 0; 0 0]
4
3
2
1
0
-1
-2
-3
-4
-5
0.13
0.135
0.14
0.145
0.15
0.155
0.16
0.165
0.17
0.175
Time (secs)

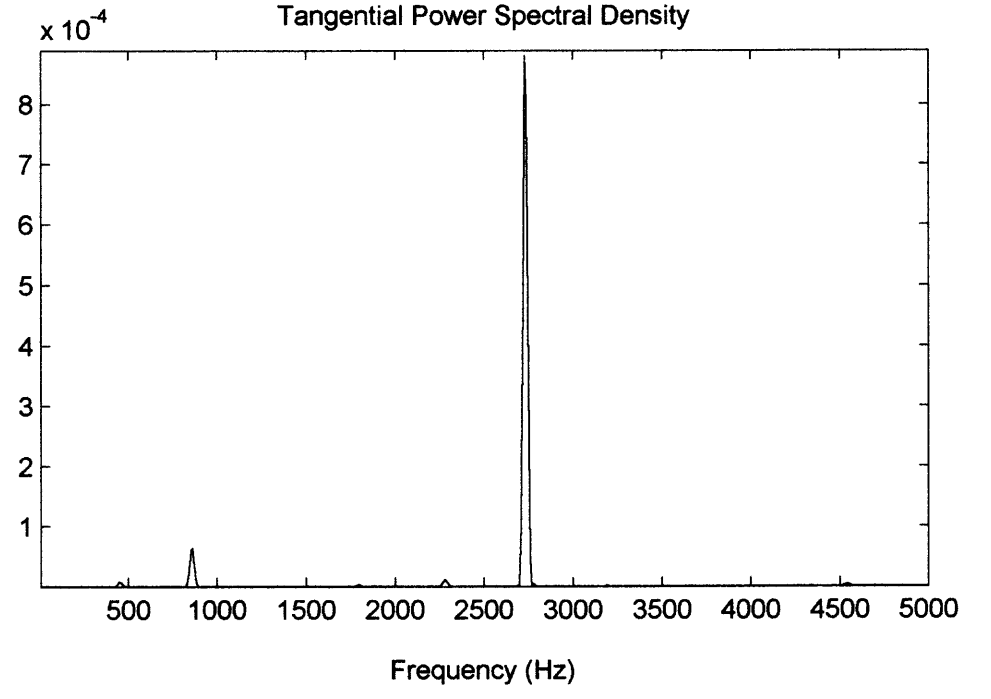
Tangential Power Spectral Density
x 10^-4
8
7
6
5
4
3
2
1
500
1000
1500
2000
2500
3000
3500
4000
4500
5000
Frequency (Hz)

Figure 11b

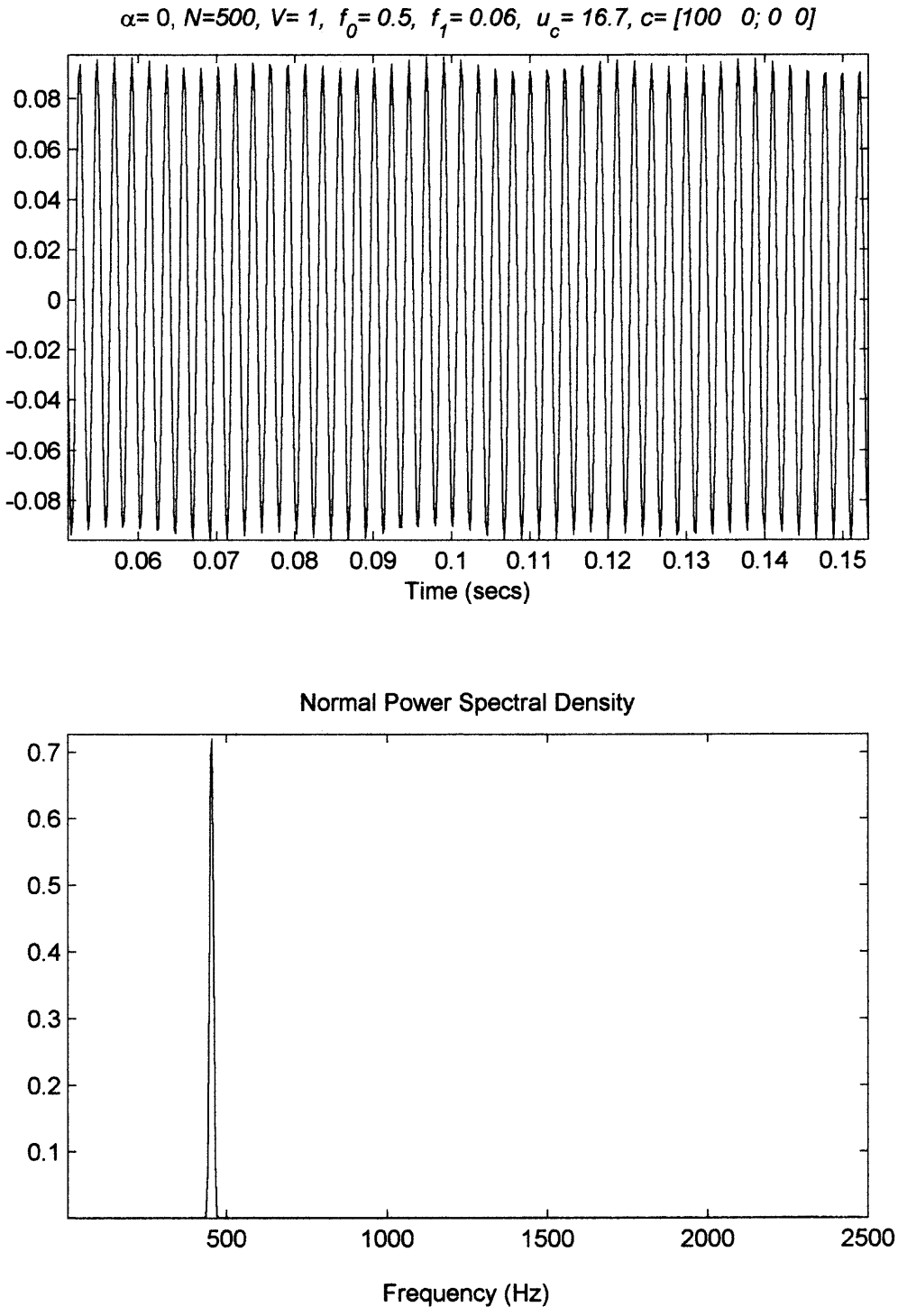
α= 0, N=500, V= 1, f0= 0.5, f1= 0.06, uc= 16.7, c= [100 0; 0 0]
0.08
0.06
0.04
0.02
0
-0.02
-0.04
-0.06
-0.08
0.06 0.07 0.08 0.09 0.1 0.11 0.12 0.13 0.14 0.15
Time (secs)
Normal Power Spectral Density
0.7
0.6
0.5
0.4
0.3
0.2
0.1
500 1000 1500 2000 2500
Frequency (Hz)

Figure 11c

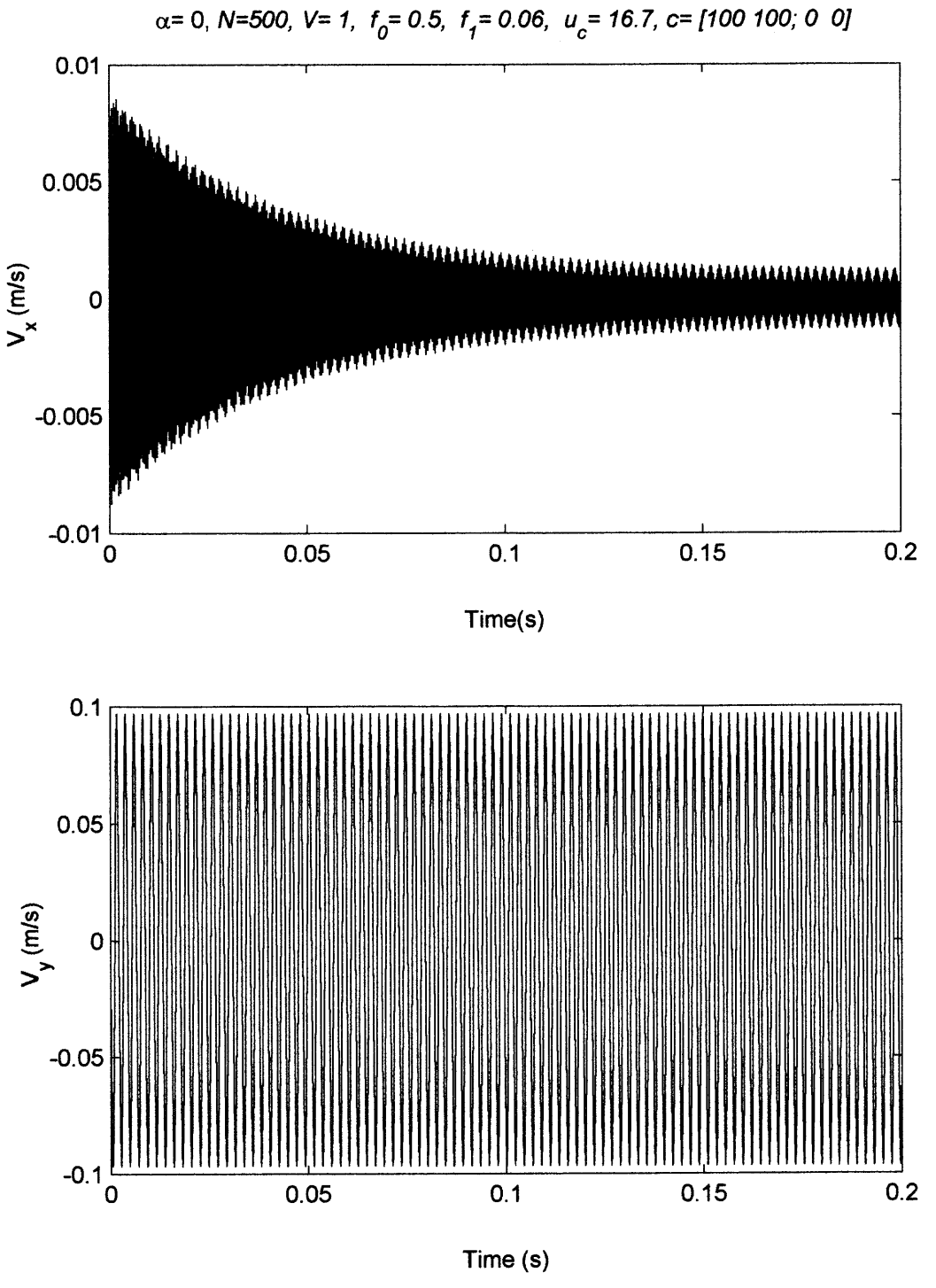
α= 0, N=500, V= 1, f0= 0.5, f1= 0.06, uc= 16.7, c= [100 100; 0 0]
0.01
0.005
0
-0.005
-0.01
Vx (m/s)
0
0.05
0.1
0.15
0.2
Time(s)
0.1
0.05
0
-0.05
-0.1
Vy (m/s)
0
0.05
0.1
0.15
0.2
Time (s)

Figure 12a

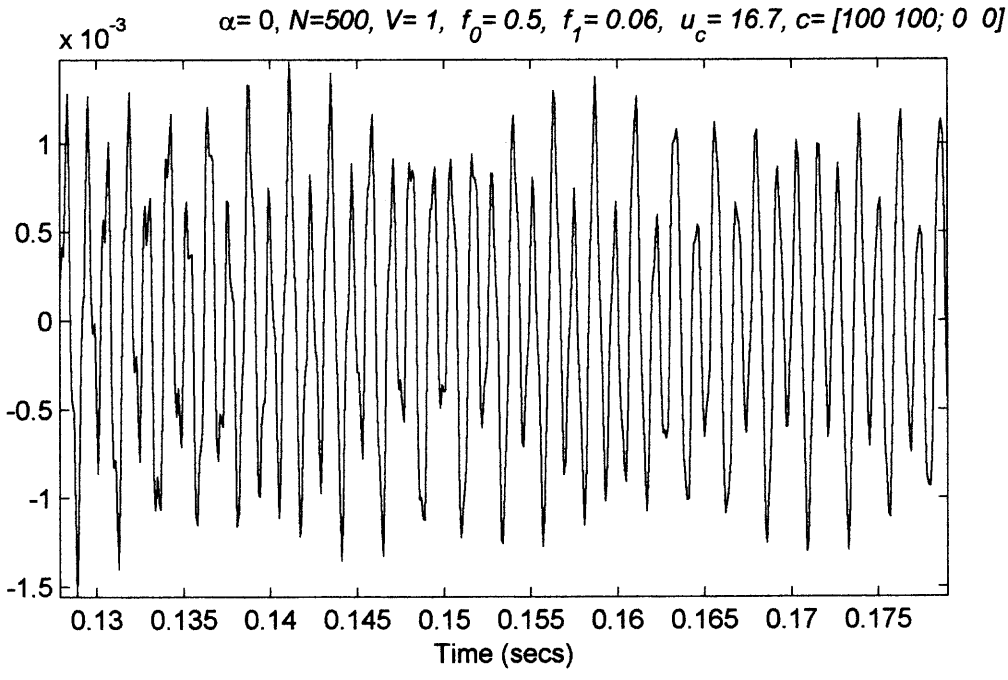
α= 0, N=500, V= 1, f0= 0.5, f1= 0.06, uc= 16.7, c= [100 100; 0 0]
x 10^-3
1
0.5
0
-0.5
-1
-1.5
0.13 0.135 0.14 0.145 0.15 0.155 0.16 0.165 0.17 0.175
Time (secs)

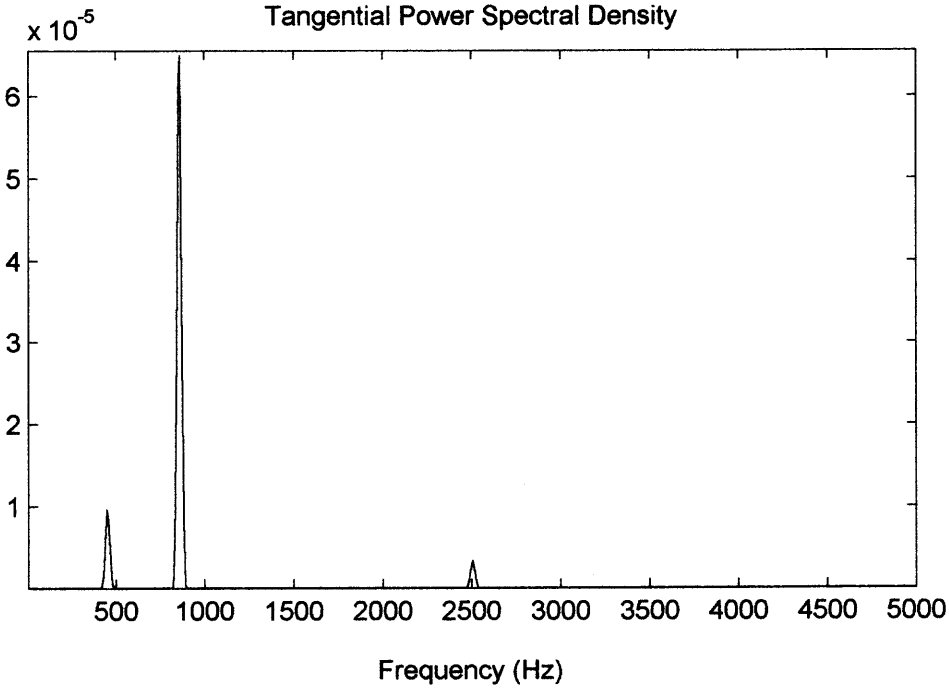
Tangential Power Spectral Density
x 10^-5
6
5
4
3
2
1
500 1000 1500 2000 2500 3000 3500 4000 4500 5000
Frequency (Hz)

Figure 12b

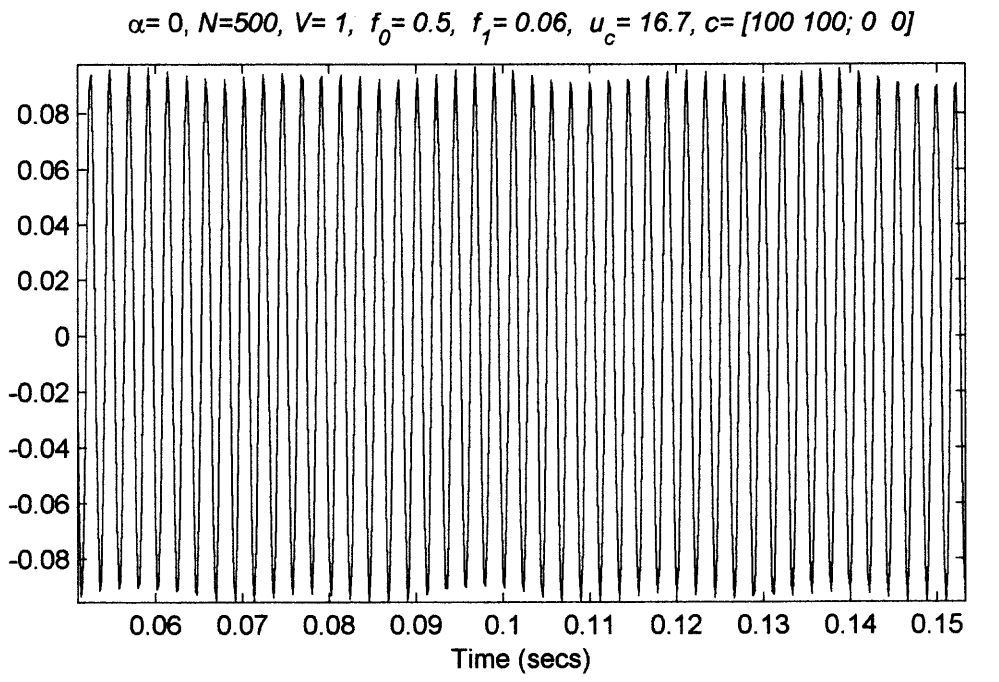
α= 0, N=500, V= 1, f0= 0.5, f1= 0.06, uc= 16.7, c= [100 100; 0 0]
0.08
0.06
0.04
0.02
0
-0.02
-0.04
-0.06
-0.08
0.06 0.07 0.08 0.09 0.1 0.11 0.12 0.13 0.14 0.15
Time (secs)

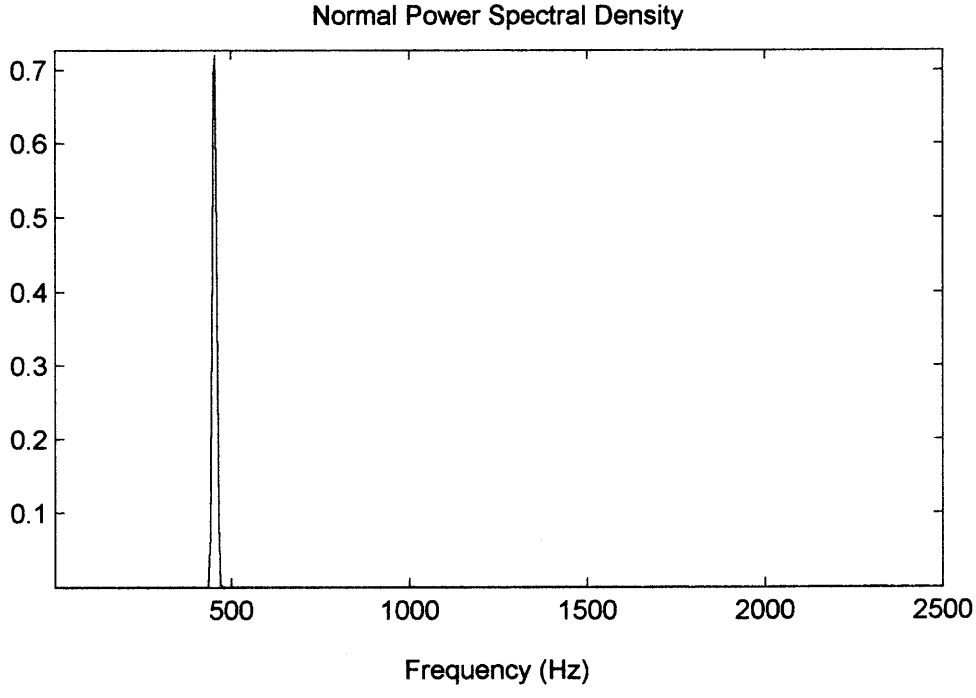
Normal Power Spectral Density
0.7
0.6
0.5
0.4
0.3
0.2
0.1
500 1000 1500 2000 2500
Frequency (Hz)

Figure 12c

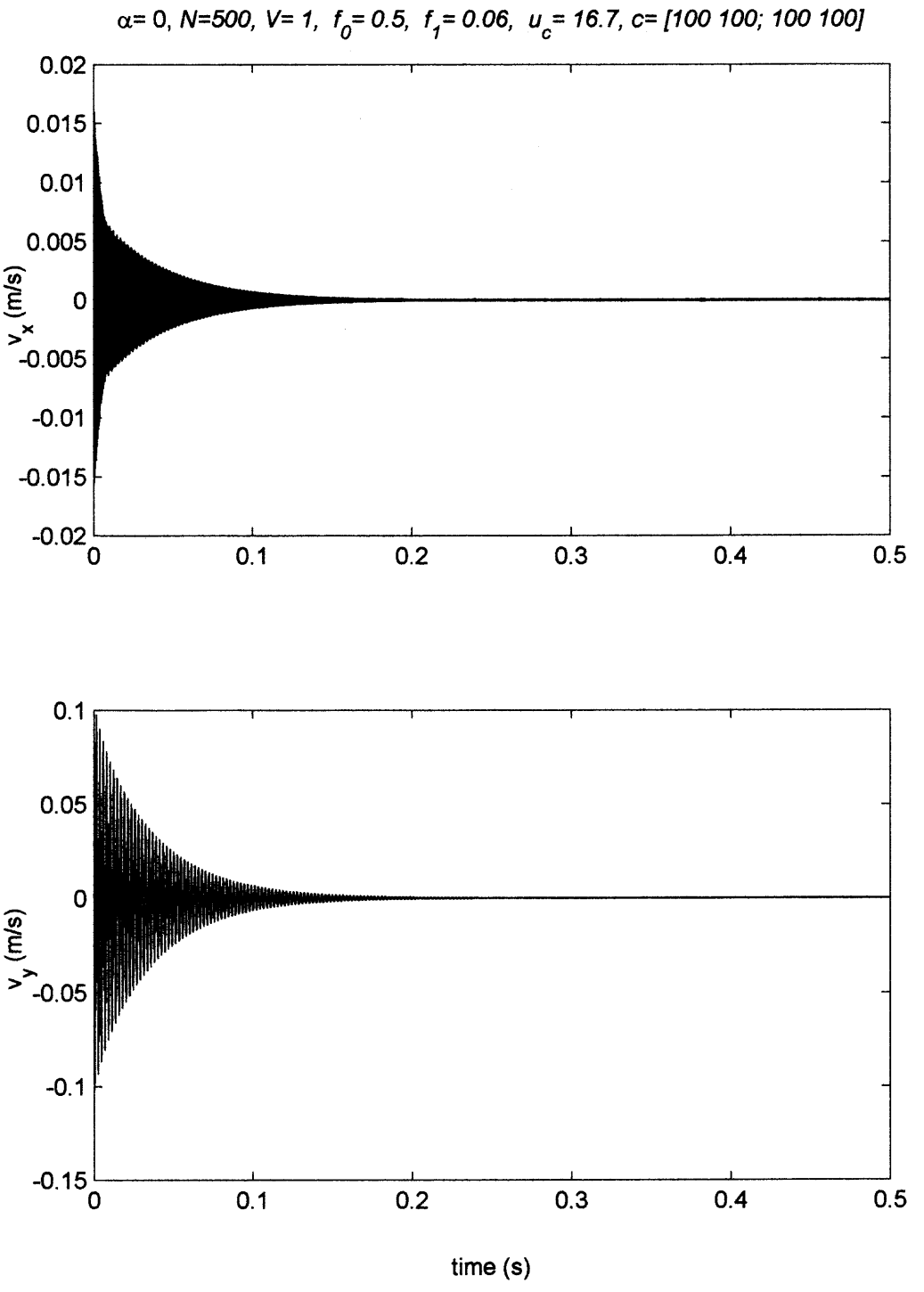

Figure 13a

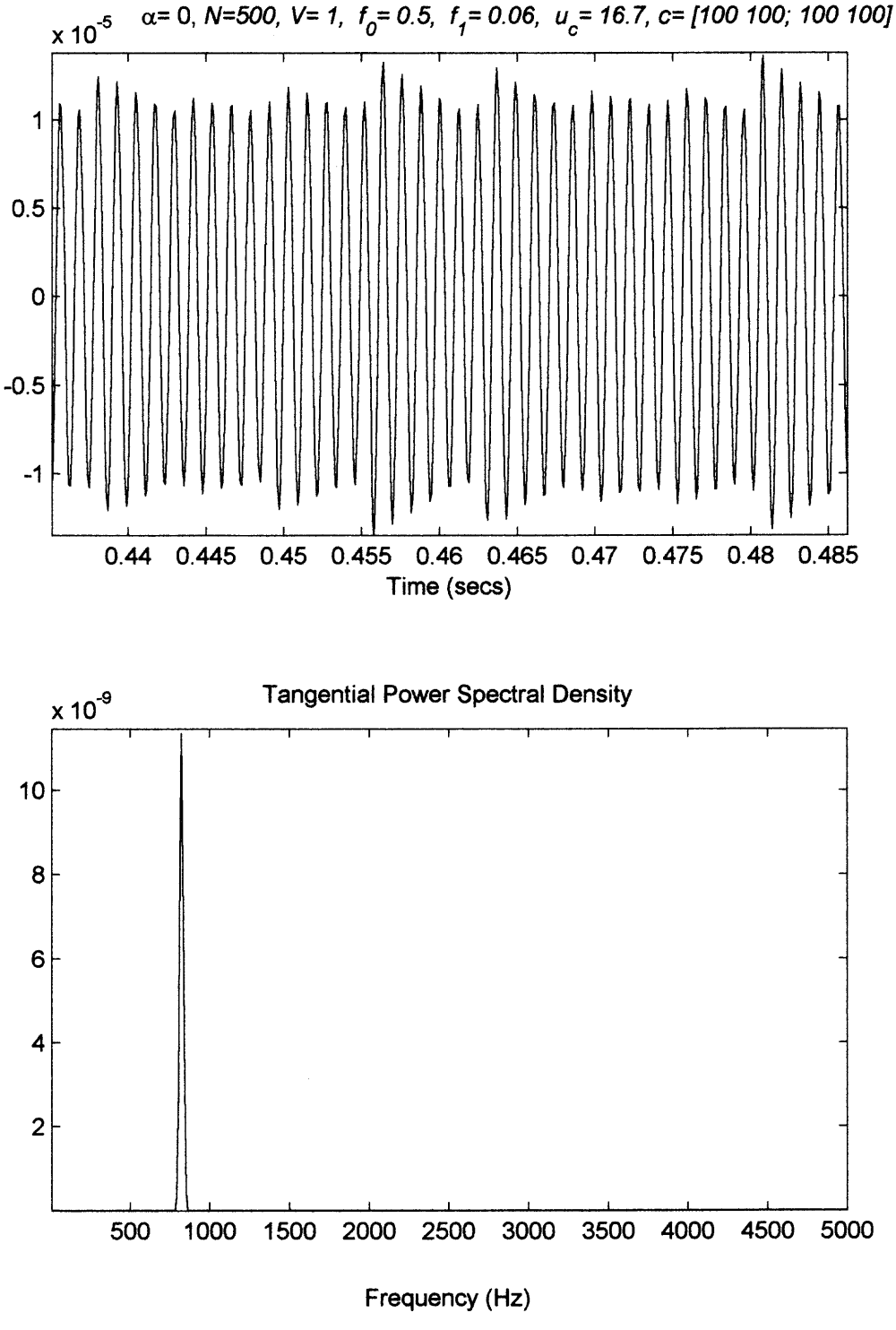
α= 0, N=500, V= 1, f0= 0.5, f1= 0.06, uc= 16.7, c= [100 100; 100 100]
x 10^-5
1
0.5
0
-0.5
-1
0.44 0.445 0.45 0.455 0.46 0.465 0.47 0.475 0.48 0.485
Time (secs)
Tangential Power Spectral Density
x 10^-9
10
8
6
4
2
500 1000 1500 2000 2500 3000 3500 4000 4500 5000
Frequency (Hz)

Figure 13b

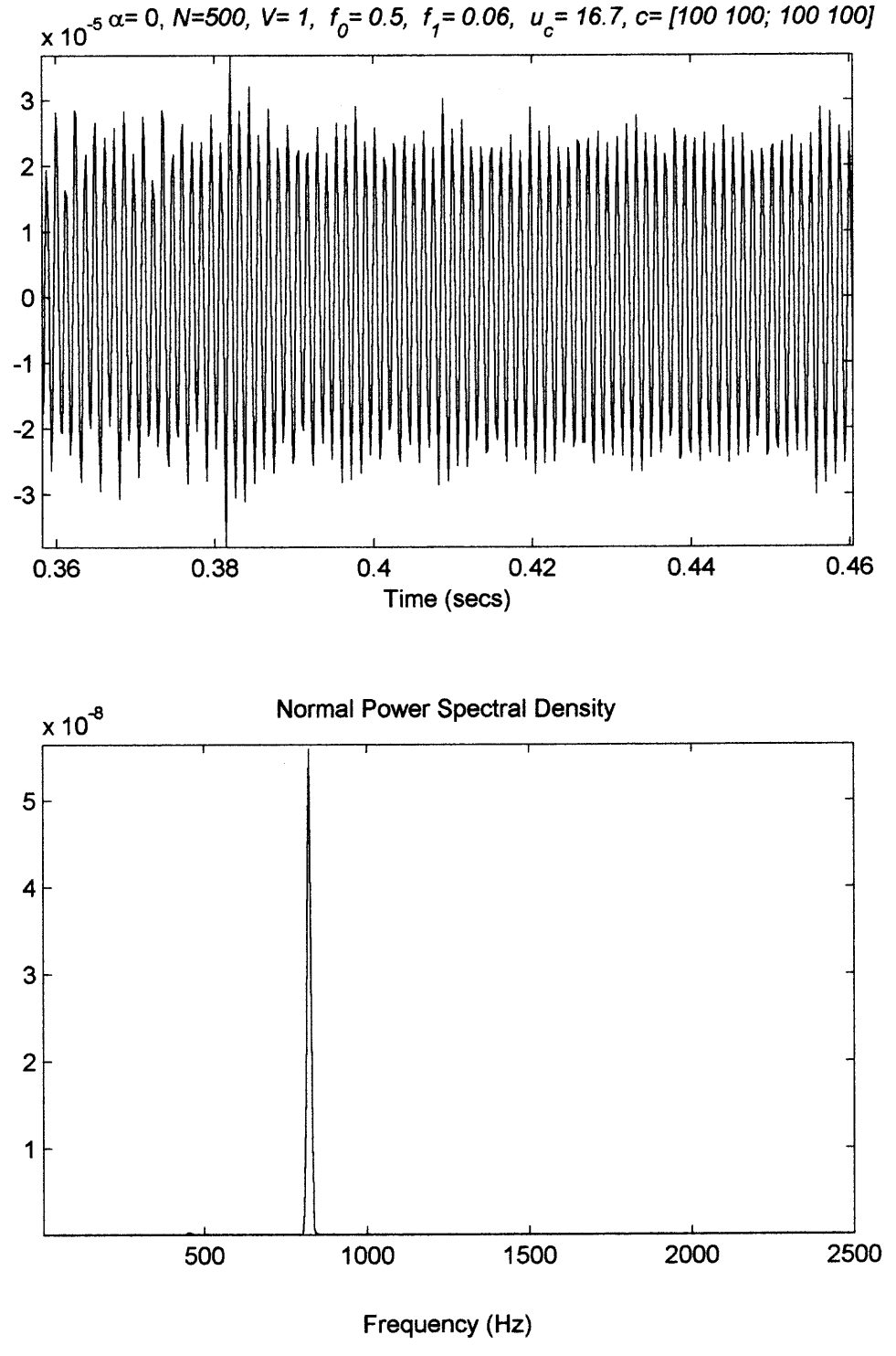
x 10^-5 α= 0, N=500, V= 1, f0= 0.5, f1= 0.06, uc= 16.7, c= [100 100; 100 100]
3
2
1
0
-1
-2
-3
0.36
0.38
0.4
0.42
0.44
0.46
Time (secs)
Normal Power Spectral Density
x 10^-8
5
4
3
2
1
500
1000
1500
2000
2500
Frequency (Hz)

Figure 13c

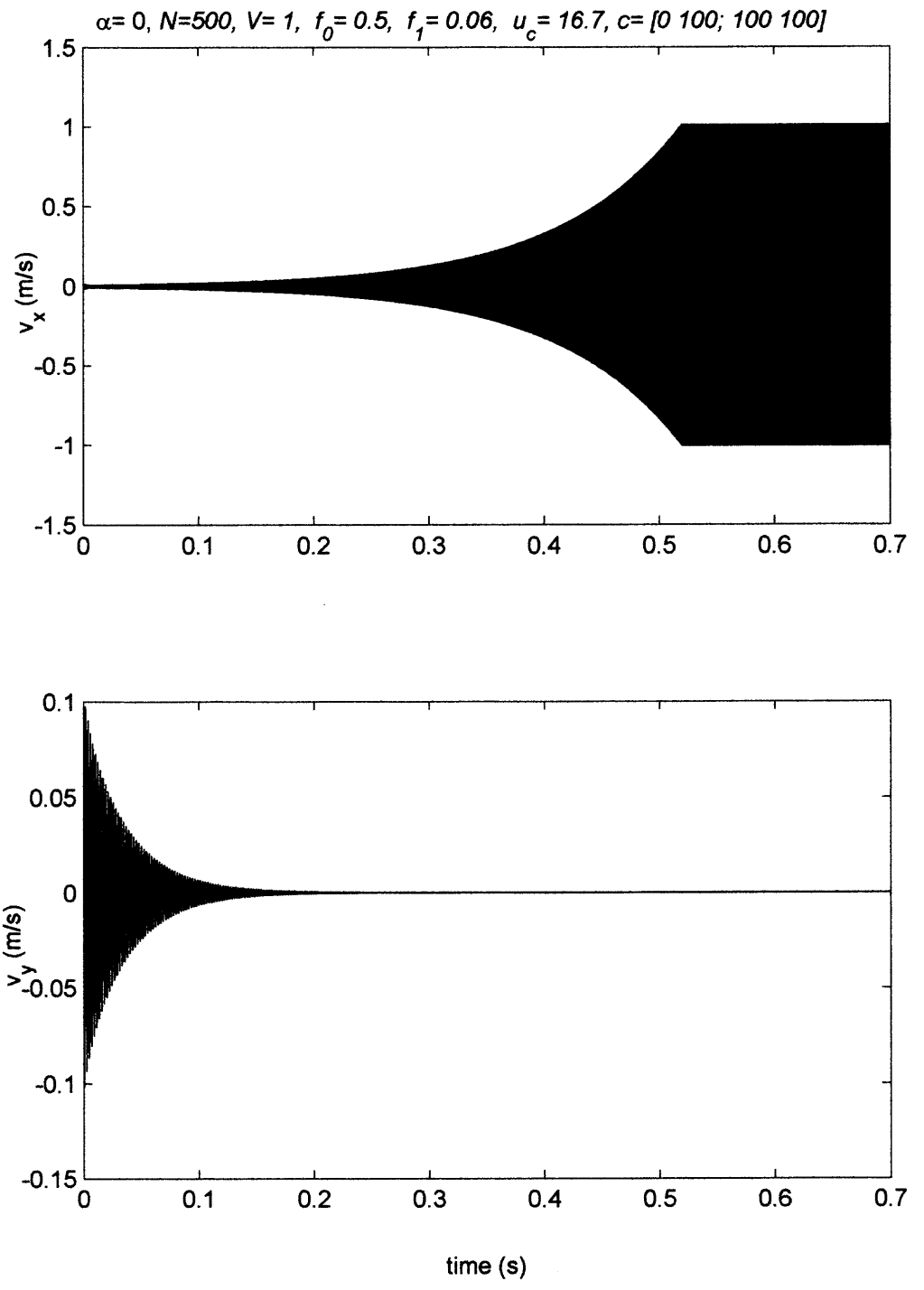

Figure 14a

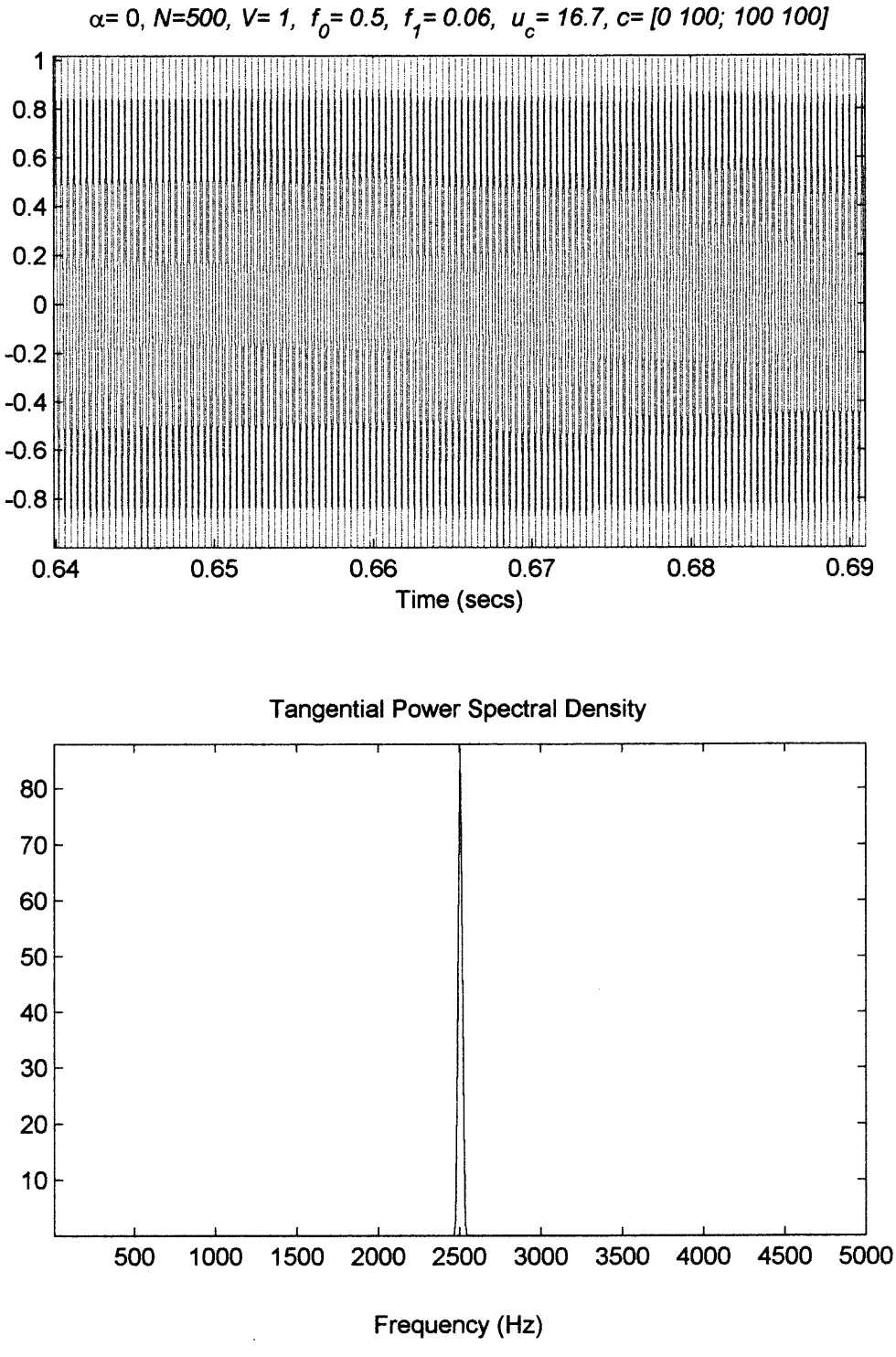
α= 0, N=500, V= 1, f0= 0.5, f1= 0.06, uc= 16.7, c= [0 100; 100 100]
1
0.8
0.6
0.4
0.2
0
-0.2
-0.4
-0.6
-0.8
0.64
0.65
0.66
0.67
0.68
0.69
Time (secs)
Tangential Power Spectral Density
80
70
60
50
40
30
20
10
500
1000
1500
2000
2500
3000
3500
4000
4500
5000
Frequency (Hz)

Figure 14b

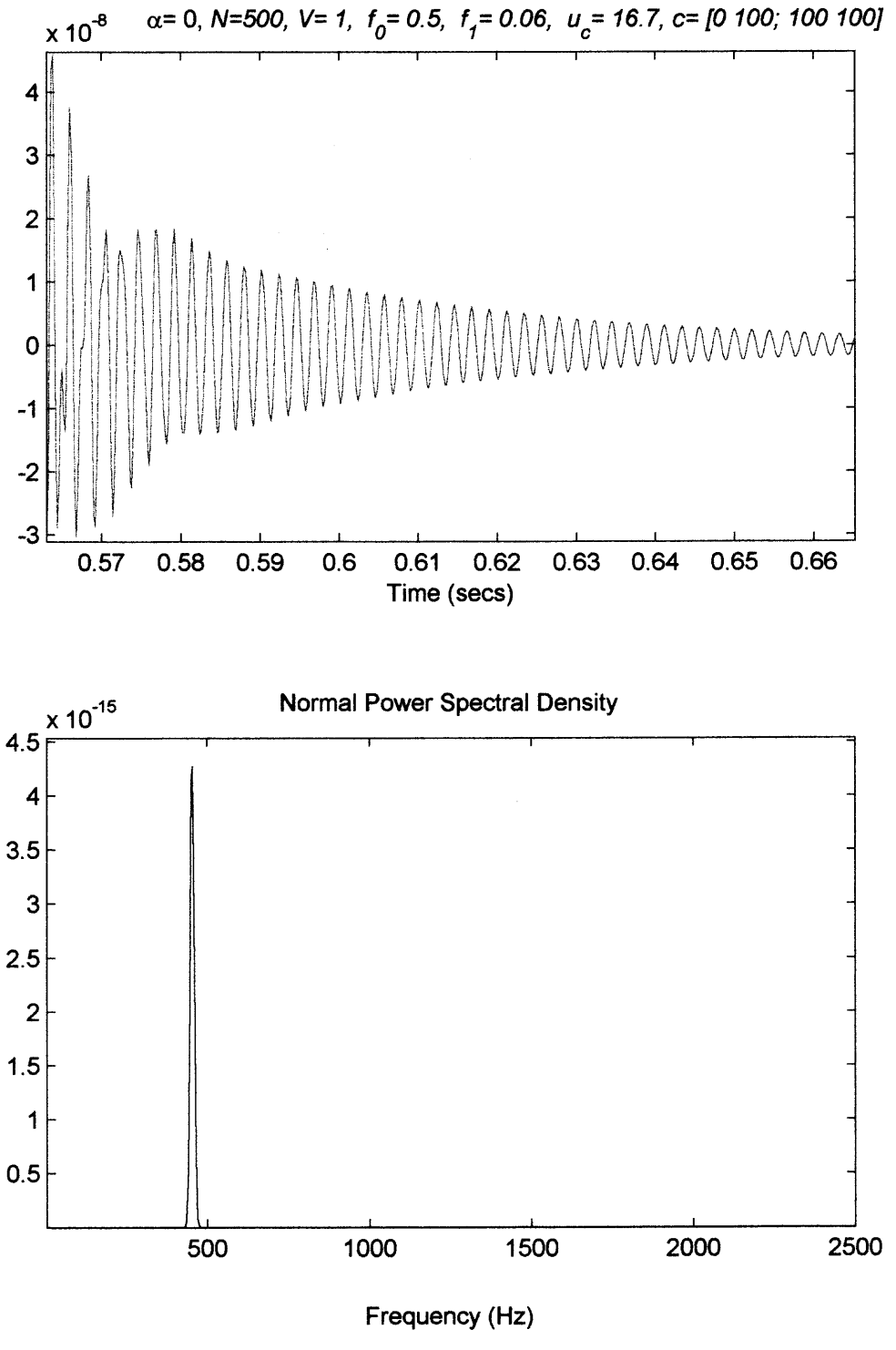
x 10^-8
α= 0, N=500, V= 1, f0= 0.5, f1= 0.06, uc= 16.7, c= [0 100; 100 100]
4
3
2
1
0
-1
-2
-3
0.57
0.58
0.59
0.6
0.61
0.62
0.63
0.64
0.65
0.66
Time (secs)
Normal Power Spectral Density
x 10^-15
4.5
4
3.5
3
2.5
2
1.5
1
0.5
500
1000
1500
2000
2500
Frequency (Hz)

Figure 14c

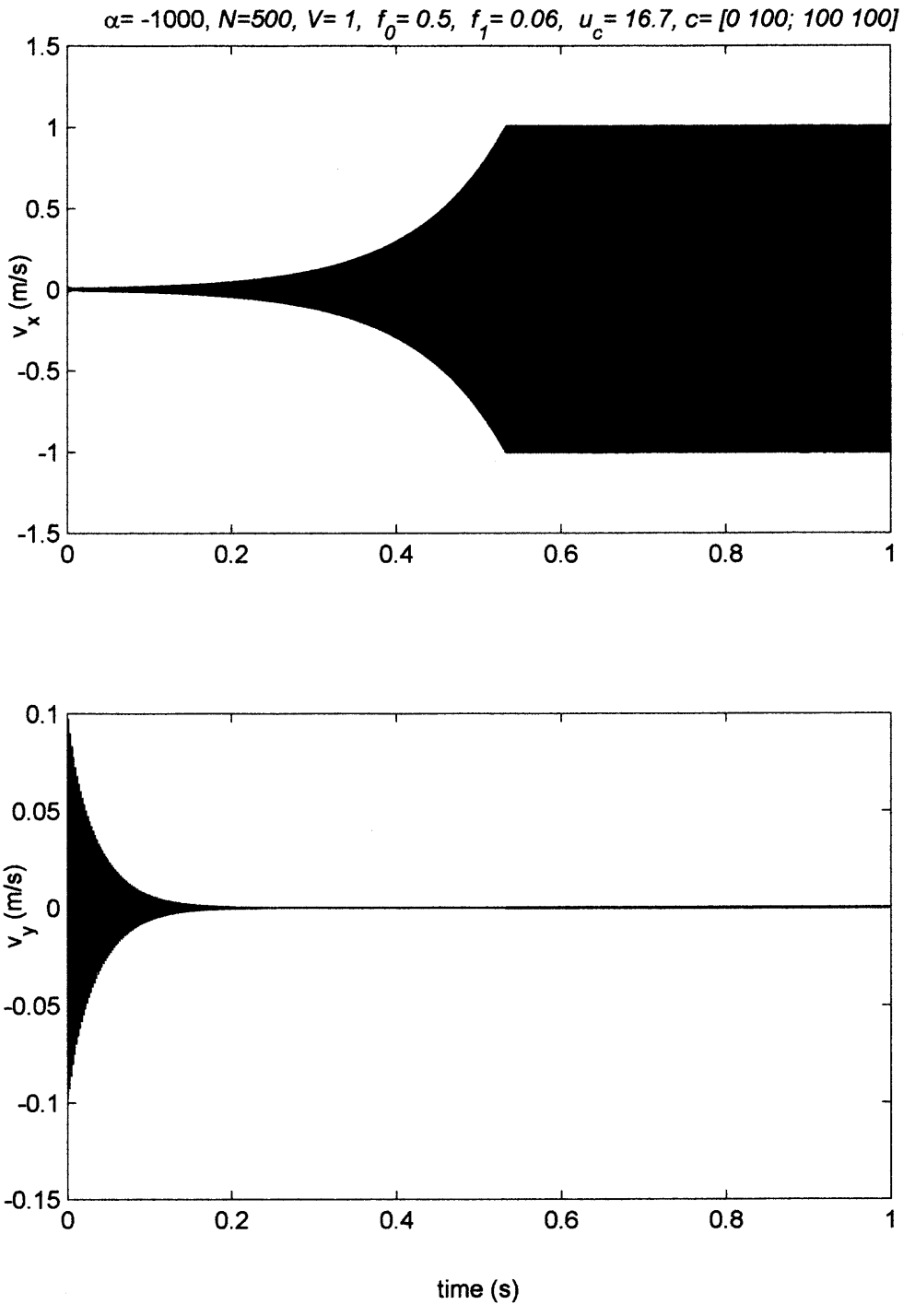

Figure 15a

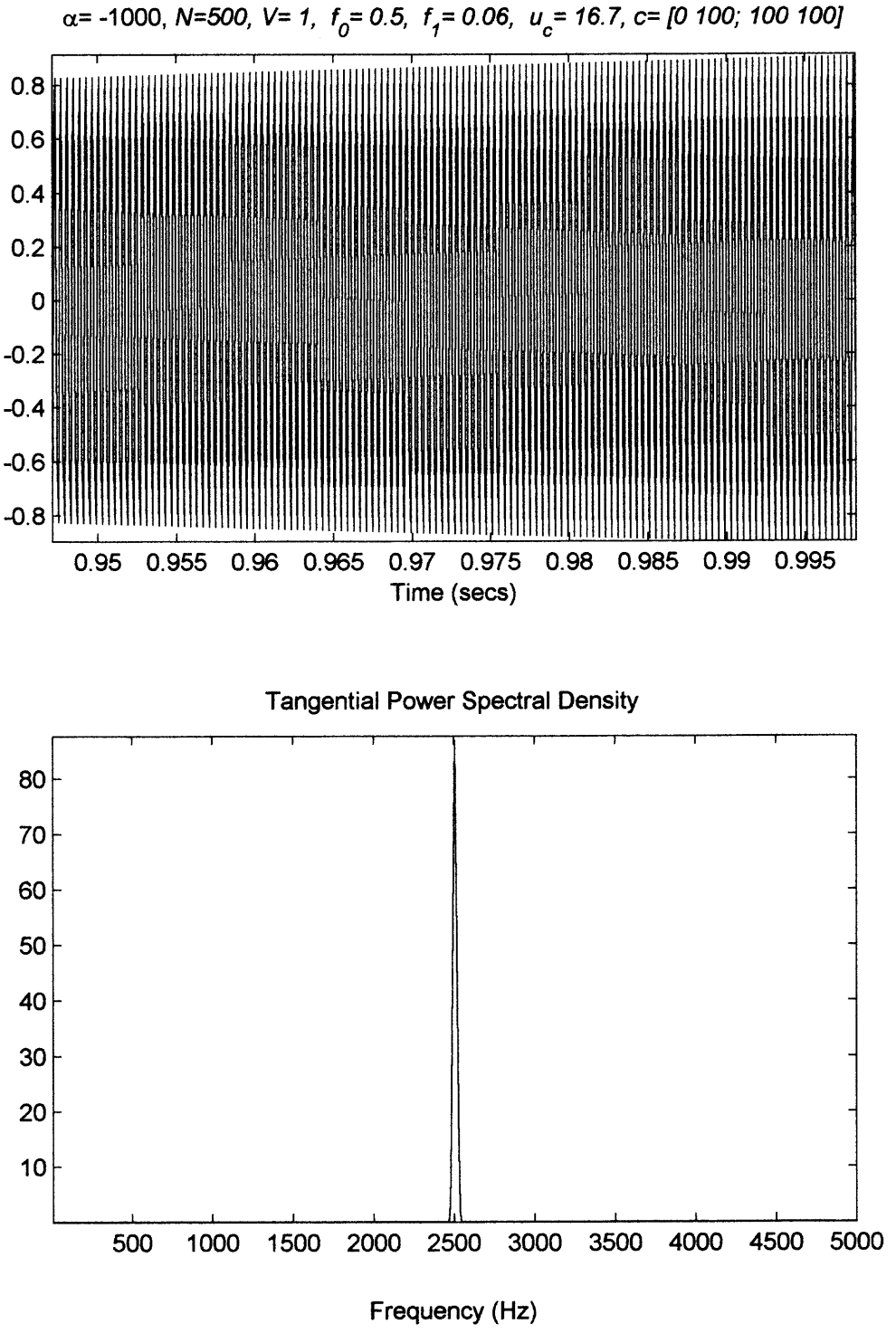
α= -1000, N=500, V= 1, f0= 0.5, f1= 0.06, uc= 16.7, c= [0 100; 100 100]
0.8
0.6
0.4
0.2
0
-0.2
-0.4
-0.6
-0.8
0.95 0.955 0.96 0.965 0.97 0.975 0.98 0.985 0.99 0.995
Time (secs)
Tangential Power Spectral Density
80
70
60
50
40
30
20
10
500 1000 1500 2000 2500 3000 3500 4000 4500 5000
Frequency (Hz)

Figure 15b

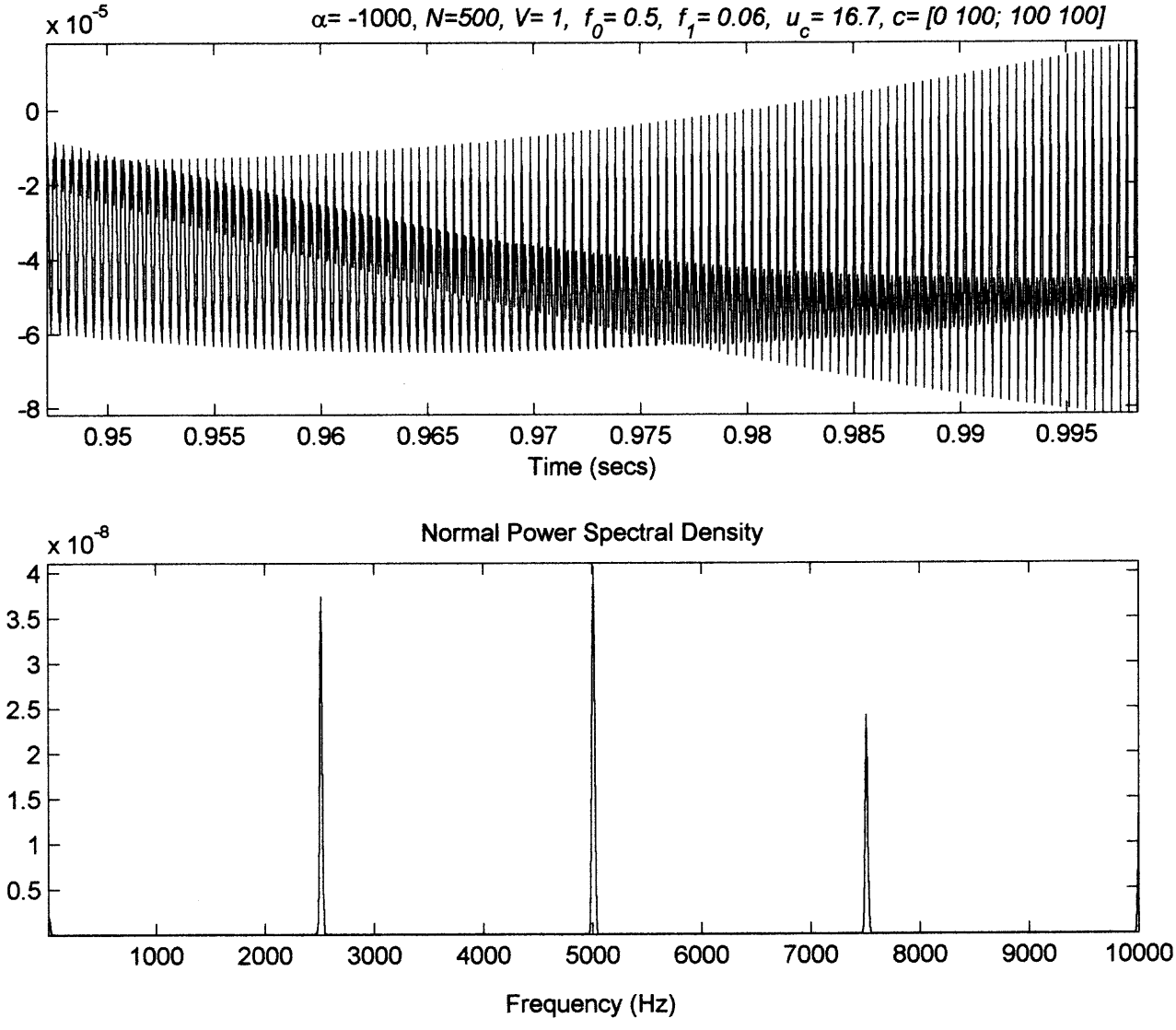
x 10^-5
α= -1000, N=500, V= 1, f0= 0.5, f1= 0.06, uc= 16.7, c= [0 100; 100 100]
0
-2
-4
-6
-8
0.95
0.955
0.96
0.965
0.97
0.975
0.98
0.985
0.99
0.995
Time (secs)
Normal Power Spectral Density
x 10^-8
4
3.5
3
2.5
2
1.5
1
0.5
1000
2000
3000
4000
5000
6000
7000
8000
9000
10000
Frequency (Hz)

Figure 15c

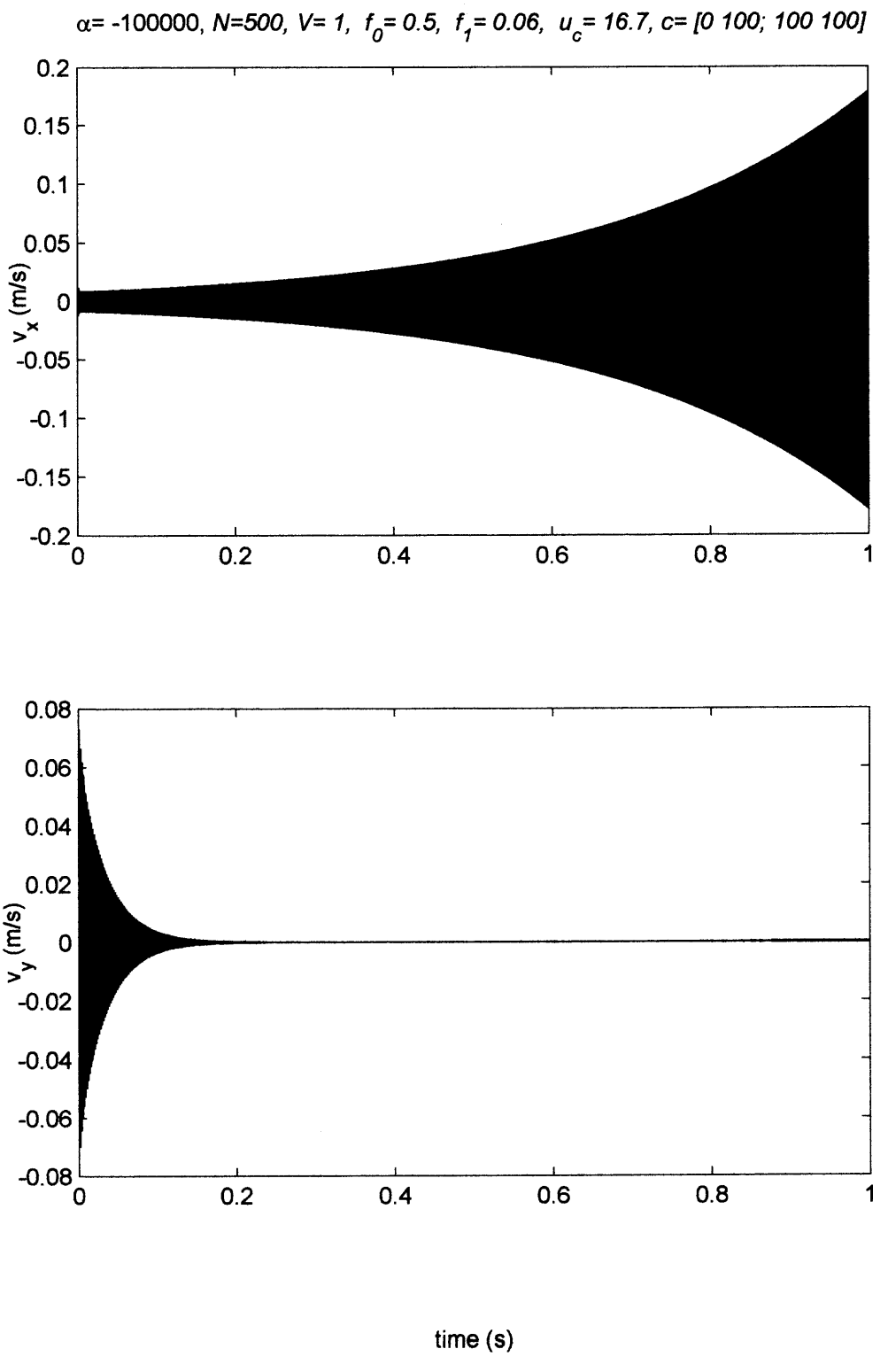
α= -100000, N=500, V= 1, f0= 0.5, f1= 0.06, uc= 16.7, c= [0 100; 100 100]
vx (m/s)
vy (m/s)
time (s)

Figure 16a

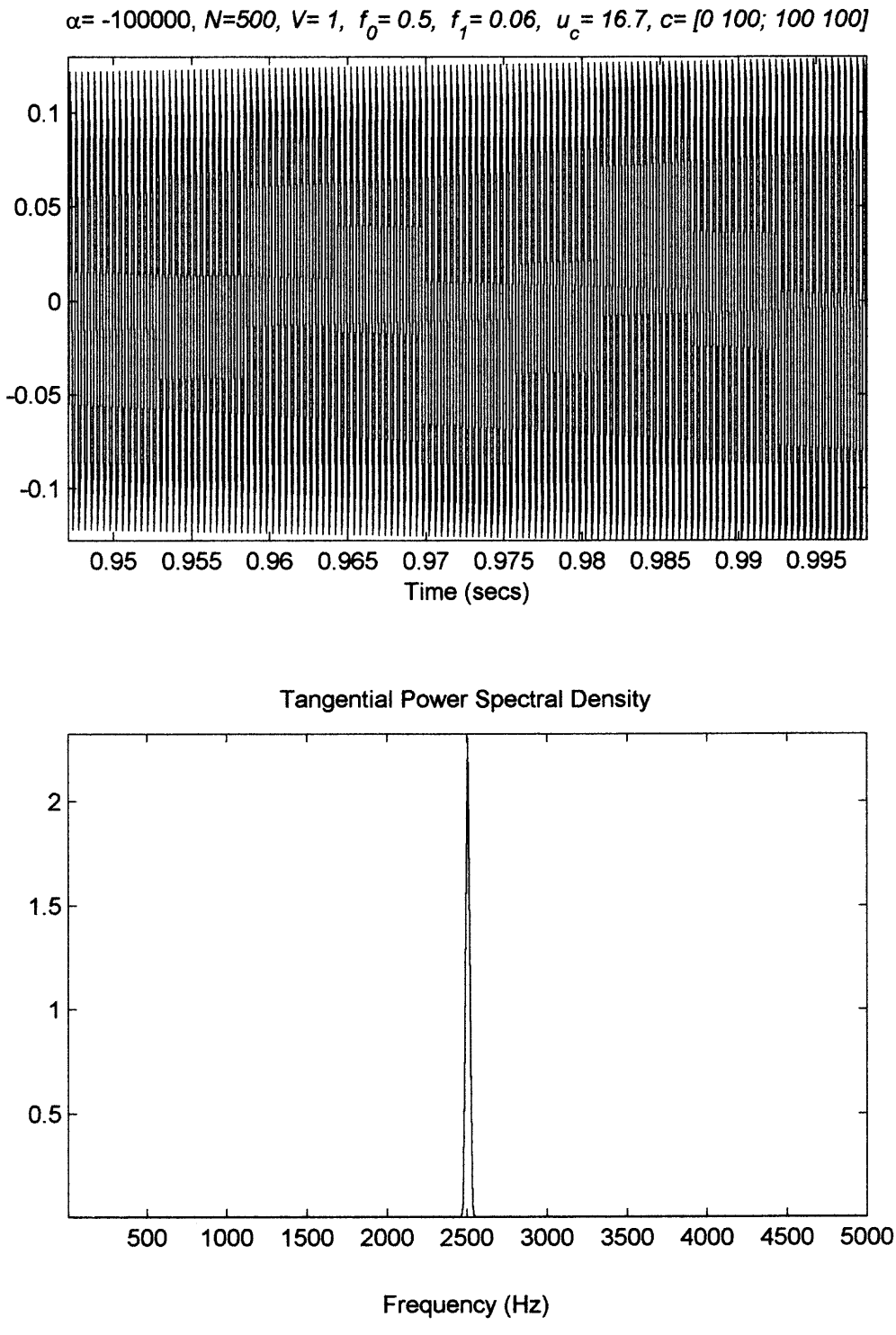
α= -100000, N=500, V= 1, f_0= 0.5, f_1= 0.06, u_c= 16.7, c= [0 100; 100 100]
0.1
0.05
0
-0.05
-0.1
0.95 0.955 0.96 0.965 0.97 0.975 0.98 0.985 0.99 0.995
Time (secs)
Tangential Power Spectral Density
2
1.5
1
0.5
500 1000 1500 2000 2500 3000 3500 4000 4500 5000
Frequency (Hz)

Figure 16b

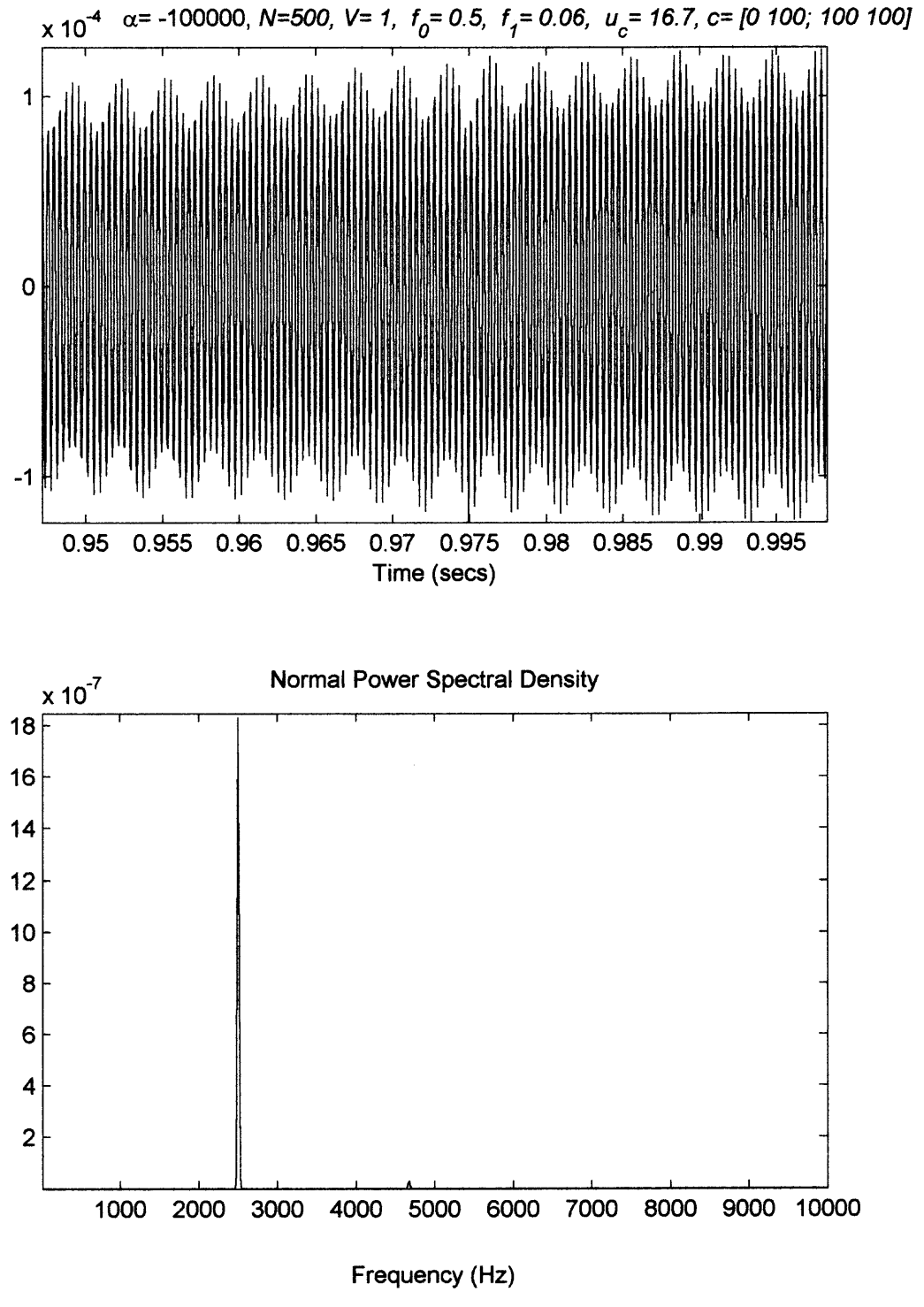
x 10^-4 α= -100000, N=500, V= 1, f0= 0.5, f1= 0.06, uc= 16.7, c= [0 100; 100 100]
1
0
-1
0.95 0.955 0.96 0.965 0.97 0.975 0.98 0.985 0.99 0.995
Time (secs)
Normal Power Spectral Density
x 10^-7
18
16
14
12
10
8
6
4
2
1000 2000 3000 4000 5000 6000 7000 8000 9000 10000
Frequency (Hz)

Figure 16c

APPENDIX B

SIMULINK PROGRAM CODE

Appendix B contains the printout of the Simulink program code. The description of program's blocks can be found in Chapter 10.

B1. Program's Interface (main page)

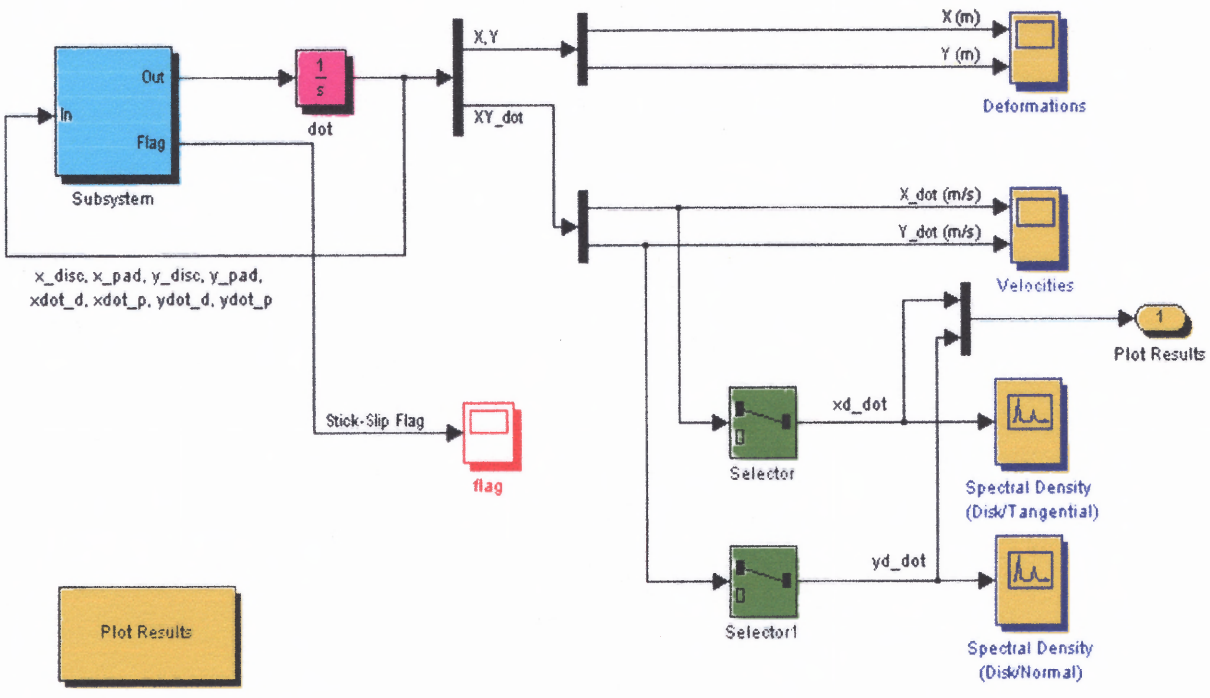

Subsystem Block

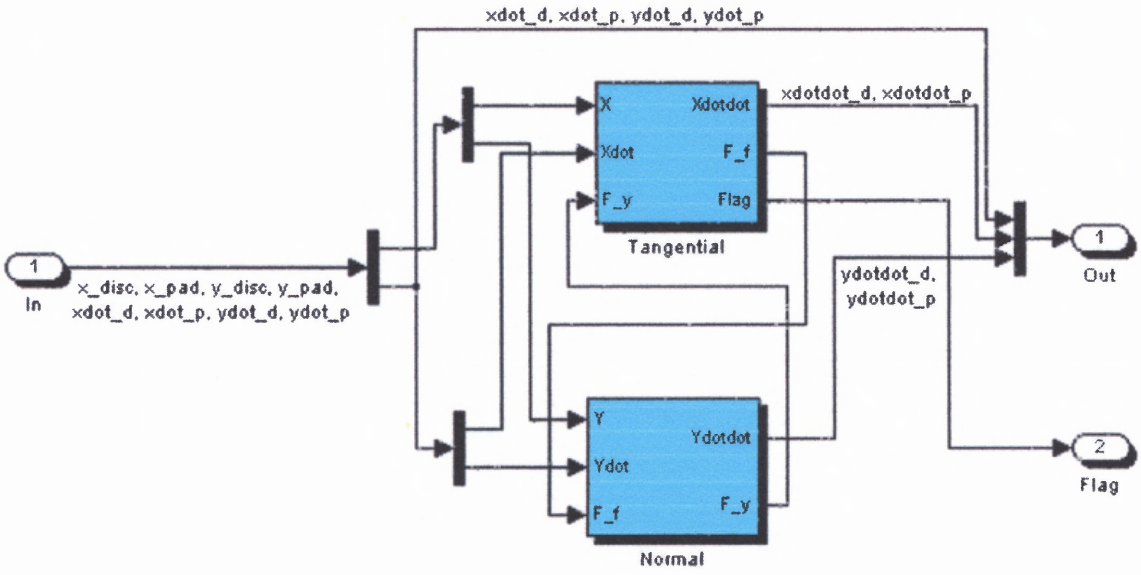

Normal Block

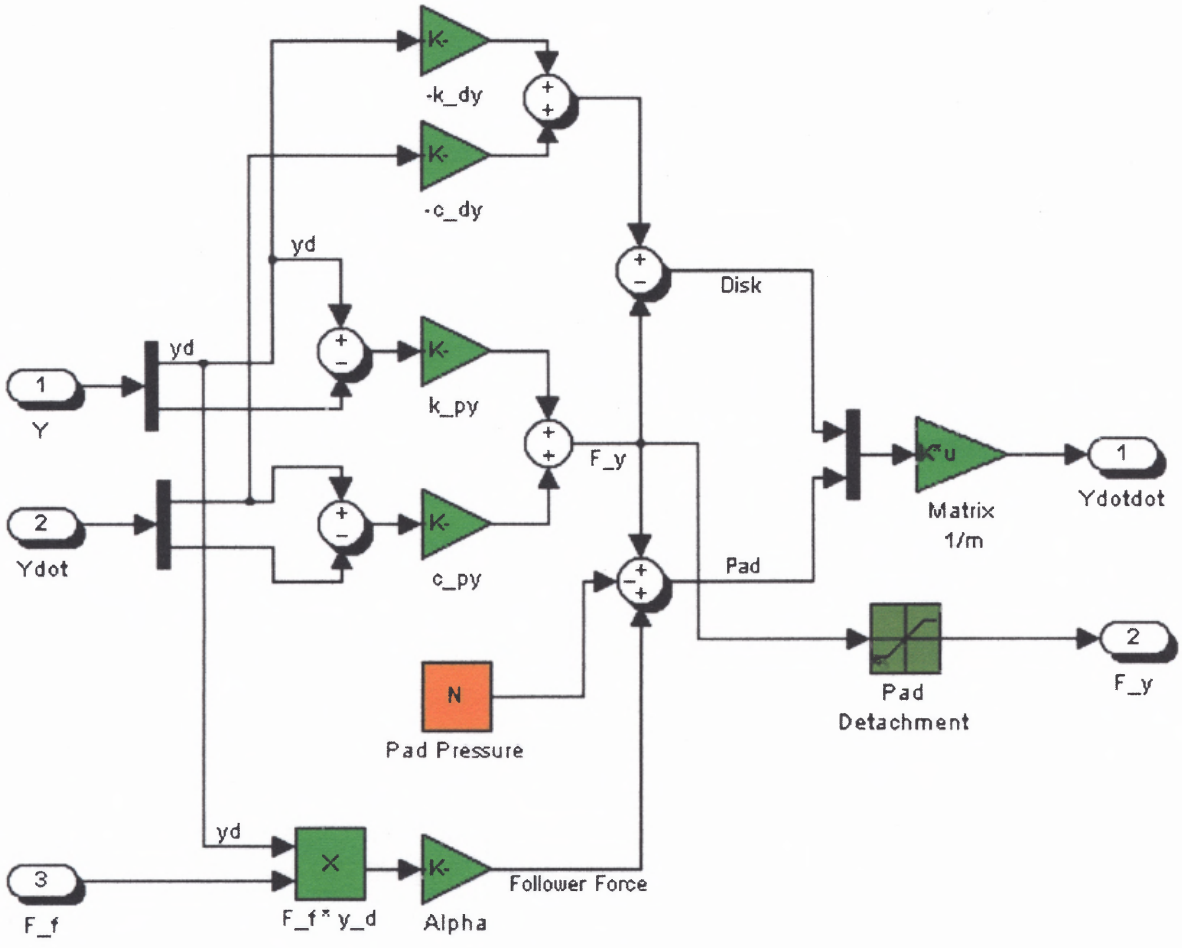

Tangential Block

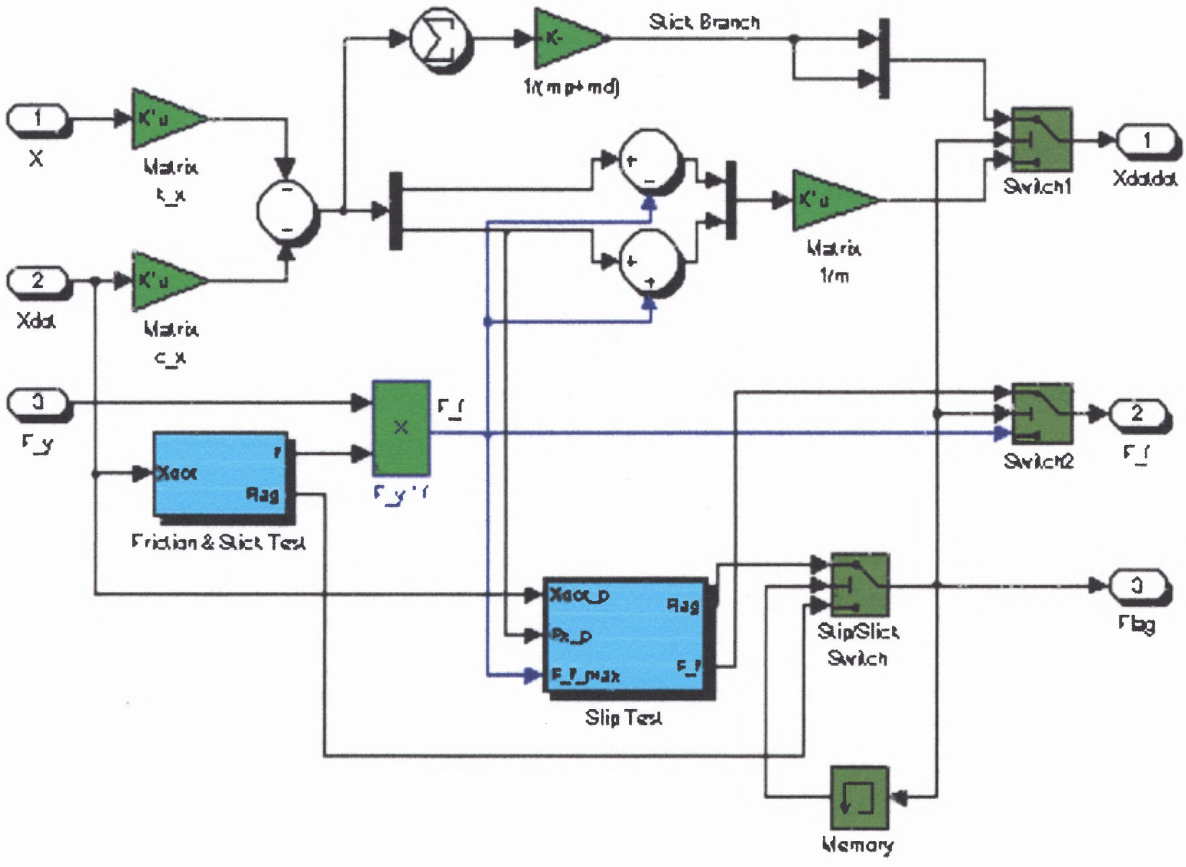

Friction and Stick Test Block

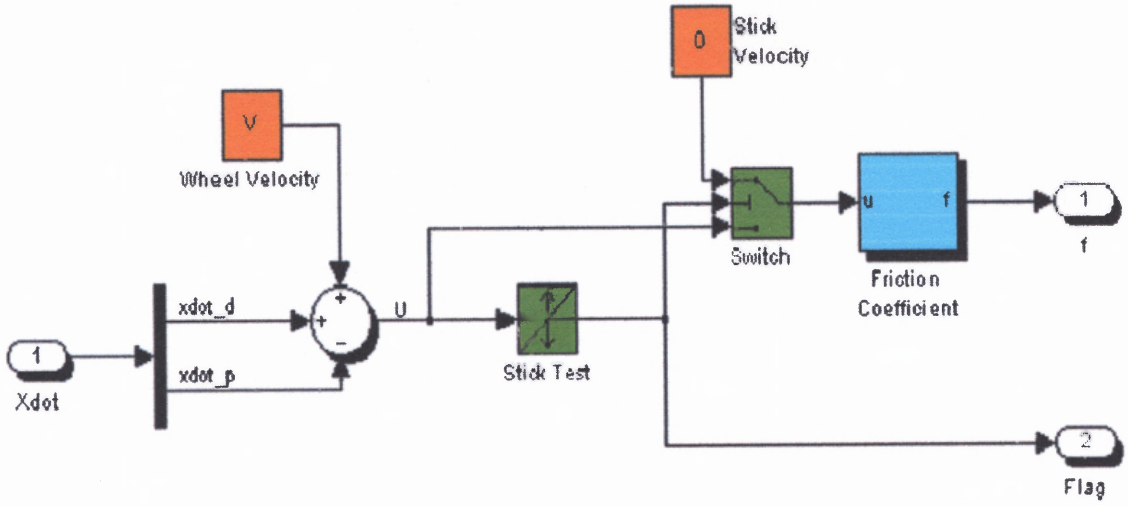

Slip Test Block

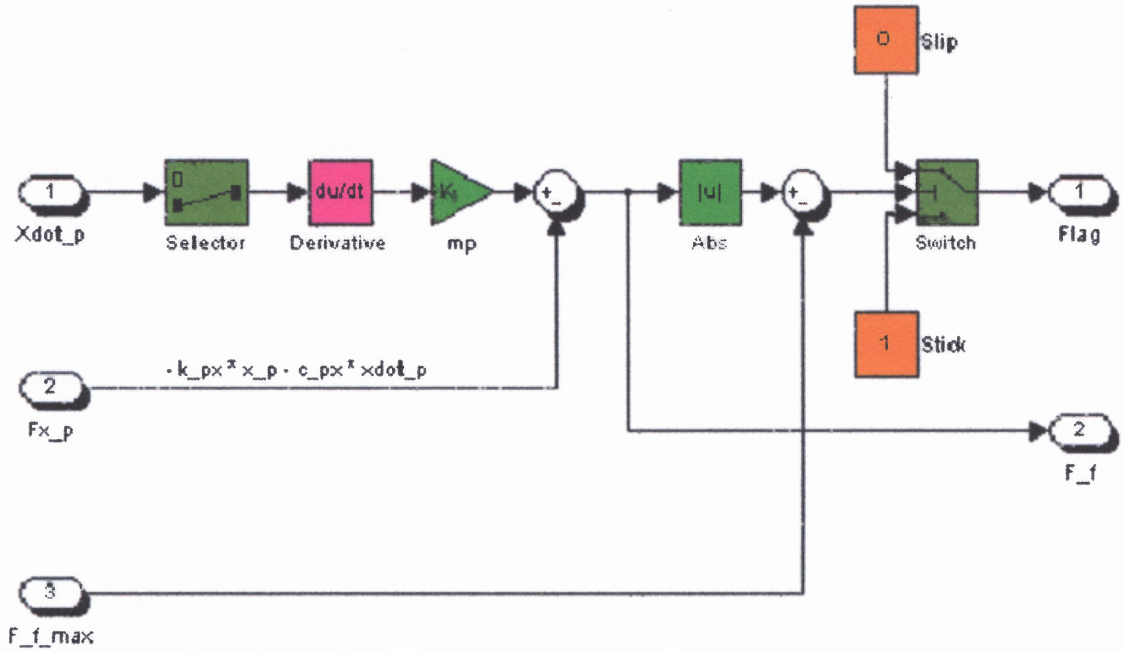

Friction Coefficient Block

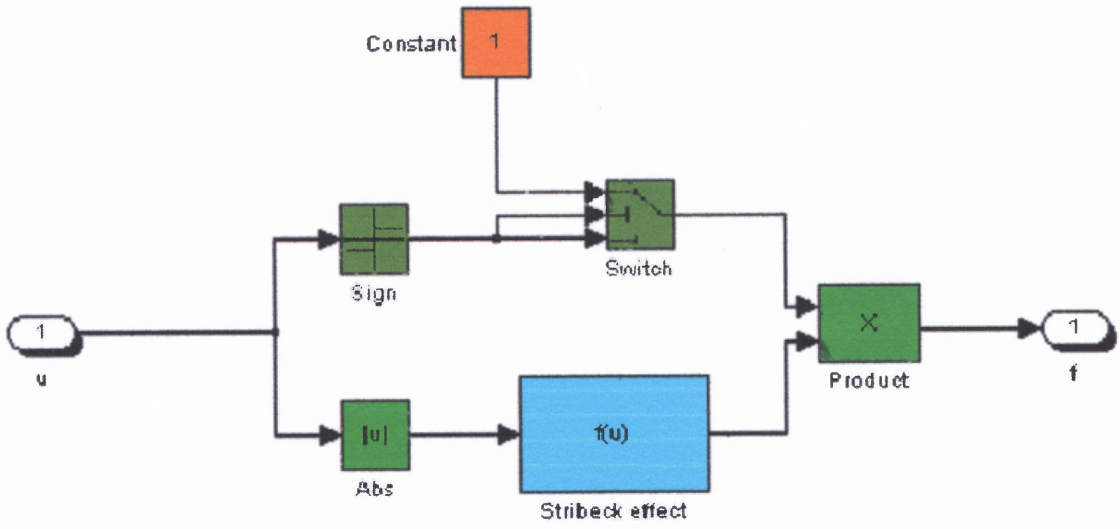

REFERENCES

1. Aviles, R., Henequet, G., Amezua, E. and Vallejo, J. (1995) "Low frequency vibrations in disc brakes at high car speed. Part II: mathematical model and simulation", Int. J. of Vehicle Design, vol. 16, No. 6, pp. 556-569.

2. Chen, F., Chen, S., Her, J. and Harwood, P. (2000) "Disc Brake Intermittent Squeal Noise Study Using Experimental Techniques Based Systematic Approach", SAE paper 2000-01-0731.

3. Chung, C., Steed, W., Kobayashi, K., and Nakata, H. (2001) "A New Analysis Method for Brake Squeal Part I: Theory for Modal Domain Formulation and Stability Analysis", SAE paper 2001-01-1600.

4. Dunlap, K. B., Riehle, M. A. and Longhouse, R. E. (1999) "An Investigative Overview of Automotive Disc Brake Noise", SAE paper 1999-01-0142.

5. El-Butch, A. M. and Ibrahim, I. M. (1999) "Modeling and Analysis of Geometrically Induced Vibration in Disc Brakes Considering Contact Parameters", SAE paper 1999-01-0143.

6. Fenny, B., Guran, A., Hinrichs, N. and Popp, K. (1998) "Historical review of dry friction and stick-slip phenomena", Appl. Mech. Rev. vol. 51, No. 5, pp. 321-341.

7. Hendricx, W., Garesci, F., Pezzutto, A. and Van der Auweraer, H. (2002) "Experimental and Numerical Modeling of Friction Induced Noise in Disc Brakes", SAE paper 2002-01-1192.

8. Mahajan, S. K., Hu, Y. and Zhang, K. (1999) "Vehicle Disc Brake Squeal Simulations and Experiences", SAE paper 1999-01-1738.

9. McDaniel, J. G., Moore, J., Chen, S. and Clarke, C. L. (1999) "Acoustic Radiation Models of Brake Systems from Stationary LDV Measurements", Proceedings of IMEC 99, 1999 International Mechanical Engineering Congress and Exposition, November 14–19, 1999, Nashville, Tennessee, USA.

10. Mottershead, J. E. Chan, S. N., and Carmell, M. P. (1994) "Parametric resonances at sub critical speeds in discs with frictional loads", Proc. Inst. Mech. Engineers, Part C, vol. 208, pp. 417-425.

11. Mottershead, J. E. (1998) "Vibration- and Friction-Induced Instability in Disks", Shock. Vib. Dig., vol. 30, pp. 14-31.

12. Mottershead, J. E., Quyang, H., Cartmell, M. P. and Brookfield, D. J. (1999) "Friction-induced vibration of an elastic slider on a vibrating disc", Int. J. of Mech. Sciences, vol. 41, pp. 325-336.

13. Mottershed, J. E. Quyang, H. and (2001a) "Unstable traveling waves in the friction-induced vibration of discs", J. of Sound and Vibration, vol. 248, pp. 768-779.

14. Mottershed, J. E. Quyang, H. (2001b) "A Bounded Region of Disc-Brake Vibration Instability", J. of Vibration and Sound, vol. 123, pp. 543-545.

15. Mottershed, J. E. Quyang, H. (2001c) "Optimal suppression of parametric vibration in discs under rotating frictional loads", Proc. Inst. Mech. Engineers, Part C, vol. 215, pp. 65-75.

16. Nishiwaki, M. (1993) "Generalized theory of brake noise", Proc. Inst. Mech. Engineers, Part D, J. Automobile Eng. Vol. 207, pp. 195-292.

17. Pilipchuk, V. N., Ibrahim, R. A., Blaschke, P. G. (2002) "Disc Brake Ring-element Modelling Involving Friction-induced Vibration", Proc. of IMAC-XX: A Conference on Structural Dynamics, February 4-7, 2002, Los Angeles, California, USA, pp. 535-541.

18. Shi, T. S., Dessouki, O., Warzecha, T., Chang, W. K. and Jayasundera, A. (2001) "Advances in Complex Eigenvalue Analysis for Brake Noise", SAE paper 2001-01-1603.

19. Watany, M., Abouel-Seoud, S., Saad, A. and Abdel-Gawad, I. (1999) "Brake Squeal Generation", SAE paper 1999-01-1735.